

# A <sup>1</sup>H NMR Pulse Gradient Spin-Echo (PGSE) Mass Transport Study of Dimethyl Oxalate and Ethylene Glycol: New Fuels for the DOFC

S. Suarez-Gustave\*, S. Greenbaum\*, S.H. Chung\*\*, E. Peled\*\*\*, T. Duvdevani\*\*\*, A. Aharon\*\*\* and A. Melman\*\*\*

\*Department of Physics  
Hunter College of CUNY  
New York, NY 10021

\*\*Department of Chemistry and Physics  
William Paterson University

Wayne, NJ, 07470

\*\*\*School of Chemistry  
Tel Aviv University  
Tel Aviv, Israel 69978

## Introduction

Fuel Cells are electrochemical devices that convert chemical energy into electrical energy. Of the many different types of fuel cells being investigated we focused on the Direct Oxidation Fuel Cell (DOFC). In the DOFC organic fuel is fed directly into the fuel cell without the need for prior modification. This makes the DOFC very attractive as the power source for electric vehicles as it offers reduce weight and volume advantages over the indirect fuel cell, which is based on the modification (reformation) of organic fuels into hydrogen.

Presently methanol is the fuel used in the DOFC. However, because of its toxicity, low boiling point and high permeability in *Nafion* - the proton conducting membrane (PCM) currently used, replacement fuels are being considered<sup>2</sup>.

To aid in the development of the DOFC, we investigated the mass transport represented by the self-diffusion coefficients (D) of methanol and two alternative fuels - dimethyl oxalate (DMO) and ethylene glycol (EG) in new low-cost nanoporous PCM's. The NP-PCM's are based on commercial poly(vinylidene fluoride), with variable pore size determined by addition of nanoscale SiO<sub>2</sub> or Al<sub>2</sub>O<sub>3</sub> particles<sup>1</sup>. EG is the most promising candidate to replace Methanol, as it is already a ubiquitous product within the automotive industry. The advantage of DMO is that it is a solid at room temperature and therefore may be added directly to the fuel cell without the need for separate fuel tank.

The use of the NP-PCM's offer several advantages over *Nafion* including: lower membrane cost, lower permeability to methanol due to smaller pores, and higher room temperature conductivities that are unaffected by metal-ion impurities (*Nafion*'s conductivity decreases significantly with added impurities)<sup>1</sup>.

Nuclear Magnetic Resonance Pulse Gradient Spin-Echo technique (NMR PGSE) was used to determine the self-diffusion of diffusing species in the systems<sup>3</sup>. The PGSE technique allows quick non-invasive measurements of the species self-diffusion and has the advantage of measuring mass transport irrespective of the number of chemical components in the diffusing specie.

## Experimental

The NMR PGSE experiments were performed using a multiply-tuned PGSE NMR probe in a 7.1T superconducting magnet interfaced with a CMX-300 spectrometer. The NMR diffusion measurements use the Hahn spin echo pulse sequence ( $\pi/2-\tau-\pi$ ) with a pair of square-shaped gradient field pulses (separated by time  $\Delta$ ) of

magnitude  $g$  and duration  $\delta$  - the first applied between the two rf pulses and the other after the  $\pi$  pulse. The echo amplitude is attenuated by an amount dependent on the change in the spins position by the process of self-diffusion in the time interval  $\Delta$ . This change may be represented by

$$A(g) = \exp[-\gamma^2 D g^2 \delta^2 (\Delta - \delta/3)]$$

where  $D$  is the self-diffusion coefficient and  $\gamma$  is the magnetogyric ratio of the spin. By fitting this equation to the echo amplitudes for a series of gradient strengths  $g$ ,  $D$  is extracted<sup>3</sup>.

Fuel/Acid mixtures consisting of 3M H<sub>2</sub>SO<sub>4</sub> and 2M of the above named fuels were prepared. Strips of the NP-PCM's were placed in each of the fuel/acid mixtures and allowed to equilibrate for 48 hours. Measurements were collected over the temperature range of 30-90°C with 20-30min sample equilibration time after each temperature change. An Oxford ITC533 temperature accessory in conjunction with a stream of dry N<sub>2</sub> gas was used to regulate the temperature to within  $\pm 1$ K.

## Results

Proton NMR spectroscopy results for the fuel/acid systems revealed multiple components - OH and CH, identifiable by their respective chemical shifts, as shown in **Fig. 1**. Of the three fuel/acid solutions DMO gave OH and CH self-diffusion coefficients lower by about a factor of two both in solution and in the NP-PCM's. EG solution had OH and CH self-diffusion values comparable to Methanol over the entire temperature range.

However, results for the EG equilibrated NP-PCM's gave OH and CH diffusion values lower by about a factor of two compared with the Methanol equilibrated membranes. Of the five NP-PCM's investigated, one particular membrane that exhibited low crossover in electrochemical evaluations gave the highest OH and CH self-diffusion values, almost independent of fuel type. **Figures 2 and 3** show Arrhenius plots of  $D$  for both the OH and CH peaks components of the equilibrated NP-PCM's and fuel/acid solutions.

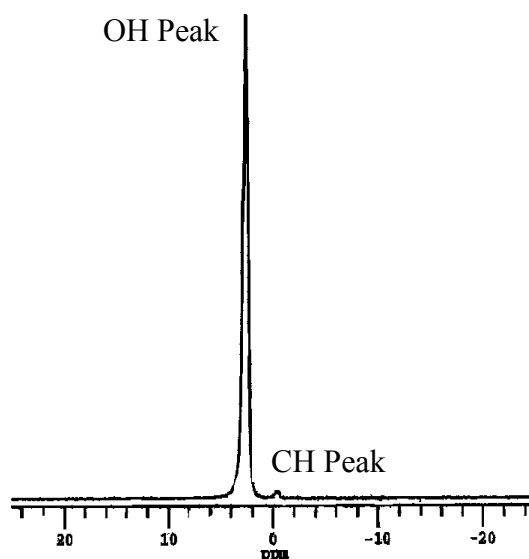


**Figure 1.** <sup>1</sup>H NMR spectrum acquired at 333K indicating the OH and CH components of the system.

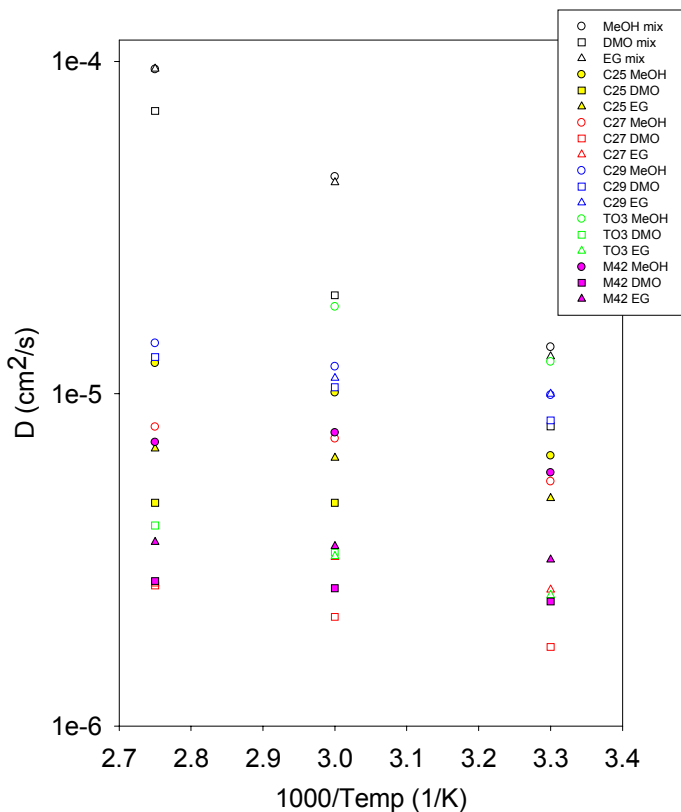


**Figure 2.** Arrhenius plot of the OH D values.

**Figure 3.** Arrhenius plot of the CH D values.

### Conclusion

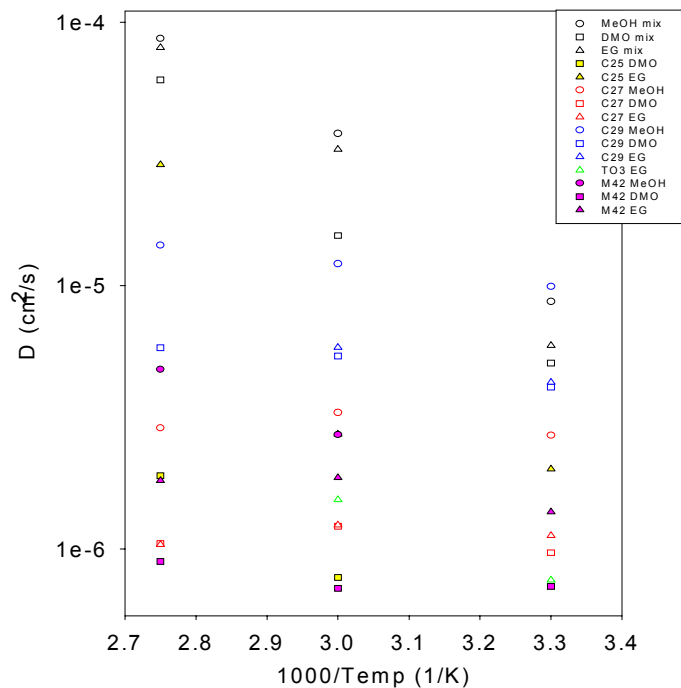
As replacement fuels for methanol, EG and DMO offers lower membrane permeability indicated by the lower values of CH self-diffusion coefficients obtained for the equilibrated NP-PCM's. Electrochemical measurements<sup>1</sup> indicate that the NP-PCM's exhibit low crossover while retaining high protonic conductivity. Although we expect to find correlations between the former and NMR-determined CH D values, and between the latter and OH D values, the present results suggest that proton transport may not be strongly correlated with OH mobility.

### Acknowledgement.

This research is supported in part by ONR.

### References

1. Peled, E.; Duvdevani, T; Aharan, A; Melman, A. *Electrochemical and Solid-State Letters*, **2000**,12 (3), 525-528.
2. Peled, E.; Duvdevani, T; Aharan, A; Melman, A. *Electrochemical and Solid-State Letters*, **2001**,4 (3), A38-A41.
3. Chung, S.H; Bajue, S; Greenbaum, S.G. *J. Chem. Phys.* **2000**, 112(19), 8515-8521.



## AGTANE (AGricultural ceTANE): An economically viable bioenergy product for compression ignited engines

A. Spataru\*

\*The ADEPT Group, Inc., 1575 Westwood Boulevard, Suite 200, Los Angeles, CA 90024-5620  
Fax: (310) 478-5658; adept@adeptgroup.net

### Introduction

Scientists at the Canadian Centre for Mineral and Energy Technology (CANMET) laboratory, Ontario, Canada, have proven at lab scale a process to convert yellow grease (YG), tallows and poultry fat to a **low sulfur, high cetane premium diesel blending stock**. This proprietary high-temperature and high-pressure process is based on a refining technology called hydrotreating. The principal output is a diesel blending stock called AGTANE (for AGricultural ceTANE).

### What is AGTANE and its purpose?

AGTANE, a mix of long-chained paraffins, is *not* a biodiesel (e.g. methyl ester). California refiners who analyzed the final product classify AGTANE as a "synthetic diesel." Paraffins are a family of hydrocarbons normally found in commercial diesel blends; esters are not. When AGTANE is blended with regular diesels, the resulting fuel burns more efficiently and with cleaner emissions. Particulate matter (PM), and NOx emissions are lowered. AGTANE compliments and reduces the volume of traditional cetane improvers.<sup>1</sup>

**Global Trends.** Convergent global trends favor production of AGTANE from discarded fats and waste oils and greases. There is also regulatory pressure towards the use of on-road diesels with low sulfur and high cetane value.

Recent research has proved synergy between AGTANE and "traditional" cetane improvers.<sup>2</sup> This synergy increases AGTANE's value. It is thought that AGTANE will be added from 3 to 12% of volume in final commercial diesel mixes.

### Test Results show that AGTANE:

- (1) linearly raises the cetane of unadditized diesel *without* a top-end limit;<sup>3</sup>
- (2) is synergistic with traditional cetane improvers;
- (3) has a low sulfur content ( $\sim 15 \pm 5 \text{ ppm}^4$ ); and
- (4) increases end-product volume by the added AGTANE volume.

### Discussion and Application

There is a growing trend to exclude YG and tallow out of the food and feed chains due to *bovine spongiform encephalopathy*, commonly known as "mad cow disease." Because YG contains a significant amount of animal fat, its sales as an animal feed component are increasingly restricted. There is an unprecedented worldwide surplus of YG. Smaller rendering plants have closed, raising health

<sup>1</sup> Cetane improvers are man-made chemicals that are added at the refinery level to diesel blends to raise the blend's cetane number. These compounds are also called "ignition improvers" Cetane is an indicator of a diesel blend's combustion performance in compression-ignited engines (same as "octane" for spark-ignited engines). As with octane, higher numbers are desirable.

<sup>2</sup> The cetane improver used in these tests was Octel CI-0801.

<sup>3</sup> The cetane value enhancing effects of traditional cetane improvers level off at some point (after an 8 or 9 point rise in cetane value).

<sup>4</sup> 15-ppm max. S<sub>2</sub> in on-road diesel is a South Coast Air Quality Management District requirement by 2005.

and environmental concerns in areas where other renderers have been unable to service.

### Conclusion

Large-scale production and commercialization of AGTANE allows the rendering industry the option to become a significant pollution remediator. The broad use of AGTANE in on-road and off-road applications will significantly reduce both NOx and PM, something not possible by burning YG in rendering plant boilers.

AGTANE production is most likely to be conducted in major urban areas where large rendering operations are located within 50 miles of petroleum refining facilities. The profitability of AGTANE plants can be further enhanced by tax breaks/incentives currently extended to biodiesel. Exchanges with leading petroleum refiners indicate on-going strong interest in AGTANE.

AGTANE may prove to be a timely solution to help meet US energy and environmental needs, while helping the agricultural sector deal with food chain concerns. As it proportionally reduces the use of petroleum-derived diesel fuel, AGTANE can reduce dependence on foreign oil and increase domestic energy security.

# BIOMASS PYROLYSIS CHEMISTRY AND GLOBAL KINETICS AT HIGH HEATING RATES

David C. Dayton<sup>a</sup>, Alexander L. Brown<sup>a,b</sup>, and John W. Daily<sup>b</sup>

<sup>a</sup>National Renewable Energy Laboratory, National Bioenergy Center  
1617 Cole Boulevard, Golden, CO 80401 USA

<sup>b</sup>University of Colorado-Boulder,  
Department of Mechanical Engineering, Boulder, CO 80309 USA

## Introduction

The initial step of biomass thermal conversion involves the primary decomposition of the lignocellulosic matrix that is composed of three interconnected polymeric materials: cellulose, hemicellulose, and lignin. Pyrolysis mechanisms typically include a superposition of the kinetic mechanisms for the individual components of the biomass material. The validity and development of these mechanisms is currently of interest [1-3]. A graphical summary of two global biomass pyrolysis models [1,3] at the experimental conditions of this study is presented in Figure 1.

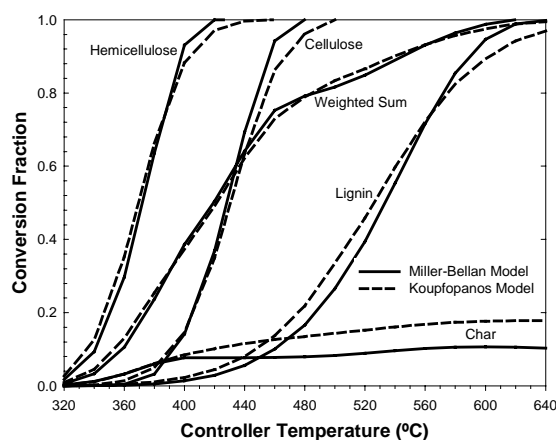


**Figure 1.** Predictions of the Miller-Bellan (solid) [1] and Koufopoulos et al. (dashed) [3] global biomass pyrolysis models at the LEFR reaction conditions.

## Experimental Methods

A new continuous feed, laminar entrained flow reactor (LEFR) was recently built and characterized [4] for determining biomass pyrolysis kinetics, gasifier tar production rates, and alkali metal release rates. This reactor is capable of heating rates on the order of  $10^3$ - $10^5$  K/s, typical of those found in developing gasifiers and in industrial boilers. This reactor is coupled to a molecular beam sampling mass spectrometer (MBMS) system to follow the chemistry of the gas phase products as they evolve during biomass thermochemical conversion processes.

To quantitatively determine biomass pyrolysis kinetics, it is important to understand in detail the many complex physical and chemical processes that a reacting particle undergoes from beginning to end in the reactor. This was the goal of a previous characterization study of the LEFR [4] in which a combination of measurements and theoretical modeling contributed to the detailed understanding of the operating qualities of the reactor. Computational Fluid Dynamics (CFD) simulations were employed to model particle trajectories and residence times and calculate gas temperature profiles. The CFD models included boundary conditions based on measured quantities (e.g. wall temperatures and gas flow rates) so credible time-temperature profiles for particles could be calculated and used in kinetic models to determine global pyrolysis rates. Temperatures are

referred to herein by the furnace temperature controller setting at which data were collected, however, it is important to realize that under set reactor conditions the particles actually undergo a specific time-temperature history [4,5].

The results of the LEFR characterization study [4] indicate it is possible to maintain kinetic, rather than heat transport control and to minimize particle velocity lag in the reactor with small ( $<50$   $\mu\text{m}$ ) particles. These guidelines were followed during an investigation of global cellulose pyrolysis kinetics [5]. In this paper we build on these initial pyrolysis studies and investigate pine (*pinus radiata*) pyrolysis kinetics, a NIST standard biomass material [6]. The LEFR pyrolysis kinetic measurements for three other NIST standards; sugarcane bagasse, poplar (*populus deltoids*), and wheat straw can be found in the references [7].

## Experimental results

The pine pyrolysis mass spectra contained mass peaks commonly associated with cellulose pyrolysis products [5]. Low temperature lignin products were also identified in the pine pyrolysis mass spectra by large peaks that correspond to the lignin precursors (p-coumaryl alcohol,  $m/z = 150$ ; coniferyl alcohol,  $m/z = 180$ ; synapyl alcohol,  $m/z = 210$ ). Higher molecular weight species with  $m/z = 272$ , and several species above  $m/z = 300$ , were also observed and are associated with lignin decomposition [8].

The pine pyrolysis mass spectra, recorded over a range of temperatures, were analyzed by multivariate analysis to group spectral elements that behave in a similar fashion and to provide a concise and reproducible method for representing a complex and extensive set of mass spectral data. This type of analysis performed on previous batch experimental results suggest that there are three distinct pyrolysis product groups (e.g. Evans and Milne, [8]). Based on the superposition theory for global biomass pyrolysis, distinct pyrolytic product groups should be evident in the primary pyrolysis products as suggested by Figure 1.

Multivariate analysis revealed four principal components that described most of the variance ( $\sim 95\%$ ) in the pine pyrolysis mass spectra. Often, a challenge with multivariate analysis techniques is assigning physical and chemical significance to the statistical relationships that are resolved. Associating the peaks identified in the reconstructed Factor Spectra, shown in Figure 1, from the pine pyrolysis mass spectral data can help to interpret the chemical nature of the four principal components.

The Primary Lignin component spectra includes all the mass peaks above  $m/z = 150$ . Most of these masses correspond to the products associated with primary lignin pyrolysis products. However, lower molecular weight species are also included in this component suggesting that pyrolysis products from other lignocellulosic constituents may be grouped in the Primary Lignin factor as well. Peaks at  $m/z = 73$ , 85, and 114 are prominent in the Primary Lignin factor spectra and the bulk of the variance of  $m/z = 144$  is attributed to this factor. These lower molecular weight peaks are generally assigned to polysaccharide pyrolysis products. Therefore, while this factor is named "Primary Lignin," the contribution from pyrolysis products of other lignocellulosic components is not completely separated.

The most dominant peak in the Tertiary factor at  $m/z = 28$  is assigned to  $\text{CO}^+$  but may have minor contributions from  $\text{N}_2^+$  and  $\text{C}_2\text{H}_4^+$ . The peak at  $m/z = 26$  is assigned to acetylene ( $\text{C}_2\text{H}_2^+$ ). Methane is a commonly recognized biomass pyrolysis product and is assigned to the peak at  $m/z = 16$ . Benzene and naphthalene are assigned to the peaks at  $m/z = 78$  and  $m/z = 128$ , respectively. These aromatic hydrocarbons are thermally stable and tend to evolve from hydrocarbons under high severity pyrolysis. The peak at  $m/z = 44$  is assigned to  $\text{CO}_2^+$  but could involve contributions from  $\text{C}_3\text{H}_8^+$ , and

$C_2H_4O^+$  as acetaldehyde or ethenol. Minor peaks at  $m/z = 92$  and  $94$  in all Tertiary factor spectra are assigned to toluene ( $C_7H_8^+$ ) and phenol,  $C_6H_6O^+$ . The identified products in the Tertiary factor are all considered tertiary biomass pyrolysis products [8]. The factor score plots (see Figure 3) show that scores of the Tertiary factor are low at low reaction temperatures, but increase with increasing pyrolysis severity, as is expected with the tertiary products.

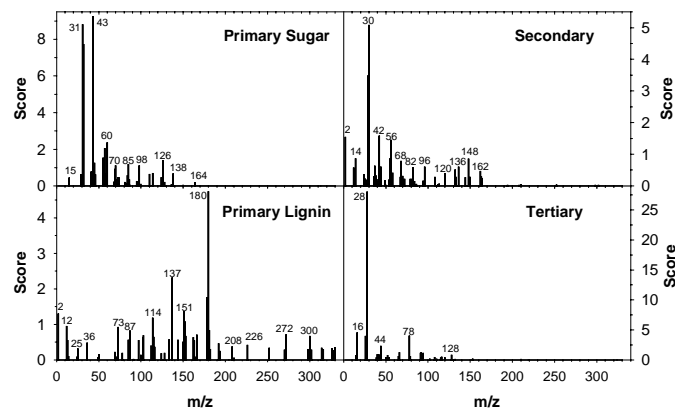


**Figure 2.** Factor spectra from the pine pyrolysis experiments based on the four-component analysis of the LEFR mass spectral data.

The Primary Sugar factor contains intense peaks at  $m/z = 32$  and  $31$  assigned to methanol ( $CH_4O^+$  and  $CH_3O^+$ ). Electron impact or thermal fragments of levoglucosan ( $C_6H_{10}O_5$ ) are assigned to peaks at  $m/z = 57$ ,  $60$ ,  $73$ , and  $98$ . The peak at  $m/z = 126$  is assigned to 5-(hydroxymethyl)-2-furfural, a common polysaccharide pyrolysis product. Other products may also contribute to the signal at  $m/z = 126$ . As discussed above, some of the lower molecular weight peaks associated with the Primary Lignin factor are also common to the Primary Sugar factor.

The Secondary factor contains prominent peaks at  $m/z = 30$  (formaldehyde),  $m/z = 42$  (ketene),  $m/z = 56$  (butene or 2-propenal),  $m/z = 68$  (furan),  $m/z = 82$  (2-methylfuran), and  $m/z = 96$  (furfural). A variety of phenolic compounds can be associated with peaks at  $m/z = 94$ ,  $108$ ,  $120$ ,  $122$ , and  $148$ . Levoglucosan has a molecular weight of  $162$  and it is tempting to assign the observed peak to the parent ion, however, it may likely result from a higher molecular weight phenolic compound. These compounds are generally identified as secondary products that form by the gas phase decomposition of larger primary pyrolysis products [8].

### Discussion and Conclusions

Factor scores determined from the pyrolysis mass spectra recorded for each of the four NIST biomass samples can be found elsewhere [7]. The variation of the average factor scores as a function of furnace controller temperature for pine pyrolysis is plotted in Figure 3. The Primary Lignin scores are highest at the lowest temperatures ( $\sim 340^\circ\text{C}$ ), which suggests that the measured relative contribution of lignin is highest at the earliest stages of pyrolysis. The model predictions for lignin pyrolysis indicate that lignin does not start reacting until the controller temperatures are set to  $400^\circ\text{C}$ . At furnace controller temperatures of  $500^\circ\text{C}$  -  $520^\circ\text{C}$ , the models predict 50% lignin conversion. Clearly, the models predict that lignin reacts much slower than is suggested by the LEFR data. These discrepancies are not completely surprising, as testing of these models with data at high heating rates has been minimal.

It is more difficult to comment on the model predictions of polysaccharide pyrolysis because the multivariate analysis of the pine mass spectral data does not clearly resolve separate contributions

from hemicellulose and cellulose pyrolysis. The pyrolysis models are a good representation of the pyrolysis regime studied in the LEFR experiments if the hemicellulose and cellulose fractions are combined into a single component in the models that gives rise to "primary sugars" as measured in the experiments.

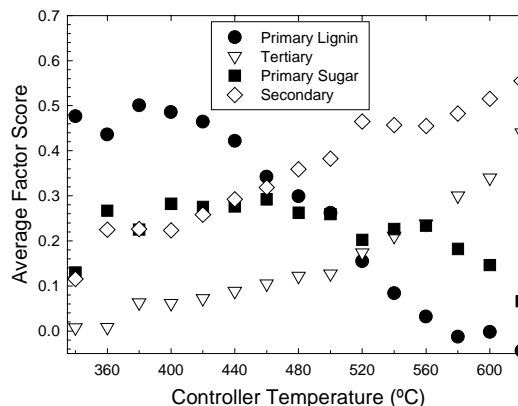


**Figure 3.** Factor scores from the pine pyrolysis experiments based on the four-component analysis of the LEFR mass spectral data.

If in fact hemicellulose and cellulose react as predicted by the two global biomass pyrolysis models, there should be distinctive pyrolysis regimes where hemicellulose contributes to the polysaccharide signals at the lowest temperatures and the cellulose pyrolysis products begin to form at higher temperatures. The models predict that 50% of the hemicellulose should have reacted as the cellulose begins to react ( $360^\circ\text{C}$  -  $380^\circ\text{C}$  in the models). The multivariate analysis of the pyrolysis mass spectral data did not clearly suggest a statistically important distinction between these two components. It is not clear from the experiments whether this is because hemicellulose and cellulose do not react in separate regimes, or because the pyrolysis products are so similar there is no mass spectral difference between early and late polysaccharide pyrolysis products. The peaks associated with polysaccharide pyrolysis products that were resolved in the Primary Lignin factor could be indicative of a cellulose/hemicellulose distinction. More detailed information is necessary before this can be confidently determined.

### References

1. Miller, R.S.; and Bellan, J. *Combust. Sci. Tech.* **1997** *126*, 97-137.
2. Di Blasi, C.; and Russo, G. In *Advances in Thermochemical Biomass Conversion vol. 2* A.V. Bridgwater, Ed., Blackie Academic and Professional: New York 1994; pp. 906-921.
3. Koufopoulos, C.A.; Maschio, G.; and Lucchesi, A. *Can. J. Chem. Eng.* **1989** *67*, 75-84.
4. Brown, A.L.; Dayton, D.C.; Nimlos, M.; and Daily, J.W. *Energy Fuels* **2001** *15*, 1276-1285.
5. Brown, A.L.; Dayton, D.C.; and Daily, J.W. *Energy Fuels* **2001** *15*, 1286-1294.
6. Milne, T.A.; Chum, H.L.; Agblevor, F.; and Johnson, D.K. *Biomass Bioenergy* **1992** *2(1-6)*, 341-366.
7. Brown, A.L. 2001. A Chemical and Kinetic Study of Cellulose and Biomass Pyrolysis at High Heating Rates. Ph.D. Dissertation, University of Colorado at Boulder.
8. Evans, R.J.; and Milne, T.A. *Energy Fuels* **1987** *1*, 123-137.

## BIOREFINERY CONCEPT DEVELOPMENT BASED ON WHEAT FLOUR MILLING

Douglas C. Elliott<sup>a</sup>, Rick J. Orth<sup>a</sup>, Johnway Gao<sup>a</sup>, Todd A. Werpy<sup>a</sup>, David E. Eakin<sup>a</sup>, Andrew J. Schmidt<sup>a</sup>, Gary G. Neuenschwander<sup>a</sup>, Anthony J. Flagg<sup>b</sup>, Jim Murry<sup>b</sup>, Lyle Lahman<sup>c</sup>, C.J. Lin<sup>c</sup>, Donald L. Mennel<sup>c</sup>, Ron Landucci<sup>d</sup>

<sup>a</sup>Pacific Northwest National Laboratory, P.O. Box 999, Richland, Washington, USA 99352

<sup>b</sup>Pendleton Flour Mills, LLC., P.O. Box 1427, Pendleton, Oregon, USA 97801

<sup>c</sup>The Mennel Milling Company, P.O. Box 806, Fostoria, Ohio, USA 44830-0806

<sup>d</sup>ProForma Systems, Inc., 13902 W. 20<sup>th</sup> Place, Golden, Colorado, USA 80401-2193

### Introduction

Wheat is the second largest agricultural commodity in the United States, with a net production of 56.1 million tonnes in 1995 (2.1 billion bushels). About half is exported, and, of the balance, 85% is dry-milled within the U.S. to produce 17.8 million tonnes of flour. The remaining 5.9 million tonnes consist of low-value byproducts, which are mostly disposed as animal feed. These byproducts, collectively referred to as millfeed, are made up of the bran, the germ, and a portion of the endosperm, which also contains a significant amount of starch not recovered in the milling process. A rough calculation suggests that millfeed is composed of up to 35% starch that originated from the endosperm.

Millfeed is not a single homogeneous stream but a collection of several streams from the process of making flour. It contains about 75% carbohydrate, 17% protein, 3% fat, and 5% mineral matter, but its composition varies, depending on the variety of wheat being processed. Millfeed production also varies slightly, depending on mill operation and variety of wheat. Flour extraction ranges from 73 to 77%; thus, the average amount of millfeed generated is about 25% by weight of the wheat introduced to the mill.

The process described in this paper is being developed to recover the starch-rich product from millfeed; process it to glucose; and convert the glucose into a commodity product, such as polyol or lactic acid. Processing the glucose from the extracted starch for polyol production is based on catalytic hydrogenation to sorbitol. Lactic acid production is based on fermentation of the millfeed-derived glucose.

In either pathway (catalytic or fermentation) to value-added products, the residual millfeed will also be an important consideration. By extracting the starch from the millfeed, the quality of the remaining material as animal feed may actually be increased by concentrating the protein content. The improved value of this starch-extracted millfeed has undergone preliminary evaluation, but needs to be validated in animal feeding tests.

### Experimental

**Glucose Production from Wheat Millfeed.** Bench-scale testing was conducted to optimize the process and provide the foundation for a process to effectively recover the starch and convert it to glucose. The process optimization testing incorporated a systematic approach of evaluating each key processing step in the order that it appears in the process; **Figure 1** illustrates those steps. The millfeed used for these tests was a soft white winter wheat all inclusive without screenings. Once the individual unit operations were tested separately, the optimized conditions were tested together to arrive at an integrated starch extraction process.

A specified amount of water was added to a 250-mL flask, and then placed in an incubator (and constantly shaken) for heat-up to a predetermined temperature. Millfeed was then added to the 250-mL flask, and it was placed back into the incubator for a predetermined time (**initial water wash**). The millfeed slurry was then removed from the incubator and **coarse filtered** via vacuum filtration for 10 min through a 4-in. Buchner filter (no filter paper used). The filtercake from the coarse filtration was dried and retained for analyses. The filtrate was collected, pH-adjusted if necessary, and placed back into the incubator for heat-up to a predetermined **liquefaction** temperature. After reaching, the specified liquefaction temperature,  $\alpha$ -amylase was added, and liquefaction was initiated.

Following the liquefaction step, the incubator temperature was adjusted to a predetermined **saccharification** temperature, and pH adjustments were made if necessary. After the desired saccharification temperature was reached, glucoamylase was added to the solution, and it was placed in the incubator for a specified saccharification time.

Following a specified time, the product from saccharification was removed, and again filtered. This second filtering operation, termed fine filtration, was conducted via vacuum filtration for 10 min, using a 4-in. Buchner funnel with Whatman #4 filter paper. Following fine filtration, the filtercake was dried and retained for analyses. The filtrate from the fine filtration step was also collected for analyses.

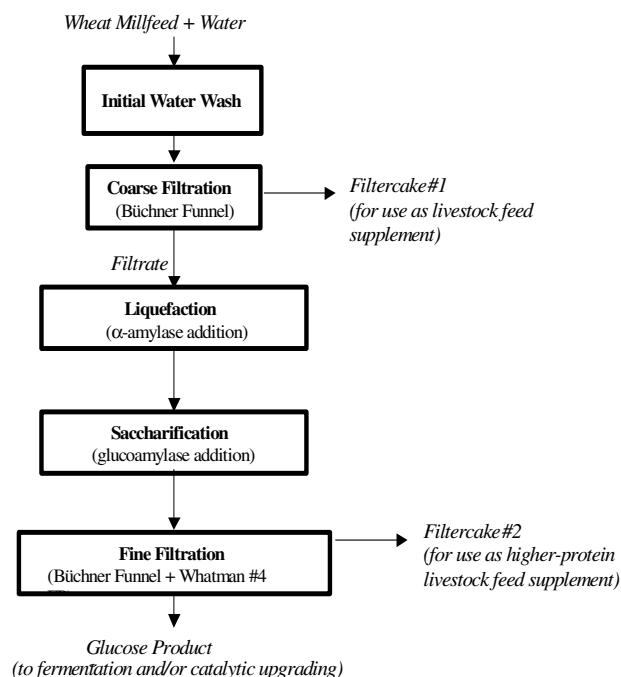


**Figure 1.** Starch Extraction Key Processing Steps

**Fermentation Development Process.** Batch and semi-batch modes were used for the lactic acid fermentation tests. In all the tests, bacterial strains of *Lactobacillus* species were selected for developing the lactic acid fermentation process. Pre-test results showed the fungal strain *Rhizopus oryzae* was unable to produce a substantial amount of lactic acid in the culture medium containing the wheat millfeed hydrolysate. However, *Lactobacillus* species were able to produce a large amount of lactic acid in the hydrolysate medium.

Fermentation media containing either reagent glucose or wheat millfeed hydrolysate were prepared. The pH of each medium was adjusted to 6.5 to 6.8 using 1 N KOH. Aliquots of 50-mL

fermentation medium were dispensed into 125-mL serum bottles, which were capped with Teflon-lined rubber septa and then wrapped with two layers of aluminum foil. After being autoclaved at 121°C for 15 min and cooled down to room temperature, each bottle was supplemented with 2 to 3 g of calcium carbonate powder, which was sterilized by baking in an oven at 121°C for at least 3 hr. The amount of added calcium carbonate depended on the glucose concentration in the hydrolysate. The medium bottles were capped with sterile septa and aluminum seals using a hand crimper, and the headspace of each bottle was purged with deoxygenated nitrogen for 5 to 10 min through a 0.2- $\mu$ m sterile filter (VWR Scientific). The ready bottles with fermentation medium were then inoculated with mature seed culture and subsequently incubated in an orbital shaker at 140 rpm. The fermentation temperature was controlled at 40°C to 45°C, depending on the testing conditions.

**Catalytic Process Development.** Glucose hydrogenation to sorbitol was chosen as the catalytic processing test case for the wheat millfeed-derived glucose. The reactor was a stirred batch reactor made of 316 stainless steel. The reactor volume was typically 300 mL with the vessel filled half full of aqueous sugar solution. The catalyst was a ruthenium on titania (rutile form) extrudate ground to powder (5 g per 150 g of feed solution). The processing conditions were 100°C and 1500 psig with hydrogen atmosphere. The slurry of feed solution and catalyst particles was stirred to maximize hydrogen contact. The reaction was allowed to proceed for 6 hr, typically, with multiple samples of product solution withdrawn throughout the reaction period. The product solutions were analyzed by liquid chromatography to determine primarily the glucose and sorbitol concentrations, but also to monitor for byproducts. The vented gas product at the end of the test was analyzed by gas chromatography to determine other byproducts (hydrocarbons or carbon oxides).

## Results and Discussion

**Glucose Production from Wheat Millfeed.** A baseline starch extraction process was developed that consists of hot water extraction of starch and filtration of fibrous animal coproduct, followed by enzymatic liquefaction and saccharification of the extracted starch with filtration of a high-protein and a lower-protein coproduct. With this process, a glucose yield of approximately 20% on a dry millfeed basis was achieved. Improvements to the baseline process, including thorough filtercake rinsing and countercurrent extraction, yielded nearly 30% glucose on a dry millfeed basis, corresponding to recovery of essentially all of the glucose value in the millfeed. Following bench-scale testing, pilot-scale testing was conducted, in which approximately 150 lb of wheat millfeed were processed. The glucose yields obtained in the pilot-scale testing were comparable to those obtained during the bench-scale testing; however, filtration was more difficult. The residual fibrous material from the pilot-scale testing was evaluated as animal feed, and the glucose-containing hydrolysate was evaluated as a feedstock for catalytic upgrading (with and without upstream separations) and fermentation.

**Fermentation Development Process.** Wheat millfeed hydrolysate was used as the primary carbon source for the lactic acid fermentation process development. Batch cultures of lactic acid fermentation were used to assess the feasibility of the fermentation process development. Three lactic acid producing strains [purchased from American Type Culture Collection (ATCC), Manassas, Virginia] were tested: *Lactobacillus rhamnosus* (ATCC 10863), *Lactobacillus delbrueckii subsp. lactis* (ATCC 12315), and *Lactobacillus rhamnosus* (ATCC 11443). All strains showed favorable lactic acid production rates at the temperature of 43°C.

Based on a mineral analysis, manganese was the only critical element lacking in the hydrolysate medium. Without the addition of

manganese, the fermentation batch culture could result in lower lactic acid yield. Under the testing conditions, the hydrolysate medium with only minimal manganese addition performed better than the culture medium containing reagent-grade glucose and other nutrients such as yeast extract and peptone. The superior performance of the hydrolysate medium is probably due to the presence of various amino acids and other nutrients.

**Catalytic Process Development.** Three versions of the wheat millfeed-derived glucose solution were used for the testing: the hydrolysis filter press product, the ultrafiltration permeate derived from the filter press product, and the nanofiltration concentrate from the ultrafiltration permeate. Results showed that further cleanup of the wheat millfeed-derived glucose stream was required before it could be used as feedstock for catalytic processing. Therefore, the ultrafiltration permeate was treated in an activated carbon bed prior to the hydrogenation to sorbitol step in order to avoid catalyst inhibition. Nanofiltration (reverse osmosis) was also demonstrated as a means to concentrate the ultrafiltration permeate prior to carbon treatment and catalytic processing.

**Support of Commercialization Efforts.** Under a contract from Pendleton Flour Mills, LCC, the process economic model was developed by ProForma Systems, Inc., with input from Pacific Northwest National Laboratory. The model development included material and energy balances built into a virtual process simulator based on Excel™ and Visual Basic™. Equipment sizing and costing calculations were dynamic in nature and adjusted with changes in the mass balance. Capital investment costs and operating costs were also estimated. Using the model, sensitivity analyses could be undertaken as well as comparisons with other technology options.

The model was used to cost a midwest green field site processing a moderate 227,273 tonne per year of millfeed. The yield of glucose was 68,182 tonne per year with 149,091 tonne per year of animal feed and 17,727 tonne per year of high-protein feed supplement. The plant capital cost estimate was \$34 million. Using a range of values for the byproducts, the range of costs and prices for the millfeed-derived glucose product was determined. These costs and prices range around the current costs and prices for corn-derived glucose. The corn costs and prices are based on a much larger (typical) corn wet mill producing 1,081,818 tonne per year of glucose. Capital cost at the different scales of operation is the major differentiating factor between the two glucose sources. According to the model, using a \$70/ton for millfeed, the glucose from wheat millfeed would cost 8.1 cents per pound.

## Acknowledgment

This development effort was conducted under a Cooperative Research and Development Agreement (CRADA) among Pacific Northwest National Laboratory; the U.S. Department of Energy; The Mennel Milling Company; and Pendleton Flour Mills, LLC. Pacific Northwest National Laboratory is operated by Battelle for the U.S. Department of Energy under Contract DE-AC06-76RL01830.

# CATALYST DEVELOPMENT FOR THE CELLULOSE GASIFICATION AND OPTIMIZATION OF THE OPERATION VARIABLES

Mohammad Asadullah, Shin-ichi Ito, Kimio Kunimori, and Keiichi Tomishige

Institute of Materials Science, University of Tsukuba, 1-1-1, Tennodai, Tsukuba-shi, Ibaraki 305-8573, Japan

## Introduction

Biomass gasification to synthesis gas is the most promising approach to share renewable energy, compared with its use as a combustion fuel. This is because the synthesis gas can be converted to clean liquid fuels or to many important bulk chemicals such as methanol, acetic acid, dimethyl ether, oxo alcohols, etc.<sup>1,2</sup> Synthetic diesel and dimethyl ether, which are promising superclean fuels in the future, can be produced with high efficiency from the synthesis gas and contribute significantly to the reduction of the net CO<sub>2</sub> emission into the atmosphere.<sup>3</sup> Furthermore, the use of renewable energy resources, agricultural and forestall biomass, would decrease the petroleum dependence of many countries. However, the biomass gasification remains problematic because of the formation of tar, a complex mixture of aromatics, during the gasification of biomass even if the process is operated at very high temperatures.<sup>4,6</sup> Although the high gasification temperature decreases the tar formation, the process is unsuitable because of high energy consumption, causing high production costs of the synthesis gas. From the economic point of view, the process should be operated at low temperature, which allows a significant savings of energy, resulting the decrease of the production costs. However, the formation of tar and char is more severe at temperatures lower than 1023 K.<sup>7</sup> The use of an efficient catalyst in the gasification reactor can solve the tar and char formation problem by cracking them to gases even at low temperature. However, some reports have demonstrated that the use of nickel based catalyst in the primary reactor unit resulted in rapid deactivation of catalyst because of carbon deposition on catalyst surface.<sup>8</sup> This challenge can be overcome by developing a suitable catalyst, which can completely convert the carbonaceous materials without the formation of any residue. We already have reported such a catalyst (Rh/CeO<sub>2</sub>), which is efficient for complete gasification of cellulose at low temperature (823 K).<sup>9</sup> This paper describes the performance of Rh catalysts on various supports, details of operating variables, and the catalyst characterization.

## Experimental

**Procedure.** The general operating system has been described in a previous paper.<sup>9</sup> However, the dependence of operating conditions was investigated here. The amounts of cellulose feedings were varied from 25 to 150 mg in a batch. In each case, 0.5 g of catalyst was used. The total flow rate of air and Ar was varied from 110 to 200 cm<sup>3</sup> min<sup>-1</sup> (STP) ( $W/F = 1 - 1.8$  g.h/mol, where  $W$  = weight of the catalyst in grams and  $F$  = flow rate of the inlet gas in moles per hour) where their ratio was always maintained at 1.2. The reactions were carried out between 723 and 873 K. Temperature difference between outside of the reactor wall and inside of the catalyst bed and also between the bottom of the distributor and the center of the catalyst bed was continuously monitored by thermocouples. Product gases in the sampling gas were calculated as concentration such as, (amount of product gas / total amount in the effluent gas) x 100.

**Catalyst.** Catalysts used in this process were Rh, Ru, Pt, Pd, and Ni loaded on CeO<sub>2</sub> and Rh loaded on various supports prepared in our

laboratory by a conventional impregnation method using an acetone solution of metal acetylacetonate such as Rh(C<sub>5</sub>H<sub>7</sub>O<sub>2</sub>)<sub>3</sub>, Ru(C<sub>5</sub>H<sub>7</sub>O<sub>2</sub>)<sub>3</sub>, Pt(C<sub>5</sub>H<sub>7</sub>O<sub>2</sub>)<sub>2</sub>, Pd(C<sub>5</sub>H<sub>7</sub>O<sub>2</sub>)<sub>2</sub>, and Ni(C<sub>5</sub>H<sub>7</sub>O<sub>2</sub>)<sub>2</sub>. All of the acetylacetonate salts with purity higher than 99% were purchased from Soekawa Chemicals. CeO<sub>2</sub> was purchased from Daiichi Kigenso Kagaku. In each case, the solution was added into the CeO<sub>2</sub> powder and stirred properly. Then the mixture was kept undisturbed for an hour. The acetone solvent was then evaporated with stirring at around 323 K, and the catalysts thus prepared were dried at around 393 K overnight. The metal loading for all catalysts was 1.2 x 10<sup>-4</sup> mol (g of catalyst)<sup>-1</sup>. In the case of the Rh/CeO<sub>2</sub> catalyst, the catalysts with 0.4 x 10<sup>-4</sup>, 0.8 x 10<sup>-4</sup>, 1.6 x 10<sup>-4</sup>, and 2.5 x 10<sup>-4</sup> mol (g of catalyst)<sup>-1</sup> were also prepared. Granules of the catalysts (60-100 mesh) were obtained by pressing, crushing, and sieving. The catalysts were pretreated before each run at 773 K under the flow of H<sub>2</sub> of 40 cm<sup>3</sup> min<sup>-1</sup> for 0.5 h. The Brunauer-Emmett-Teller (BET) surface areas of fresh (after H<sub>2</sub> treatment) and used Rh/CeO<sub>2</sub> catalysts were determined by a Gemini (Micrometrics).

## Results and Discussion

We have previously investigated various types of support materials and supported metal catalysts for cellulose gasification in a batch-feeding and fluidized-bed reactor at 823 K (Table 1).<sup>9</sup> In this paper we also investigated the performance of Rh catalyst on various supports and the results are included in Table 1. In the noncatalytic reaction the C conversion was only 53% which was remarkably increased by the presence of CeO<sub>2</sub>, ZrO<sub>2</sub>, TiO<sub>2</sub>, or MgO support materials on the bed. However, the synthesis gas formation increased only by the presence of CeO<sub>2</sub>. Because CeO<sub>2</sub> has shown the performance for cellulose gasification on the basis of the C conversion as well as the formation of synthesis gas, we prepared CeO<sub>2</sub>-supported various types of metal catalysts and tested them in the gasification reaction. As shown in Table 1 only Rh/CeO<sub>2</sub> promoted the C conversion as well as the formation of CO and H<sub>2</sub> drastically. Interestingly enough, complete C conversion was achieved when Rh/CeO<sub>2</sub> was used as a catalyst. The loading of Rh on other supports caused lower C conversion and higher methane formation that ultimately decreased the amounts of CO and H<sub>2</sub>. The promoting effect of metals supported on CeO<sub>2</sub> is as follows: Rh >> Ru > Pt ≈ Pd > Ni.

It is a fact that the temperature of the catalyst bed greatly affects the cellulose gasification. In this work the influence of temperature on the C conversion and product distribution has been evaluated in the interval of 723-873 K and is shown in Figure 1. As expected, the C conversion increased with increasing reaction temperature, and became 100% at 823 K. At or above this temperature, the product gas analysis revealed that the total C in cellulose converted to gas. At lower temperatures than 823 K, some of the tar and/or char did not take part in either the combustion or the reforming reaction. On the other hand, the gas composition was greatly varied with increasing temperature. The amounts of H<sub>2</sub> and CO increased remarkably, however, the amount of CH<sub>4</sub> increased slightly with increasing temperature. Furthermore, the amount of CO<sub>2</sub> expectedly decreased with increasing temperature.

The variation of the C conversion and product distribution with the cellulose feeding amount in a batch is shown in Figure 2. It can be seen that 100% C conversion was achieved until 50 mg of cellulose was used in a batch. A higher amount of cellulose than 50 mg caused a decrease of C conversion. Although the CO<sub>2</sub> formation slightly increased when 150 mg of cellulose was used, the formation of CO and H<sub>2</sub> decreased.

**Table 1. Effects of Various Supports and Supported Metal Catalysts on the Gasification of Cellulose<sup>a</sup>**

Catalyst	Yield of gases / $\mu\text{mol}$				$\text{H}_2/\text{CO}$	C to gas wt%
	CO	$\text{H}_2$	$\text{CO}_2$	$\text{CH}_4$		
None	160	90	790	30	0.6	53
$\text{CeO}_2$	330	630	860	120	1.9	71
$\text{MgO}$	260	430	960	60	1.7	70
$\text{TiO}_2$	240	560	1040	40	2.3	71
$\text{ZrO}_2$	180	490	1020	110	2.7	71
$\text{Al}_2\text{O}_3$	200	480	720	60	2.4	53
$\text{SiO}_2$	220	230	680	60	1.0	52
$\text{Rh}/\text{CeO}_2$	670	1290	1060	120	1.9	100
$\text{Ru}/\text{CeO}_2$	490	1010	1050	130	2.1	91
$\text{Pd}/\text{CeO}_2$	360	830	1180	70	2.3	87
$\text{Pt}/\text{CeO}_2$	360	850	1080	120	2.3	85
$\text{Ni}/\text{CeO}_2$	280	740	1150	50	2.6	80
G-91 <sup>b</sup>	450	760	990	180	1.7	87
$\text{Rh}/\text{CeO}_2^c$	370	920	1160	300	2.5	100
$\text{Rh}/\text{ZrO}_2$	450	680	1150	250	1.5	98
$\text{Rh}/\text{Al}_2\text{O}_3$	340	660	1210	260	1.9	98
$\text{Rh}/\text{TiO}_2$	220	800	960	370	3.6	84
$\text{Rh}/\text{MgO}$	360	820	1010	170	2.3	83
$\text{Rh}/\text{SiO}_2$	400	720	698	160	1.8	68

<sup>a</sup>50 mg cellulose (C, 1850  $\mu\text{mol}$ ;  $\text{H}_2$ , 1543  $\mu\text{mol}$  and  $\text{O}_2$ , 772  $\mu\text{mol}$ ). <sup>b</sup>Commercial steam reforming catalyst: Ni, 14%;  $\text{Al}_2\text{O}_3$ , 65-70%; CaO, 10-14% and  $\text{K}_2\text{O}$ , 1.4-1.8%. <sup>c</sup>Catalyst was placed in a secondary bed.

**Table 2. Effect of W/F on the Carbon Conversion and Product Distribution<sup>a</sup>**

W/F	$\text{O}_2$ supply	Yield of gases / $\mu\text{mol}$				C to gas %
		CO	$\text{H}_2$	$\text{CO}_2$	$\text{CH}_4$	
$\text{g h mol}^{-1}$	within 50 s/ $\mu\text{mol}$					
1	696	1534	2930	2523	268	78
1.2	578	1595	3101	2605	304	81
1.4	496	1398	2880	2534	204	75
1.8	409	1044	2226	2149	154	61

<sup>a</sup> Cellulose 150 mg (C, 5555  $\mu\text{mol}$ ;  $\text{H}_2$ , 4629  $\mu\text{mol}$  and O, 4629  $\mu\text{mol}$ ).

The influence of W/F on the C conversion and product distribution has been studied at 823 K using 150 mg of cellulose, and the results are summarized in Table 2. An increase of W/F caused the variation of two factors in this system: an increase of the residence time and a decrease of oxygen supply. The highest C conversion (81%) and product yield were achieved in the case of W/F = 1.2  $\text{g h mol}^{-1}$ .

Figure 3 shows the performance of the  $\text{Rh}/\text{CeO}_2$  catalyst with various loading amounts for the gasification of 50 mg of cellulose in a

batch at 823 K. The C conversion and synthesis gas yield dramatically increased with an increase in the loading amount and reached 100% C conversion when the Rh loading of  $1.2 \times 10^{-4}$  mol (g of catalyst)<sup>-1</sup> was used. However, it is contrary to the fact that the higher loading amount of Rh than  $1.2 \times 10^{-4}$  mol (g of catalyst)<sup>-1</sup> decreased the C conversion. On the other hand, the formation of  $\text{CH}_4$  increased with an increasing in the Rh loading, which ultimately decreased the yield of synthesis gas. Ceria alone also gave the higher amount of methane. Actually, ceria is an effective catalyst for CO hydrogenation giving mainly  $\text{C}_1$ - $\text{C}_5$  hydrocarbons.<sup>10,11</sup> In fact  $\text{Ce}^{3+}$ , which is generated under reducing atmosphere has been recognized as an active site for CO hydrogenation reaction.<sup>12</sup>

**Table 3. BET surface area of  $\text{Rh}/\text{CeO}_2$  catalyst**

No. of batch reaction	BET surface area/ $\text{m}^2 \text{g}^{-1}$
0	59
1	24
5	24
10	23
20	21

Table 3 shows the BET surface area of  $\text{Rh}/\text{CeO}_2$  of both fresh and used catalysts. This value was  $59 \text{ m}^2 \text{g}^{-1}$  before reaction, however, it was decreased drastically to  $24 \text{ m}^2 \text{g}^{-1}$  during the first batch of cellulose gasification reaction. However, fortunately the decreasing trend of surface area was very slow and it was almost constant in successive reactions. The catalytic activity did not change significantly even after 20 times of batch feeding of cellulose.

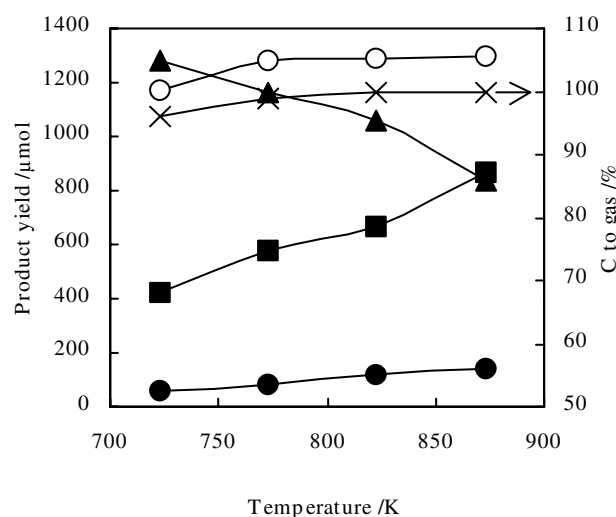


**Figure 1.** Effect of temperature on the  $\text{Rh}/\text{CeO}_2$  (0.5 g) catalyzed gasification of cellulose (50 mg; C, 1850  $\mu\text{mol}$ ;  $\text{H}_2$ , 1543  $\mu\text{mol}$  and  $\text{O}_2$ , 772  $\mu\text{mol}$ ) with air ( $60 \text{ cm}^3 \text{ min}^{-1}$ ). ■ : CO, O:  $\text{H}_2$ , ●:  $\text{CH}_4$ , ▲:  $\text{CO}_2$  and X : C-conversion.

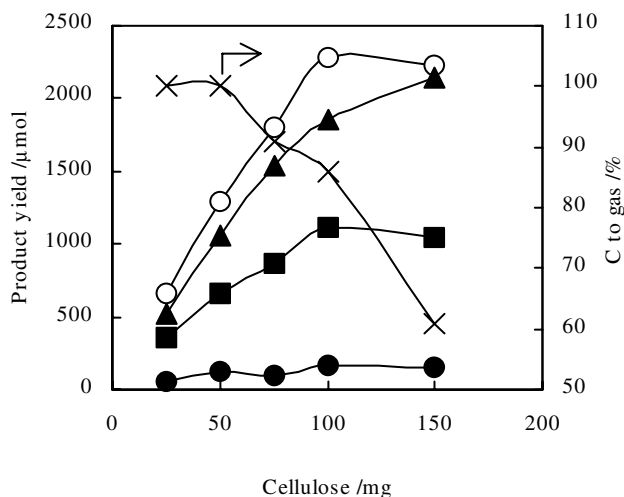


**Figure 2.** Effect of cellulose feeding amount in a batch on the C conversion and product distribution at 823 K. ■ : CO, O: H<sub>2</sub>, ●: CH<sub>4</sub>, ▲: CO<sub>2</sub> and X, C conversion.

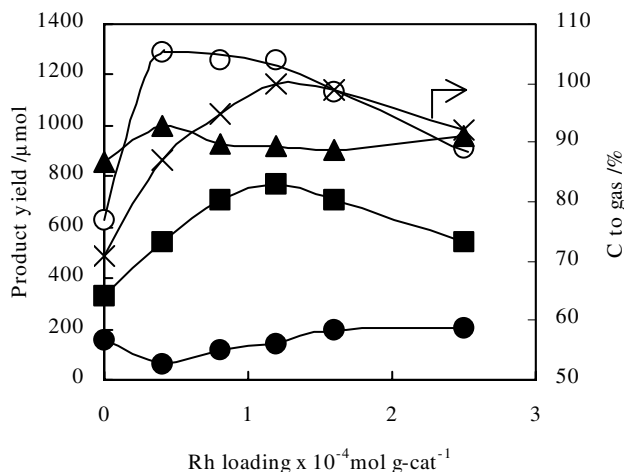


**Figure 3.** Effect of the amount of metal loading on the C-conversion and product distribution. ■ : CO, O: H<sub>2</sub>, ●: CH<sub>4</sub>, ▲: CO<sub>2</sub> and X : C-conversion.

### Conclusions

Rh supported on CeO<sub>2</sub> only exhibited multifunction in this reaction such as increasing the C conversion as well as CO and H<sub>2</sub> formation. On the other hand, the formation of methane was inhibited on the catalyst. Total carbon conversion was achieved at temperatures above 823 K when up to 50 mg cellulose was used in a batch on Rh/CeO<sub>2</sub> catalyst of Rh loading  $1.2 \times 10^{-4}$  mol (g of catalyst)<sup>-1</sup>. Although the surface area decreased suddenly in the first reaction, it was almost constant in the successive reactions and the reactivity remained constant.

### Acknowledgement

This research was supported by the Future Program of Japan Society for the Promotion of Sciences under the Project "Synthesis of Ecological High Quality of Transportation Fuels" (JSPS-RFTF98P01001).

### References

1. Tanaka, Y.; Yamaguchi, T.; Yamasaki, K.; Ueno, A.; Kotera, Y. *Ind. Eng. Chem. Res.* **1984**, *23*, 225.
2. Beaker, E. G.; Mitchell, D. H.; Mudge, L. K.; Brown, M. D. *Energy Progress* **1983**, *3*, 226.
3. Shikada, T.; Ohno, Y.; Ono, M.; Mizuguchi, M.; Tomura, K.; Fujimoto, K. *Stud. Surf. Sci. Catal.* **1998**, *119*, 515.
4. Caballero, M. A.; Corella, J.; Aznar, M. P.; Gil, J. *Ind. Eng. Chem. Res.* **2000**, *39*, 1143.
5. Miccio, F.; Moersch, O.; Spliethoff, H.; Hein, K.R.G. *Fuel* **1999**, *78*, 1473.
6. Brage, C.; Yu, Q.; Chen, G.; Sjöström, K. *Biomass Bioenergy* **2000**, *18*, 87.
7. Bangala, D. N.; Abatzoglou, N.; Martin, J.-P.; Chornet, E. *Ind. Eng. Chem. Res.* **1997**, *36*, 4184.
8. Baker, E. G.; Mudge, L. K.; Brown, M. D. *Ind. Eng. Chem. Res.* **1987**, *26*, 1335.
9. Asadullah, M.; Tomishige, K.; Fujimoto, K. *Catal. Commun.* **2001**, *2*, 63.
10. Maruya, K.; Inaba, A.; Maehashi, T.; Domen, K.; Onishi, T. *J. Chem. Soc., Chem. Commun.* **1985**, 487.
11. Arai, T.; Maruya, K.; Domen, K.; Onishi, T. *Bull. Chem. Soc. Jpn.* **1989**, *62*, 349.
12. Arai, T.; Maruya, K.; Domen, K.; Onishi, T. *J. Catal.* **1993**, *141*, 533.

# THE CATALYTIC EFFECT OF CARBON-SUPPORTED RUTHENIUM ON THE DEPOLYMERIZATION OF HYDROLYTIC LIGNIN

Caroline E. Burgess, David J. Clifford, and Justin R. Horvath

Penn State University, The Energy Institute,  
209 Academic Projects Bldg., University Park, PA 16803

## Introduction

Biomass consists of an assortment of recalcitrant polymers such as cellulose and lignin. Prior to use in gasification streams, these polymers are subjected to degradation/depolymerization reactions for the purpose of liberating smaller, more volatile and reactive species.

It is well known that carbohydrates can be depolymerized in an acid hydrolysis reaction with the depolymerization effectively catalyzed using a carbon-supported ruthenium catalyst (1-5). Under relatively mild conditions, carbon-supported ruthenium can also effectively catalyze the hydrogenation of highly hindered aromatic rings, such as those found in rosin (6, 7). More recently, alumina-supported ruthenium and other forms of ruthenium have been studied as hydrodesulfurization and coal liquefaction catalysts (8-11).

While it is known that ruthenium can catalyze carbohydrate depolymerization, less is understood when reacting whole biomass, as hydrolytic lignin remains and must be separated from the catalyst. Base hydrolysis at 280-320°C has been used to solubilize and react the hydrolytic lignin to phenolic compounds (2, 12). However, little is known about the effect of the ruthenium on the hydrolytic lignin under the base hydrolysis reaction conditions. In this study, the catalytic effect of ruthenium on the degradation of lignin polymers has been explored.

## Experimental

Commercially available hydrolytic lignin was obtained from Aldrich Chemical Co. and used as the starting material. Reagent grade sodium hydroxide and concentrated hydrochloric acid were also obtained from Aldrich. The ruthenium catalyst (5% ruthenium loaded on a carbon support) was obtained from Aldrich.

Reactions were performed with and without ruthenium catalyst. For the latter, the catalyst loading was a 1% metal loading. Tubing reactors (~25 mL) were loaded with 1.5 g of hydrolytic lignin and 10 mL of 10% aqueous sodium hydroxide. The reactors were initially purged with nitrogen to remove air and charged to 4.5 MPa with hydrogen gas. An ebulating sand bath was utilized to obtain temperatures of 280, 300 and 320°C in three experiments, each of which had a residence time of 1 hour.

The reacted materials were processed according to the flow chart shown in Figure 1. Solid and liquid products were separated by filtration. The liquid material was then acidified to a pH of approximately 2.0 and separated into acid-soluble and acid-insoluble fractions. Acid-soluble compounds were then extracted with diethyl ether, which was then evaporated to determine yield. Not all acid soluble compounds were soluble in diethyl ether. The yield of residual acid-solubles and gases were determined by difference.

The ether soluble fraction was analyzed by gas chromatography-mass spectrometry (GC-MS) using a Shimadzu QP-5000 mass spectrometer. The acid-soluble fraction was analyzed using a Chemagnetics M100S solid-state nuclear magnetic resonance (NMR) spectrometer operating at a field strength of 2.4 T and utilizing a spinning speed of 3.5 kHz. The technique of cross polarization with magic angle spinning was employed.

To simplify the discussion, the ether-soluble fraction will be referred to as LMW (low molecular weight), the acid-insoluble as

HMW (high molecular weight), and the residual soluble material following extraction with diethyl ether as AS-LMW (acid-soluble-low molecular weight) materials.

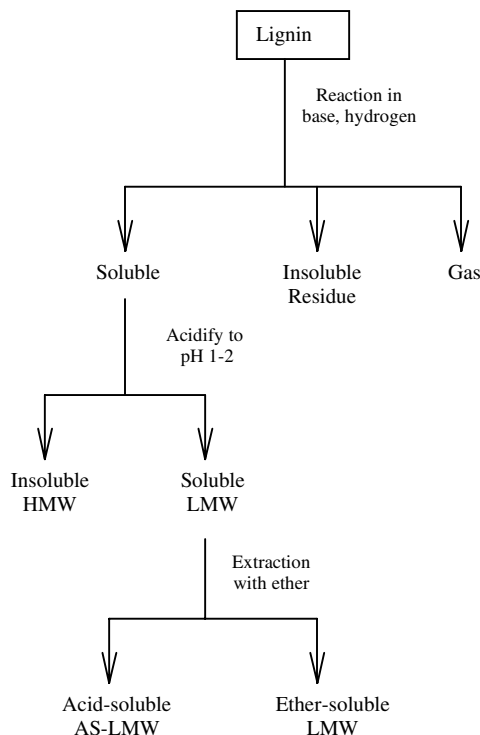


Figure 1: Schematic of procedure to separate products.

## Results and Discussion

**Non-catalytic Reactions.** Table 1 shows the conversions and yields of HMW, LMW and AS-LMW/gas fractions for 280, 300 and 320°C reaction conditions. In each case, conversion to either LMW, HMW, or AS-LMW/gas was nearly complete. Shown in Figure 2 are the GC-MS chromatograms for the LMW fraction and in Figure 4 are solid-state <sup>13</sup>C-NMR spectra for the HMW fraction. Relative yields, which are listed in Table 1, indicate that as the reaction severity increases, the yield of HMW product and LMW product decreases, while the AS-LMW/gas yield increases, particularly at 320°C.

**Table 1. Conversion and Yield Data for Reaction of Hydrolytic Lignin With and Without Ruthenium Catalyst**

Reaction Temp (°C) <sup>a</sup>	Catalyst	Conversion (wt %)	Yield HMW (wt %)	Yield LMW (wt %)	Yield AS-LMW/Gas (wt %) <sup>b</sup>
280	none	99.7	52.0	22.1	25.6
300	none	98.1	38.2	14.6	45.3
320	none	98.6	24.0	8.1	66.5
280	Ru	97.6	22.6	27.5	47.5
300	Ru	90.4	23.6	23.7	43.1
320	Ru	93.5	21.2	16.9	55.4

<sup>a</sup> All reactions were run for 1 hour, under 4.5 MPa of hydrogen.

<sup>b</sup> Yield determined by difference.

GC-MS analyses of the LMW fraction (Figure 2) show a product distribution of primarily phenols and catechols, which are compounds typical of lignin degradation reactions. At 280°C, guaiacol is a major product, as well as other methoxyl-substituted aromatic compounds. As the reaction temperature increases, the abundance of methoxyl-substituted aromatics dramatically decreases, with 2,6-di-tert-butyl-p-cresol surviving the more degradative conditions.

Based on the solid-state NMR data (Figure 4), the HMW fraction was found to undergo reactions consistent with those previously reported in lignin maturation investigations (13-19). The primary reaction results in the loss of methoxyl (Figure 4: 74 ppm) and catechol (Figure 4: 148 ppm) functionality with some preservation of phenol-like moieties (Figure 4: 154 ppm).

**Catalytic Reactions.** When reactions were carried out in the presence of ruthenium catalyst, the conversion was slightly lower than for the corresponding reactions without ruthenium. At all three reaction temperatures, yield of HMW does not change significantly, while the LMW decreases with increasing reaction temperature. However, the depolymerization of the starting material appears to be suppressed under the catalytic reaction conditions at the higher reaction temperature.

GC-MS analyses of the LMW fraction (Figure 3) show the fraction is composed primarily of phenols and catechols, similar to non-catalytic reaction conditions. At 280°C, guaiacol is a major product, as well as other methoxyl-substituted aromatic compounds. As the reaction temperature increases, the methoxyl-substituted aromatics dramatically decrease, with 2,6-di-tert-butyl-p-cresol surviving the more degradative conditions.

The HMW fraction yield did not change as significantly with temperature. The most notable effect on functional group distributions was the loss of the methoxyl (Figure 5: 74 ppm) moieties, while there was some preservation of catechol (Figure 5: 148 ppm) and phenol (Figure 5: 154 ppm) groups within the structure.

**Comparison of Non-catalytic and Catalytic Reactions.** At 280°C, the extent of depolymerization appears greater for the catalytic reactions. The AS-LMW/gas yield is higher for the catalyzed reaction, and NMR of the HMW fraction shows a greater loss of oxygen functionality when catalyst is in the reaction. The GC-MS data for the LMW also shows fewer oxygen substituted compounds compared to the non-catalytic reaction, another indication of an increased rate of reaction.

However, at 300 and 320 °C, the ruthenium appears to suppress the depolymerization of the hydrolytic lignin compared to the non-catalyzed reactions. The AS-LWM/gas yield is lower for the catalytic reactions. Results of NMR analyses suggest that for the non-catalyzed reactions, the HMW fraction loses more oxygen functionality, particularly as phenols and catechols while the aromaticity increases, compared to the catalytic reactions. The GC-MS data obtained for the LMW fractions indicates a lower percentage of oxygenated compounds, with relatively more substituted aromatics, than in the catalytic reactions.

So what is the role of the ruthenium under these reaction conditions? Ruthenium is a known hydrogenation catalyst, particularly selective for hydrogenating carbonyl functional groups and hindered aromatics (1, 6, 7). However, the hydrogenation activity is highest at 25-200°C. At temperatures of 200-300°C, it has been reported that dehydrogenation activity of aromatics is more dominant (20-21). The reaction system we are investigating is slightly different in that it is a base hydrolysis as well as a hydrogenation reaction.

As observed in the non-catalytic reaction, it is thought that the base participates in breaking the  $\beta$ -O-4 bonds. As radicals are generated through the reaction of the hydrolytic lignin, at 280°C, the ruthenium may be catalyzing the capping of methoxyl radicals with

hydrogen and keeping the radicals from re-reacting with the HMW structure. At higher temperatures, the ruthenium appears to promote hydrogenation of the oxygen radicals on the aromatic structures and preserve the phenols and catechols in the HMW structure. It may also function to hydrogenate the carbonyl groups on the generated monomers.

While ruthenium catalyst might suppress the complete gasification of the hydrolytic lignin, it does appear to selectively hydrogenate and retain some oxygen in the solid carbonaceous material. The possible result would be less oxygen in the gas products and less CO/CO<sub>2</sub> generation. Rather than focusing on the complete depolymerization of lignin, the goal could be to focus on finding value-added applications for the products in order to improve the economics for the entire process.

## Conclusions

Results indicate that the overall lignin conversion is reduced slightly with increasing temperature compared to non-catalytic reactions. Acid-insoluble compounds retain oxygen functionality, as determined by solid state <sup>13</sup>C NMR, when compared to their non-catalytic counterparts. For all reactions, the NMR data showed the oxygen is lost as ether, phenol, and catechol moieties. However, in the non-catalytic reactions, the rate of loss of these moieties and the increase in aromaticity is greater than in the catalytic reactions. If the ruthenium does act to suppress the depolymerization of hydrolytic lignin at higher temperatures, it may selectively suppress loss of oxygen and therefore produce less CO/CO<sub>2</sub>. In that case, making value added materials from the remaining material could increase the viability of the entire process. Future work will include using an inert gas, such as N<sub>2</sub> in the reaction, determining the gas composition and yield with and without hydrogen, and searching for uses of the remaining solid.

**Acknowledgement.** Funding for the project has been provided by the Energy Institute and the Center for Environmental Chemistry and Geochemistry at Penn State University.

## References

- (1) Gilman, G. and Cohn, G., *Adv. Catalysis*, **1957**, 9, 733.
- (2) Vasyunina, N.A., Balandin, A.A., Chepigo, S.V., and Barysheva, G.S., *Bull. Acad. Sciences USSR (Chem.)*, **1960**, 1419.
- (3) Robinson, J.M., Banuelos, E., Barber, W.C., Burgess, C.E., Chau, C., Chesser, A.A., Garrett, M.H., Goodwin, C.H., Holland, P.L., Horne, B.O., Marrufo, L.D., Mechalke, E.J., Rashidi, J.R., Reynolds, B.D., Rogers, T. E., Sanchez, E.H., Villarreal, J.S., *ACS Div. of Fuel Chem. Preprints*, **1999**, 44 (2), 224-227.
- (4) Robinson, J.M., Herndon, P.T., Holland, P.L., Marrufo, L.D., *Org. Proc. Res. & Dev.*, **1999**, 3 (5), 352-356.
- (5) Robinson, J.M., *U.S. Patent No. 5,516,960*, "Process for producing hydrocarbon fuels," **May 14, 1996**.
- (6) Glasebrook, A.L., Hoffman, A.N., and Montgomery, J.B., *U.S. Patent No. 2,776, 276*, "Rosin hydrogenation," **Jan. 1, 1957** ((as reported by A.E. Rea and M. Bebbington in "Annotated Bibliography on Ruthenium, Rhodium, and Iridium as Catalysts," International Nickel Company: New York, 1959).
- (7) Montgomery, J.B., Hoffman, A.N., Glasebrook, A.L., Thigpen, J.I., *Ind. Eng. Chem.*, **1958**, 50, 313.
- (8) Liaw, S.J., Lin, R.G., Raje, A., and Davis, B.H., *Appl. Catalysis A-Gen.*, **1997**, 151 (2), 423.
- (9) Wojciechowska, M., Pietrowski, M., and Czajka, B., *Catalysis Today*, **2001**, 65 (2-4), 349.
- (10) Suzuki, T., Yamada, H., Yunoki, K., and Yamaguchi, H., *Energy Fuels*, **1992**, 6 (4), 352.

- (11) Kondo, K., Kawanishi, T., Ikenaga, N., and Suzuki, T., *Fuel*, **2001**, *80* (7), 1015.
- (12) Burgess, C.E., Robinson, J.M., O'Hara, K., Rashidi, J.R., Sanchez, E.H., and Greenwood, P.F., *ACS Div. of Fuel Chem. Preprints*, **1998**, *43* (2), 335-339.
- (13) Hayatsu, R., McBeth, R.L., Scott, R.G., Botto, R.E., and Winans, R.E., *Org. Geochem.*, **1984**, *6*, 463.
- (14) Pang, L.S., Vassallo, AM., and Wilson, M.A., *Org. Geochem.*, **1990**, *16* (4-6), 853.
- (15) Hatcher, P.G., *Org. Geochem.* **1990**, *16* (4-6), 959.
- (16) Hatcher, P.G., Faulon, J-L., Wenzel, K.A., and Cody, G.D., *Energy Fuels*, **1992**, *6*, 813.
- (17) Behar, F. and Hatcher, P.G., *Energy Fuels*, **1995**, *9*, 984.
- (18) Buchanan, III, A.C., Britt, P.F., and Struss, J.A., *Energy Fuels*, **1997**, *11*, 247.
- (19) Freitas, J.C.C., Bonagamba, T.J., and Emmerich, F.G., *Energy Fuels*, **1999**, *13*, 53.
- (20) Borisov, P.R., and Stepanov, S.S., *Sci. Reports Moscow State University*, **1936**, No. 6, 347 (as reported by A.E. Rea and M. Bebbington in "Annotated Bibliography on Ruthenium, Rhodium, and Iridium as Catalysts," International Nickel Company: New York, 1959).
- (21) Holroyd, R., and Peel, D.H.P., U.S. Patent No. 2,411,726, "Catalytic dehydrogenation," Nov. 26, 1946 (as reported by A.E. Rea and M. Bebbington in "Annotated Bibliography on Ruthenium, Rhodium, and Iridium as Catalysts," International Nickel Company: New York, 1959).

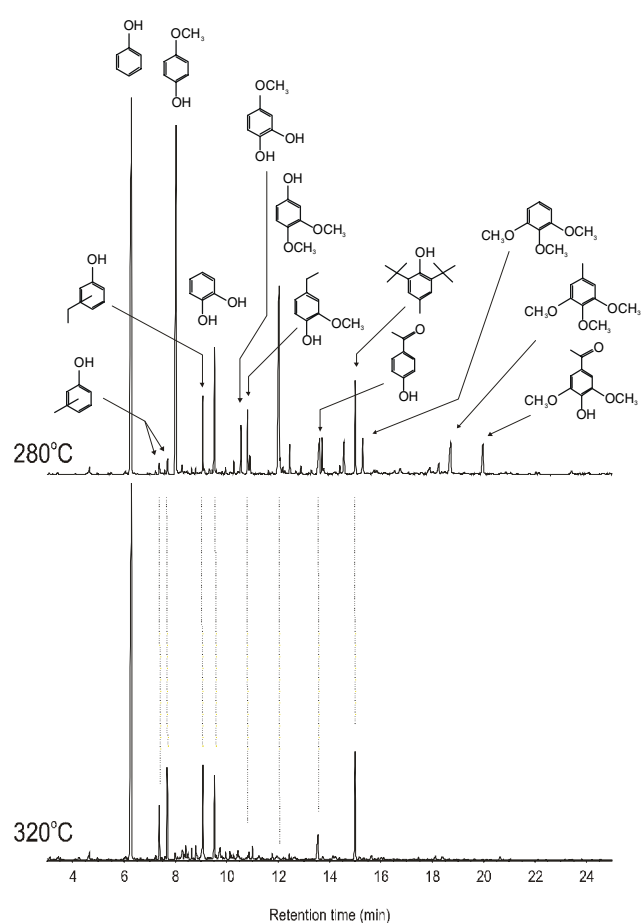


**Figure 2:** GC-MS spectra of LMW for non-catalytic reactions at 280 and 320°C.

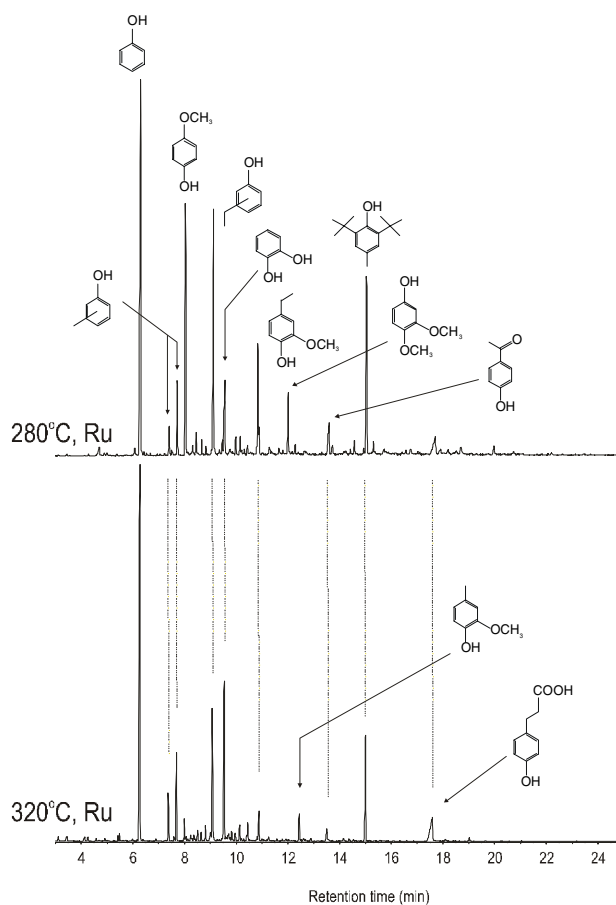


**Figure 3:** GC-MS spectra of LMW for catalytic reactions at 280 and 320°C.

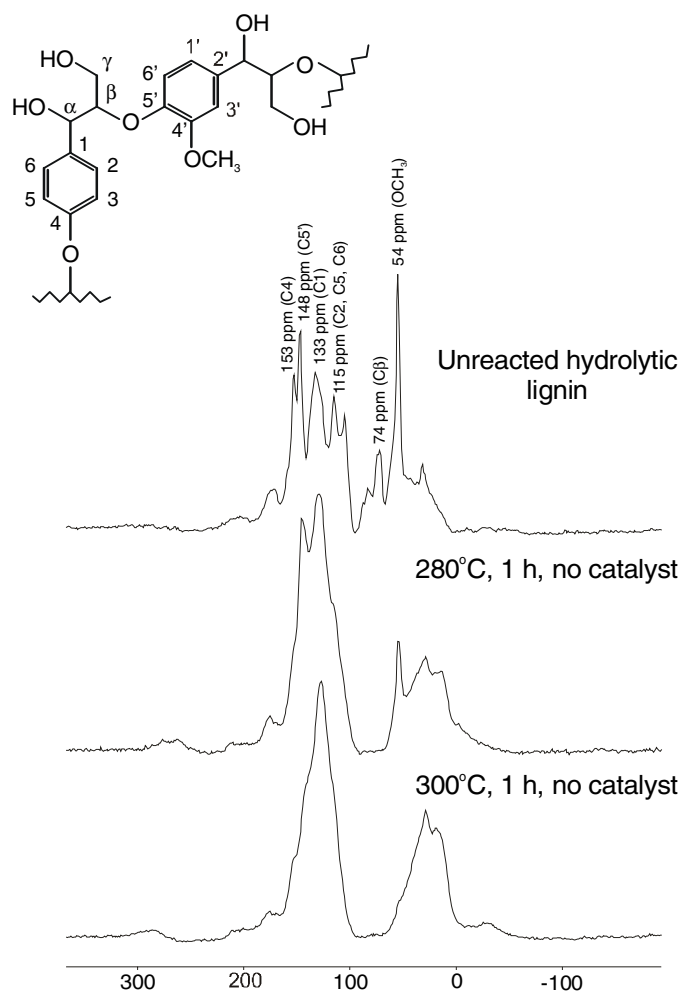


**Figure 4:**  $^{13}\text{C}$  NMR spectra of unreacted lignin and catalytically reacted HMW at 280 and 300°C.

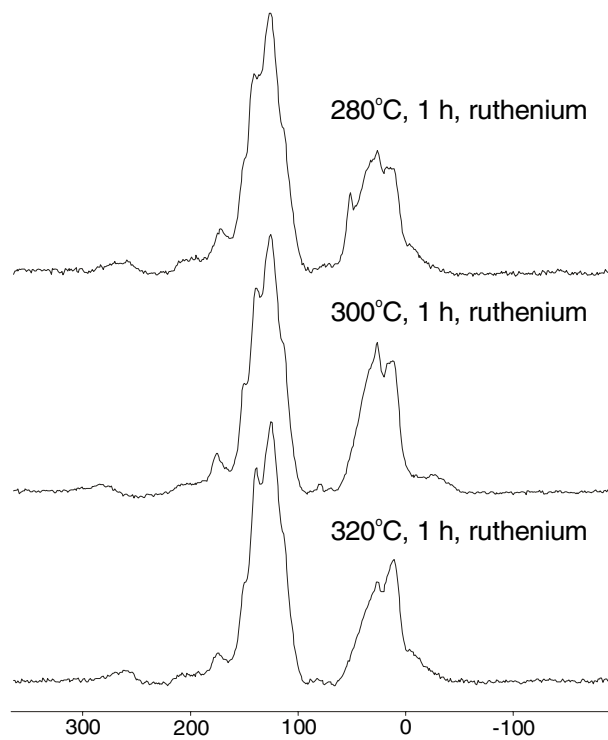


**Figure 5:**  $^{13}\text{C}$  NMR spectra of reacted HMW from catalytic reactions at 280, 300, and 320°C.

## CONVERSION OF LIGNIN INTO A HYDROCARBON PRODUCT FOR BLENDING WITH GASOLINE

David K. Johnson<sup>a</sup>, Esteban Chornet<sup>a,b</sup>, Wlodzimierz Zmierzczak<sup>c</sup>  
and Joseph Shabtai<sup>c</sup>

<sup>a</sup> National Renewable Energy Laboratory, 1617 Cole Blvd., Golden, CO, USA 80401 Fax: 303-384-6363; david\_johnson@nrel.gov; <sup>b</sup> University of Sherbrooke, Canada; <sup>c</sup> Department of Chemical and Fuels Engineering, University of Utah, Salt Lake City, UT 84112

### Introduction

Lignin is present (15-30 wt%) in all lignocellulosic biomass. Ethanol production from biomass feedstocks will always generate lignin containing residues. Thus, lignin supply will progressively increase as ethanol plants using straw, forest residues, etc., are implemented in the future<sup>1</sup>. Adding value to this residue will significantly enhance the competitiveness of biomass-to-ethanol conversion. Lignin, a cross-linked amorphous phenolic polymer, is the biomass component with highest energy content (9000 - 11000 Btu/lb compared to 7300 - 7500 for cellulose). Lignin can be combusted to provide heat and/or power for the ethanol process, and could provide some excess power to generate additional revenue. Given the molecular nature of lignin it is also conceivable to convert lignin into added value end products, especially fuel components. Previous process development studies in our project have focused on converting lignin to reformulated gasolines and gasoline blending components<sup>2,3</sup>.

Lignin-derived products must be compatible with the evolving regulations for transportation fuels. There are specific compositional requirements for gasoline limiting the level of aromatic compounds in gasoline<sup>4</sup>. For Federal Phase II Reformulated Gasoline (RFG), the limits are 1 percent benzene and 25 percent by volume total aromatics. In California, the Phase III RFG specification is an average of 22 percent aromatics or less. For non-RFG gasoline, the aromatic content is limited to the refinery's 1990 baseline level. Gasoline volatility (90% should distill below 167 °C) and Reid Vapor Pressure (RVP, should be 48-56 kPa) are also important specifications. Octane number ((R+M)/2) determines gasoline fuel grade and ranges from 85 to 93. It is the current goal of this project to convert lignin into a hydrocarbon product compatible with blending in gasoline that has an octane number greater than 110.

The sulfur-in-gasoline rule, issued in December 1999, greatly reduced the amount of sulfur to be allowed in gasoline by 2005. The new regulations for light-duty vehicles greatly reduced the allowable emissions of NO<sub>x</sub>, NMOG and particulates. Automakers say these standards can only be achieved if virtually sulfur-free gasoline is available. It is estimated that the required desulfurization of gasoline could reduce aromatics levels in gasoline and create a loss of 0.5 octane numbers. The predicted phase-out of MTBE, an oxygenate and octane enhancer, will exacerbate the nationwide shortage of octane. This may permit introduction of an aromatic octane-blending agent without an increase in permitted aromatics levels. If the lignin-derived octane enhancer has the same octane number as xylene (i.e., 106), then 1.7 percent could be blended to remedy the octane loss without exceeding the original aromatics content of gasoline. On this basis, the potential US market for a lignin-derived octane enhancer could be 142,800 barrels per day or 2.2 billion gallons per year<sup>4</sup>.

This project is thus targeted to obtain the necessary scientific and technological data with which to evaluate the economics and markets for converting lignin into valuable fuel components.

The main source of lignin from Biomass-to-Ethanol processes is the high molecular weight lignin remaining in the solid residue after saccharification and fermentation (SSF) of the dilute acid pretreated

biomass. The lignin is soluble in aqueous basic solutions, and can be readily separated by solubilization from the protein, unconverted carbohydrate, and other non-lignin materials present in the residue.

The process strategy is to depolymerize the lignin by base catalysis, using moderately high temperatures and short reaction times. To minimize the cost of base recovery only low levels of soluble base are used, just sufficient to dissolve the lignin. The resulting intermediate is a base catalyzed depolymerized (BCD) product that consists of monomeric and oligomeric phenolics. The BCD product is isolated by acidification and then solvent extraction of the raw BCD product. Catalytic hydroprocessing (HPR) is then used to convert the extracted BCD product into a mixture of monomeric aromatic hydrocarbons very similar to components already found in gasoline. HPR utilizes catalysts with hydrodeoxygenation (HDO) and hydrocracking (HCR) activity to remove all remaining oxygen and break the interaromatic C-C linkages.

The target characteristics for the hydrocarbon product are:

Distillation characteristics

-95% should distill <200 °C

Chemical composition

-C + H > 99.5%

-S content <0.01% (100ppm)

-Aromatic hydrocarbons > 65%

-No detectable phenols

Octane value

-Blending octane number ((R+M)/2) > 110

Reed Vapor Pressure

-Mandated limits vary

-Maximum levels range from 7 - 10 psi

A process flow sheet has been constructed for the process of converting lignin into a high-octane hydrocarbon fuel blending component. From this the production cost for the BCD-HPR product has been estimated at \$0.60 - 0.75/gallon. This estimate assumed the plant received a fraction of the lignin from a 600 tpd ethanol plant. Performance targets used in the calculations included that 100% of the lignin in the SSF residue could be solubilized to give a feed with an 8% lignin concentration. The cost of base recovery was minimized by limiting the soluble base concentration to 1% or less in the lignin depolymerization step. The overall yield of hydrocarbon product in the gasoline boiling range was assumed to be 70% of the theoretical yield, equivalent to about 50% on a mass basis. Extraction of the depolymerized lignin intermediate assumed that it could be performed with a relatively low cost solvent such as the BCD-HPR product or a process stream found in a petroleum refinery.

The value of high-octane ((R+M)/2 = 110) hydrocarbon fuel blending components has been estimated based on the Annual Energy Outlook projection of \$20 - 25 / bbl for crude oil in 2010, and that the value of an octane boosting product is in the range of 0.7 - 1.4 cents per octane gallon<sup>5</sup>. The value of the lignin-derived gasoline blending component should be in the range of \$0.97 - 1.14 per gallon based on these assumptions. Thus if performance targets can be met it should be possible to utilize the lignin from a bioethanol plant to enhance the competitiveness of biomass-to-ethanol conversion.

### Results and Discussion

**Base Catalyzed Depolymerization.** Initially, systematic studies on the BCD reaction were performed at the U of U using stirred autoclaves. The effects of reaction time, temperature, and pressure, base type and concentration, and the solvent used, were examined. High yields of depolymerized lignin (60%-80%) were obtained at moderate temperatures and short reaction times.

**Table 1. Comparison of Starting Lignin to BCD Products**

	Alcell Lignin	LZD-7	LZD-19
Volatiles (by GC)	0%	36% ± 14%	33% ± 13%
Mn	870	470	530
Mw	2400	680	830
<sup>13</sup> C NMR data (Number of Cs per 6 C <sub>Ar</sub> )			
Aliphatic C	2.9	2.6	2.5
Methoxyls	1.3	0.7	0.3
Methyls	0.6	0.9	0.9
Ar-OH	0.8	1.7	1.6
C=O	0.1	0.4	0.5
Elemental Analysis Data			
C%	66.6	68.8	70.9
H%	5.9	6.5	6.4
O% by difference	27.5	24.5	22.6

Mn = Number-average molecular weight of peracetylated BCD;  
Mw = Weight-average molecular weight of peracetylated BCD.

As can be seen from the data in Table 1 the BCD reaction causes the lignin to be partially depolymerized from a mixture of dimers through nonamers into a mixture of monomers through trimers. Chemical analysis indicates that demethoxylation occurs during the BCD reaction, mostly through loss of the methyl group. The largest identifiable component of the BCD products is normally catechol. Analyses also indicate that all oxygen containing functionalities in the lignin side-chain are lost apart from a few that are converted to carbonyls. Figure 1 shows the average reaction chemistry that occurs during a BCD reaction.

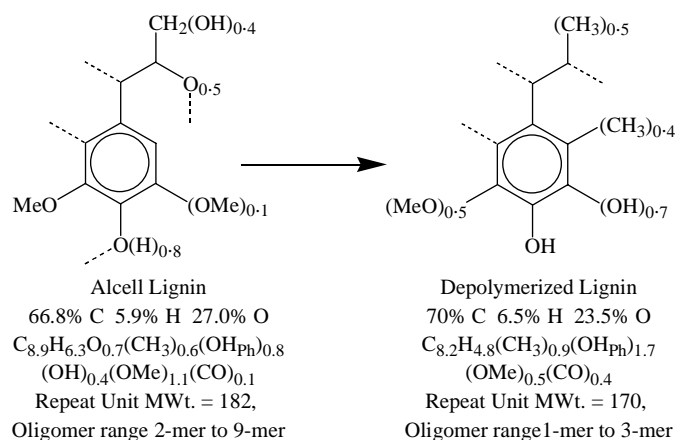


**Figure 1.** Average reaction chemistry for BCD reactions performed under aqueous conditions.

The depolymerization reaction has been scaled up into a flow reactor at the U. of Utah capable of processing 100g of lignin per hour.

**Hydroprocessing** Depolymerized lignin samples have been hydroprocessed at the U. of Utah into products that are predominately mixtures of aromatic and naphthenic hydrocarbons that could be blended with gasoline. Catalysts and reaction conditions are still being optimized so that the product meets all

target specifications. Analyses of the BCD-HPR products, performed at NREL (Figure 2), indicate that complete deoxygenation with minimal hydrogenation is not easily attained.

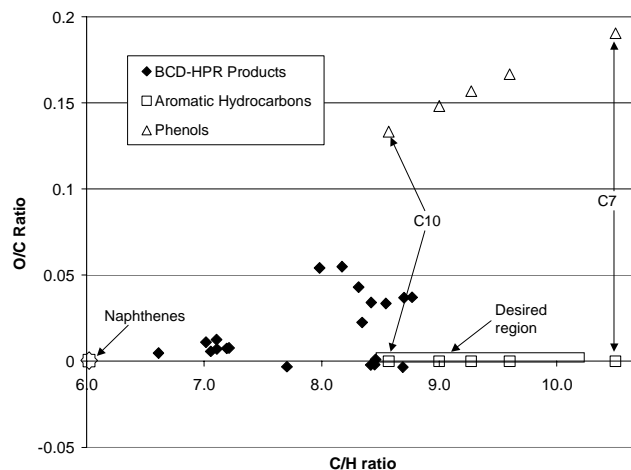


**Figure 2.** Variation of O/C ratio with C/H ratio for BCD-HPR products made at the U. of Utah.

A flow reactor has been brought into operation at the U. of Utah for production of sufficiently large samples (up to 1L) so that fuel property tests can be performed on lignin-derived hydrocarbon products. Standard tests for distillation (ASTM D86) and vapor pressure (ASTM D5191) have shown that the products are close to meeting these gasoline specifications. Standard tests (ASTM D2700 and D2699) of 10 – 50% blends of HPR-BCD products with unoxxygenated gasoline have given blending octane numbers for the products of 82 – 97. Higher values are obtained when hydrogenation is limited, minimizing formation of naphthenes.

### Conclusions

A process for converting the lignin in residues from biomass-to-ethanol processes is being developed. Significant progress has been made towards developing a process that has commercial potential. Increased yields, better control of hydroprocessing, and decreasing the cost of base recovery are the most important improvements that still need to be made.

**Acknowledgement.** We wish to thank the US DOE OTT Office of Fuels Development (Director John Ferrell) for funding this work, and NREL and DOE Ethanol Program managers, Robert Wooley and Gerson Santos-Leon, for their support.

We would also like to thank several of our colleagues at NREL., including Mark Davis and Justin Sluiter for their assistance in performing some of the analyses of the samples, plus Kelly Ibsen, and the Process Engineering group for technoeconomic analyses.

### References

- Handbook on Bioethanol: Production and Utilization. Wyman, C.E. Ed., Taylor & Francis, Washington, DC: 1996; pp 105-118.
- Shabtai, J., Zmierczak, W., and Chornet, E. Proc. 3rd Biomass Conf. of the Americas, Elsevier, 1997, Vol. 2, pp 1037-1040.
- Shabtai, J., Zmierczak, W., and Chornet, E. U.S. Patent 5,959,167.
- Sinor, J.E. "Review of Market for Octane Enhancers" NREL report (NREL/SR-580-28193), May 2000.
- Unzelman, G.H., Natl. Petrol. Ref. Assn. Ann. Mtng., San Francisco, CA, March 1995.

# DIRECT FORMATION OF AROMATICS FROM BIOPOLYMERS DURING LATE-STAGE, HIGH-SEVERITY PYROLYSIS

Robert J. Evans, Mike J. Looker, and Mark N. Nimlos

National Bioenergy Center  
National Renewable Energy Laboratory  
1617 Cole Blvd.  
Golden, CO 80401

## Introduction

The formation of aromatics from biomass pyrolysis by gas phase cracking of the primary products has been well documented.<sup>1-3</sup> Since biopolymers may undergo solid-phase chemical transformations during devolatilization, minor amounts of aromatics may be formed directly from this altered solid phase. Recently, Hajaligol et al<sup>4</sup> reported the direct formation of aromatics from preformed, biopolymer chars heated to 400 - 600 °C. Even if minor compared to the bulk volatile product slate, these aromatics may be significant when compared to the gas phase sources of aromatics under biomass conversion systems such as a fluid bed gasifier.

We report here methodology and results showing this effect directly from biopolymers. Two-stage pyrolysis was used to show the effect of composition and thermal history on the products evolving from the solid phase. Cellulose and pectin were used as model biopolymers and as a matrix to which other model compounds were added. The samples were heated in two stages:  $T_1 = 350$  °C, for 7 minutes,  $T_2 = 700$  °C, for an additional 5 minutes. Molecular Beam Mass Spectrometry (MBMS) was used to observe the evolution of volatile products.

## Experimental

The reactor shown in **Figure 1** was used to first expose the sample to low-temperature ( $T_1$ ) pyrolysis conditions in flowing Helium for seven minutes where some of the sample weight was lost as volatile products. The remaining material is then slid into a hotter region of the furnace ( $T_2$ ) where a second devolatilization event is observed.

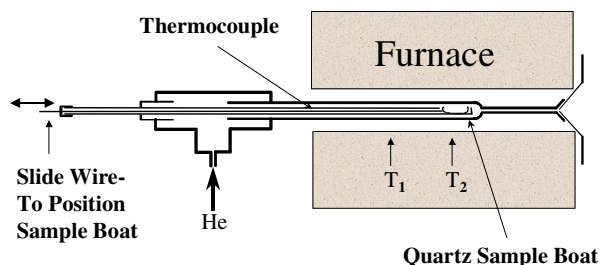


**Figure 1.** The pyrolysis reactor for variable-temperature pyrolysis studies. The sample is slid to a position and held at the low target temperature ( $T_1$ ) then slid further into the reactor to expose the sample to a subsequent high reaction temperature ( $T_2$ ).

A 50:50 mixture of pectin and cellulose was used as the base-case starting material, or matrix. The pectin was from Acros Organics Inc. and the cellulose was from Sigma Chemical Inc. We selected a sample of cellulose that gave a full range of pyrolysis products, including levoglucosan and hydroxyacetaldehyde, which is more representative of the product distribution found in biomass than a highly purified sample, such as Avicel<sup>1</sup>. A higher char yield is also

obtained from this cellulose, which means that a reasonable sample of char persists for further evaluation at a higher temperature. A 250 mg sample of the matrix was used resulting in a solid phase after the  $T_1$  treatment of ~50 mg. To study the condensed-phase reactions of other materials, mixtures with the matrix were made at a 10% level of additive and the resulting products compared to those derived from the matrix alone. This approach is necessary since some materials of interest will simply evaporate when studied as a neat sample in this fashion. However, when in the presence of the matrix, these volatile materials may undergo solid-forming reactions as the vapors or thermal reaction products interact with the charring matrix material and hence approximate what happens in biomaterials with complex cell wall structures.

**Molecular Beam Mass Spectrometry.** The study of pyrolysis by MBMS has been fully described previously.<sup>1</sup> The hot gases exiting the reactor are expanded through an orifice on the apex of a sampling cone into the stage one vacuum at 40 mtorr. The pressure difference is sufficient for free-jet expansion, which quenches the products and allows the full range of products, including light gases, high-molecular-weight compounds, and reactive products, to be simultaneously sampled and analyzed. A molecular beam, collimated through a second expansion, enters an ion source, where approximately 25 eV electron impact ionization is used to form ions that are analyzed by a quadrupole mass filter.

**Multivariate Data Analysis.** Factor analysis was used to identify subspectra of the time-resolved mass spectra collected during  $T_2$ . Two subspectra were identified using the methods of Windig et al.<sup>5</sup> and fractional concentrations were calculated for each spectra.

## Results and Discussion

During exposure of the sample to low-temperature ( $T_1$ ) pyrolysis conditions for seven minutes some of the sample weight was lost as volatile products. The remaining material is then quickly ramped up to high temperature ( $T_2$ ) where a second devolatilization event is observed typically resulting in a total of 75% weight loss from both stages. Volatiles continued to evolve from the remaining 25% char during a maturation phase with no clearly defined end point. A typical experiment is shown in **Figure 2**.

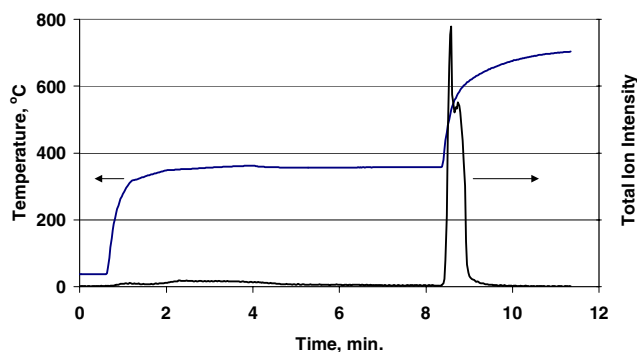


**Figure 2.** Time-resolved behavior of pectin/cellulose in a two-temperature pyrolysis experiment. The sample is slid to the position for  $T_1$  (350 °C) and held for 7 minutes. Product evolution occurs at this low temperature but is not of interest for this experiment. The remaining solid is then slid to the position for  $T_2$  (700 °C) and held until product evolution stops.

Experiments were performed to evaluate the yield of char from neat pectin and cellulose at typical settings of  $T_1$  and  $T_2$ . The char yields for the pectin were higher than for the cellulose sample. The residue yield at  $T_1=350$  °C is 30% for both pectin and cellulose with no significant effect of time at  $T_1$  (5 vs 10 minutes). There is no

evidence that these residues have been converted to a thermally stable form. The point of this experiment is to put the material through a treatment of appropriate severity to make an assessment of potential impact of short thermal pretreatments on aromatic hydrocarbon formation. This timeframe and solid matrix also permits an assessment of potential reactions between the evolving solid structure and other substances of interest that are added and compared to the matrix alone. The residue yields at  $T_2$  from 700 to 800 °C were independent of both the  $T_1$  and  $T_2$  temperatures that were studied and consistently around 20% for pectin and 10% for cellulose. We conclude that the low temperature treatment is insufficient to influence the amount of fixed carbon that will result from the high temperature treatment, but the chemical nature of that material may still be influenced by this treatment. We conclude that the parameters of this experiment are not critical to the observations of product formation from char and therefore are more likely to be relevant to a wide range of conditions where chars form. The main purpose of the low temperature treatment is to allow prompt chemical modifications of the material and reactions between co-reactants prior to higher severity pyrolysis

The devolatilization product composition at  $T_2$  is predominantly primary products like what is observed at  $T_1$ . To separate the primary products evolving from the remaining unaltered starting material and that which is evolving from the thermally altered matrix material, time-resolved factor analysis of the  $T_2$  mass spectra was performed. This series of mass spectra were subjected to self-modeling factor analysis and resulted in two distinct subspectra. The resolution of the  $T_2$  curve into these two profiles is shown in **Figure 3**.

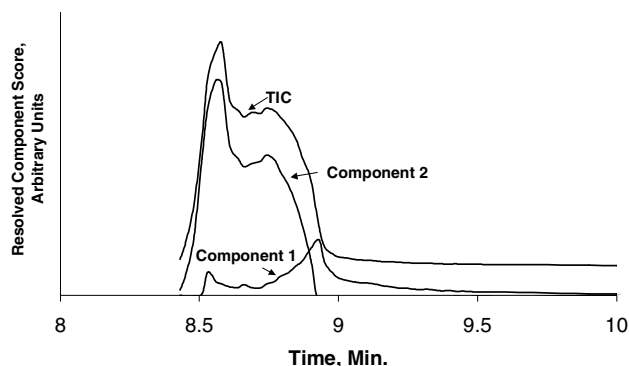


**Figure 3.** Time-resolved factor analysis of the  $T_2$  evolution profile (TIC) showing evolution curves for the two subspectra shown in Figures 4 and 5.

Component Spectrum 1, shown in **Figure 4**, is a mixture of monoaromatics ( $m/z$  78, benzene;  $m/z$  92, toluene;  $m/z$  106 xylenes), phenols ( $m/z$  94, phenol;  $m/z$  108, cresol;  $m/z$  122, methylcresol), furans ( $m/z$  67, 82 methyl furan), along with CO ( $m/z$  28) and  $CO_2$  ( $m/z$  44). Polynuclear aromatic hydrocarbons were not detected in this experiment, but higher aromatics, such as naphthalene, were seen in other experiments, especially after the major evolution of  $T_2$  products is finished.

Component spectrum 2, shown in **Figure 5**, is a typical carbohydrate primary pyrolysis product. The evolution profiles (**Figure 3**) of the two component spectra over the  $T_2$  event are different with the primary products (component 2) reaching a maximum earlier. The aromatic/phenols continue to evolve and reach a maximum after the primaries are finished.

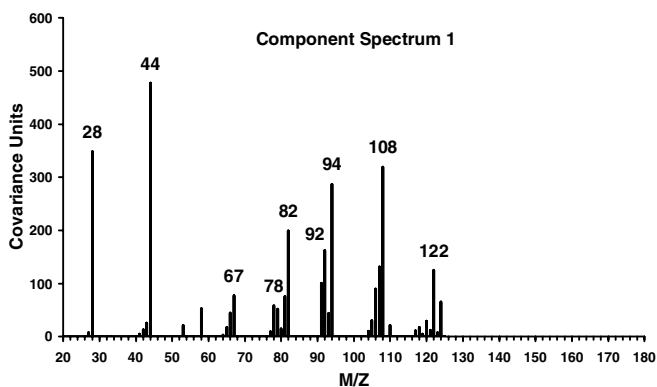


**Figure 4.** Component spectrum 1 in the time-resolved factor analysis of data in Figure 3.

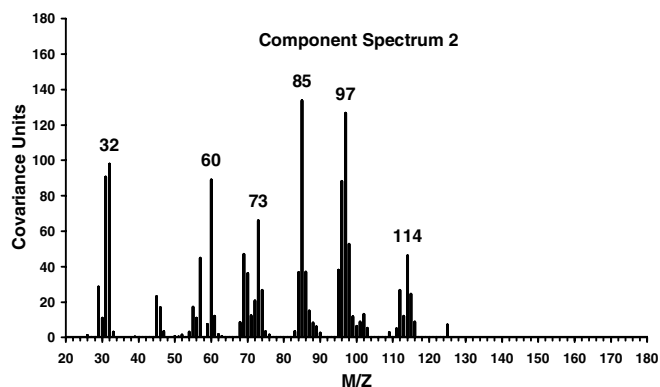


**Figure 5.** Component spectrum 2 in the time-resolved factor analysis of data in Figure 3.

**Effect of Additives.** Other biomaterials were tested by adding to the pectin/cellulose matrix and subjected to the same two temperature heating sequence. The following showed an enhancement of the yield of the aromatic/phenolic group: lignin, chlorogenic acid, rutin, proline and linolenic acid. It was surprising that lignin did not show a more significant enhancement. A possible explanation is the lignin addition leads to a more thermally stable residue that does not release low molecular weight volatiles.

## Conclusions

In summary, two sub-spectra were evident during high severity pyrolysis of biopolymer samples that had been thermally pretreated: the primary pyrolysis products that also evolved at  $T_1$  and a later evolving group of products that includes phenols and aromatics.

**Acknowledgement.** The authors gratefully acknowledge the financial support from Philip Morris USA, Inc. and discussions with Mohammad Hajaligol that initiated this work.

## References

1. Evans R.J.; Milne, T.A. *Energy & Fuel* **1987**, 1,123.
2. McGrath T.; Sharma R.; Hajaligol, M. *Fuel* **2001**, 80, 1787.
3. Shin, E.-J.; Nimlos, M. R.; Evans, R. J. *Fuel* **2001**, 80, 1697.
4. Hajaligol, M.; Waymack, B.; Kellogg, D. *Fuel* **2001**, 80, 1787.
5. Windig W.; Lippert J.L.; Robbins, M.J.; Kresinske, K.R.; Twist, J.P.; Snyder, A.P. *Chemometrics and Intell. Lab.* **1990**, 9, 7.

## The effect of inorganics on the formation of PAH during low temperature pyrolysis of cellulose

Thomas E. McGrath, Jason A. Hoffman\*,  
Jan B. Wooten and Mohammad R. Hajaligol

Philip Morris USA, Research Center, Richmond, VA 23234

\*Current Address: MCV School of Pharmacy, Richmond, VA, USA

### Introduction

The effect of inorganic salts on the pyrolysis of cellulose has been extensively studied.<sup>1</sup> It is well known that the presence of inorganic salts can: lower the primary pyrolysis temperature, increase the char yield by accelerating decomposition reactions, increase or decrease the rate of oxidation of the aromatic component of the char, and increase or decrease the heat released from the oxidation of char to CO<sub>2</sub>. Although a wealth of information exists, relatively little is known about the effect of inorganic salts on the low temperature formation of polycyclic aromatic hydrocarbons (PAHs).

In an effort to explore the effect of the main indigenous cations found in biomass on the formation of PAHs we have investigated the effect of Na, K, and Ca on the formation of PAHs from cellulose. Cellulose samples loaded with varying weight percentages of sodium, potassium, and calcium were pyrolyzed at temperatures up to 600 °C. The major components of the cellulose tars were characterized using gas chromatography – mass spectroscopy (GC-MS). The effect of mono- and divalent cations on the aromaticity of chars formed at 300 °C was studied using nuclear magnetic resonance spectroscopy (NMR). Although the absolute yields of PAHs at temperatures up to 600 °C may not be significant relative to the higher yields of PAHs formed at elevated temperatures, their formation and yields are deemed important during the smoldering combustion of biomass materials.

### Experimental

A schematic of the experimental setup is given in Fig. 1. The experimental apparatus consisted of a quartz tube placed inside a heated zone. The zone had an internal diameter of 2.5 cm and an isothermal length of ca. 7 cm. Helium was used as the carrier gas at a flow rate of 120 cm<sup>3</sup>/min. A Cambridge pad placed in a special assembly immediately at the end of the zone was used to collect the product tar condensate. The temperature of the sample in the heated zone was measured using a chromel/alumel (K type) thermocouple. The thermocouple was also used to transport the quartz boat, containing the cellulose samples, to and from the heated zone.

**Materials.** The cellulose sample was obtained from FMC Corporation, and the inorganic salts were obtained from Acros and Aldrich. The cellulose is a microcrystalline purified and depolymerized  $\alpha$ -cellulose derived from fibrous plants (Avicel PH-102). Cellulose samples with 0.1, 1, and 5% w/w of NaCl, KCl, CH<sub>3</sub>COOK, and CaCl<sub>2</sub>, respectively, were prepared by dissolving the desired amount of the salt in water and then adding 2.5 g of cellulose powder to the aqueous salt solution. Samples were stirred for 4 hours and then placed in an oven at 45 °C for 12 hours. A mortar and pestle was used to grind the samples into a fine powder. A cellulose sample that under went the same procedure was used as the control.

**Experimental Procedure.** A 500 mg sample was placed in the quartz boat that initially rested in an unheated section of the tube before the heated zone (see Fig. 1). The Cambridge pad assembly was placed on the exit side of the furnace and the exit line was maintained at ~250 °C to minimize any condensation of the product tar prior to reaching the pad. After the furnace had reached the

respective set temperature, the sample was pushed to a pre-determined location in the furnace and pyrolyzed for 10 minutes. The Cambridge pad was removed, placed in an amber screw capped vial, and the washings from the cambridge pad assembly were added to the vial. A total solvent level of 5 ml of methanol was used and the vial was left to stir overnight. The residence time of gas phase pyrolysis products in the isothermal section of the reactor was calculated to be approximately 4 s at a furnace temperature of 600 °C.

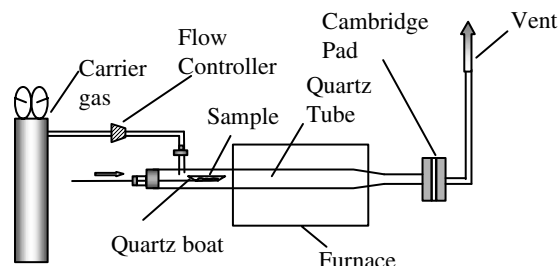


Figure 1. Schematic diagram of apparatus setup

The product condensates were analyzed by GC-MS using a HP 6890 GC equipped with a HP 5973 quadrupole MSD analyzer in the scanning mode. 14 PAH were studied that consisted of two to six condensed aromatic rings. The experimental error in PAH yield measurements varied between 10 to 30%. It should be realized that PAH constituted only a small fraction of the product which was a complex mixture of mostly oxygenated organic compounds. Besides the PAH mentioned above, the tar also contained other PAH, mainly methyl substituted PAH that were not considered in the analysis of this study.

Cross-polarized magic angle spinning (CPMAS) <sup>13</sup>C nuclear magnetic resonance (NMR) was used to characterize cellulose chars formed at 300 °C. Elemental analysis (EA) of cellulose chars was carried out by Galbraith Laboratories, Inc., Knoxville, TN, USA. The NMR and EA data are not reported here.

### Results and Discussion

Varying the cation loading from 0.1 to 5% w/w increased the amount of char formed and decreased the overall weight loss of cellulose samples. The weight loss data for cellulose samples loaded with 5% w/w of NaCl, KCl, CH<sub>3</sub>COOK, and CaCl<sub>2</sub> is given in Table 1. Char yields are expressed on an ash free basis. All cation loaded cellulose samples gave higher char yields and lower tar yields with respect to the control. The Na loaded cellulose sample experienced the highest weight loss of the cation loaded samples. The KCl and CH<sub>3</sub>COOK cellulose samples experienced very similar weight losses, while the Ca loaded cellulose sample experienced the lowest weight loss.

The constituents of the product tar condensate derived from the control and cation loaded samples were characterized using GC-MS. The yield of levoglucosan was significantly affected by the presence of cations on the cellulose matrix, decreasing as the cation concentration increased. The above weight loss and levoglucosan yield data is consistent with what has been reported in the literature.<sup>1</sup>

PAH yields were higher from the cation loaded samples compared to the control. PAH yields were calculated on a  $\mu$ g/g of sample and on a  $\mu$ g/g of char basis. The yields of PAH formed from the cation loaded cellulose samples were found to increase with an increase in cation loading. Na and K loaded cellulose samples gave similar PAH yields. When PAH yields were expressed on a  $\mu$ g/g of

char basis the control and the cation loaded samples gave very similar yields of PAHs.

**Table 1. Weight Loss of Cation Loaded Cellulose Samples**

<sup>a</sup> Material	Zone I Temperature at 600 °C		
	<sup>b</sup> Char (mg)	<sup>c</sup> Tar (mg)	<sup>d</sup> Total Wgt. Loss
Cellulose	36	252	93%
Cell. + NaCl	59	210	84%
Cell. + KCl	69	210	81%
Cell. + CH <sub>3</sub> COOK	71	191	81%
Cell. + CaCl <sub>2</sub>	94	183	76%

a = 500 mg sample pyrolyzed

b = Amount of char formed after 10 min at 600 °C in zone I calculated on an ash free basis

c = Amount of tar collected after 10 min at 600 °C in zone I

d = Percent weight lost from sample after 10 min at 600°C in zone I

A comparison of PAH yields formed from the pyrolysis of Na, K, and Ca loaded cellulose samples is given in Fig. 2(a). PAH yields are expressed on a µg/g of sample basis. All three cation loaded samples gave higher PAH yields compared to the cellulose control. The yields of most 2 to 3 ring PAH are very similar for all three cation loaded samples. The yields of 4 ring PAH are lower for the Ca loaded cellulose sample with respect to the other samples. PAH yields were also calculated on a µg/g of char basis as shown in Fig. 2(b). The yields of PAHs from the control and Na and K loaded samples are very similar while the yields of 3 and 4 ring PAH are lower for the Ca loaded sample.

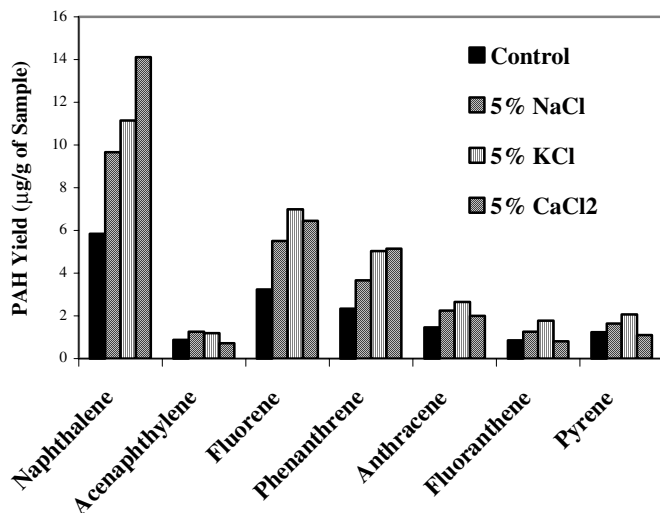


**Figure 2(a).** PAH yields for the pyrolysis of cation loaded cellulose samples at 600 °C. PAH yields expressed on a µg/g of sample basis.

It is well known that the presence of inorganic salts can increase the char yield. If PAH formation at low temperatures is attributable to precursors formed in the solid char matrix over the 400 to 600 °C temperature range,<sup>2,3</sup> then one might expect an increase in PAH yields as the char yield increases. This assumption appears to hold true for the Na and K loaded samples. Although the Ca loaded samples gave the highest char yields, the lower yields of 3 and 4 ring

PAH may indicate a higher degree of cross-linking in this char relative to the other samples.

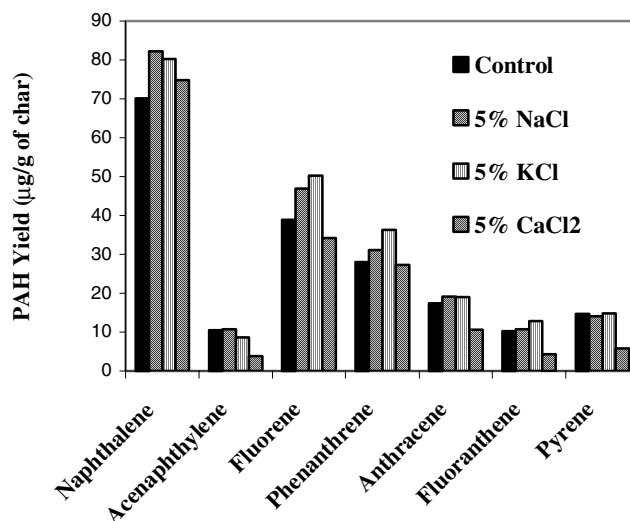


**Figure 2(b).** PAH yields for the pyrolysis of cation loaded cellulose samples at 600 °C. PAH yields expressed on a µg/g of char basis.

### Conclusions

The addition of Na, K, and Ca inorganic salts to cellulose increases char yields and decreases tars yields. The yields of primary decomposition products were significantly affected. Increasing the cation loading decreases the yields of levoglucosan and increases the yield of char formed. PAH yields increased with an increase in cation concentration when yields were expressed on a µg/g of sample basis. The yields of PAHs formed were generally very similar when the yields were normalized on a µg/g of char basis. PAH yields from the control and from the Na and K loaded cellulose samples were very similar while lower yields of 3 to 4 ring PAH were formed from Ca loaded samples and this may be attributable to a more highly cross-linked char. Anion effects were also observed: changing the anion from Cl<sup>-</sup> to CH<sub>3</sub>COO<sup>-</sup> for K loaded samples significantly lowers levoglucosan yields and increases the amount of naphthalene and fluorene formed.

**Acknowledgement.** The authors are grateful to the Philip Morris U.S.A. management for the support of this research. The assistance of B. Miller and K. Patel is also gratefully acknowledged.

### References

- (1) Shafizadeh, F., *The Chemistry of Solid Wood*, Edt. Roger Rowell, American Chemical Society, Washington, DC, **1984**
- (2) Sekiguchi, S., Shafizadeh, F., *Journal of Applied Polymer Science*, **1984**, 29, 1267-1286, Pan, W-P., Richards, G.N., *J. Anal. Appl. Pyrolysis*, **1989**, 16, 117-126, Liodakis, S.E. et al., *Thermochim. Acta*, 1996, 278, 99-108. Soares, S., et al., *European Polymer Journal*, **2001**, 37, 737-745
- (3) E.W. Robb, W.R. Johnson, J.J. Westbrook, and R.B. Seligman, *Beitrag zur Tabakforschung*, **1966**, 3, 597. B.E. Waymack and D.S. Kellogg, *Fuel Chemistry Division Preprints*, **2001**, 46, 198.
- (4) T. McGrath, G. Chan, M. Hajaligol, "Low Temperature Mechanism for the Formation of Polycyclic Aromatic Hydrocarbons from the Pyrolysis of Cellulose", submitted to *J. Anal. Appl. Pyrol.*, **2001**.

# EFFECTS OF RESTRICTED MASS TRANSPORT ON THERMOLYSIS OF LIGNIN MODEL COMPOUNDS

A. C. Buchanan, III, Phillip F. Britt, and Michelle K. Kidder

Chemical Sciences Division  
Oak Ridge National Laboratory  
Bethel Valley Road  
P.O. Box 2008, MS-6130  
Oak Ridge, Tennessee 37831-6130

## Introduction

Lignin is a renewable resource whose complex structure, chemical and thermal reactivity, and potential for use in a variety of commercial products continues to draw considerable attention.<sup>1,2</sup> Our research has been focusing on the thermolysis mechanisms of model compounds that represent structural elements in native lignins (e.g.  $\beta$ -O-4 and  $\alpha$ -O-4 aryl ether linkages)<sup>1a</sup> and in processed lignins (e.g. diphenylmethane linkages from acidic or alkaline treatments in pulping).<sup>1b,c</sup>

We studied in detail the pyrolysis mechanism of phenethyl phenyl ether (PhCH<sub>2</sub>CH<sub>2</sub>OPh, PPE), the simplest model of the  $\beta$ -O-4 aryl ether linkage, in the liquid and vapor phases at 330-445 °C.<sup>3</sup> Two competitive free radical decay pathways were found to be operative, including a significant rearrangement pathway involving an O,C-phenyl shift in the PhCH<sub>2</sub>CH•OPh intermediate. Recently, mechanistic studies of methoxy-substituted PPEs, representative of guaiacyl and syringyl units in lignin, have been conducted under high temperature, short contact time conditions (500 °C, < 1 s) using the flash vacuum pyrolysis (FVP) technique.<sup>4</sup> These studies revealed a rich variety of intramolecular transformations for intermediate methoxy-substituted phenoxy radicals. Currently, we are investigating other important PPE structures, such as  $\alpha$ -alcohols PhCH(OH)CH<sub>2</sub>OPh,<sup>5</sup> under FVP conditions.

Another aspect of our research has been investigation of the impact of potential mass transport limitations on thermolysis products, kinetics, and mechanisms through the use of silica-immobilized model compounds for structures in coal and lignin. This has been accomplished through the use of model compounds immobilized on the surface of silica nanoparticles via a Si-O-C<sub>aryl</sub> linkage. The results of extensive investigations into the pyrolysis mechanisms of hydrocarbon models for structures in coals have been recently reviewed.<sup>6</sup> In this paper, we will summarize our current understanding of the significant role that mass transfer limitations can play in altering reaction pathways for lignin model compounds compared with fluid phase behavior. Initial results from current studies, which focus on the detailed investigations of hydrogen transfer steps under diffusional constraints, will also be presented.

## Experimental

**Preparation of Surface-Attached Materials.** Procedures for the preparation of the surface-attached phenethyl phenyl ether,<sup>7</sup> benzyl phenyl ether,<sup>8</sup> diarylmethane,<sup>9</sup> and 1,3-diphenylpropane<sup>10</sup> models have been described. In general, the precursor phenol was adsorbed onto the dried (200 °C, 4h) surface of a fumed silica (Cabosil M-5, Cabot Corp., 200 m<sup>2</sup> g<sup>-1</sup>, ca. 4.5 SiOH nm<sup>-2</sup> or 1.5 mmol SiOH g<sup>-1</sup>) by solvent evaporation from a benzene slurry. Surface-attachment was performed in a sealed, evacuated (2 x 10<sup>-6</sup> torr) Pyrex tube at 200-225 °C for 0.5-1.0 h in a fluidized sand bath. Unattached phenol was removed by either sublimation at 225-270 °C for 1 h under dynamic vacuum (5 x 10<sup>-3</sup> torr), or Soxhlet extraction with dry benzene. Surface coverage analysis was performed on 150-200 mg samples dissolved in 30 mL 1N NaOH overnight. A phenol such as 4-phenylphenol or 4-(2-phenylethyl)phenol in 1N NaOH was added as an internal standard. The solution was acidified with HCl, and extracted with methylene chloride or diethyl ether (3 x 7 mL). The combined organic layer was typically washed with water (1 x 10 mL), dried over MgSO<sub>4</sub>, filtered, and the solvent removed under reduced pressure. Silylation with *N,O*-bis(trimethylsilyl)-trifluoroacetamide (BSTFA) in pyridine (2.5 M, 0.30 mL) produced

the corresponding trimethylsilyl ether. GC analysis was conducted on a Hewlett Packard 5890 Series II gas chromatograph employing a J & W Scientific 30 m x 0.25 mm DB-1 or DB-5 column and flame-ionization detection. Multiple assays provided surface coverages with reproducibility of  $\pm 2$  %. Two-component surfaces were prepared by co-attachment of the probe and spacer phenols in an analogous manner.<sup>10</sup>

**Pyrolysis Procedure.** The pyrolysis apparatus and procedure have been described previously.<sup>6-10</sup> In brief, a weighed amount of sample (0.4-0.6 g) was placed in one end of a T-shaped Pyrex tube, evacuated, and sealed at ca. 2 x 10<sup>-6</sup> torr. The sample was inserted into a preheated temperature-controlled ( $\pm 1.0$  °C) tube furnace, and the other end placed in a liquid nitrogen bath. The volatile products collected in the trap were dissolved in acetone (0.1-0.3 mL) containing internal standards and analyzed by GC and GC-MS. Surface-attached pyrolysis products were similarly analyzed after digestion of the silica in aqueous base, addition of internal standards, and silylation of the resulting phenols to the corresponding trimethylsilyl ethers as described above for the surface coverage analysis.

## Results and Discussion

**Aryl Ethers.** Silica-immobilized phenethyl phenyl ether ( $\approx$ PhCH<sub>2</sub>CH<sub>2</sub>OPh,  $\approx$ PPE) and benzyl phenyl ether ( $\approx$ PhOCH<sub>2</sub>Ph,  $\approx$ BPE) have been studied as models of the corresponding  $\beta$ -O-4 and  $\alpha$ -O-4 aryl ether linkages in lignin, where " $\approx$ " is used to denote the Si-O-C<sub>aryl</sub> linkage to the silica surface. Pyrolysis of  $\approx$ PPE at 375 °C revealed that the free-radical chain decay mechanism observed earlier for fluid-phase PPE remains operative on the surface.<sup>7</sup> Selectivity in formation of the two sets of products (Figure 1) arises from formation of radicals at the  $\alpha$ - and  $\beta$ - carbon sites (Figure 2). This

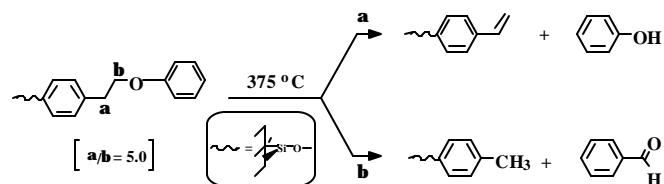


**Figure 1.** Principal products from pyrolysis of surface-immobilized PPE.

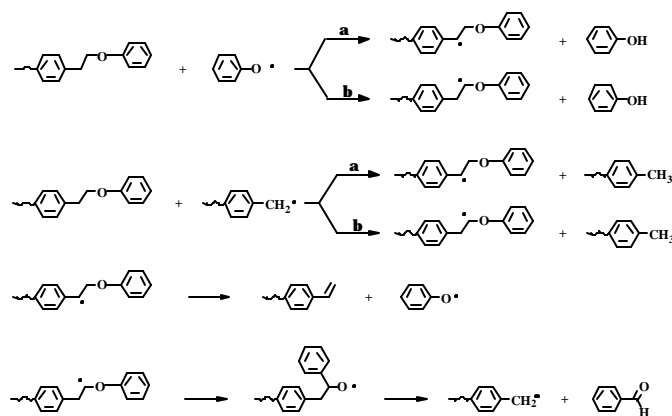


**Figure 2.** Radical chain propagation steps in pyrolysis of  $\approx$ PPE.

$\alpha/\beta$ -path selectivity was found to vary in a predictable manner with changes in substitution on the PPE framework, and the rearrangement path involving the O,C-phenyl shift remained significant in all cases.

However, in dramatic contrast to solution-phase behavior, where dilution of PPE in biphenyl solvent had no impact on the  $\alpha/\beta$ -

spacer molecules ( $\approx$ BP) caused a significant change in the product selectivity.<sup>7</sup> For example, the  $\alpha/\beta$ -path selectivity for  $\approx$ PPE/ $\approx$ BP (1:10 mol ratio) increased 4-fold to a value of ca. 20 compared with similar surface coverages of  $\approx$ PPE alone. Similar results were found when naphthalene was employed as the surface diluent, and the selectivity change must be attributable to the restrictions on mass transport. Our current hypothesis, depicted in Figure 3, is that the rigid aromatic spacer molecules introduce steric constraints that hinder the O,C-phenyl shift for the  $\beta$ -carbon radical that is the critical step in the rearrangement path. The reduced rate

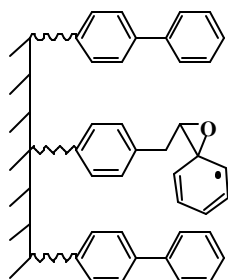


**Figure 3.** Steric constraints on O,C-phenyl shift on the silica surface in the presence of aromatic spacer molecules.

for this step would permit interconversion of  $\beta$ - and  $\alpha$ -radicals via hydrogen transfer and result in larger values for the  $\alpha/\beta$ -path selectivity. Interestingly, if a more flexible spacer molecule is employed, such as diphenylmethane, the steric constraints on the rearrangement path appear to be largely removed. Clearly, an improved understanding of the dynamics of molecular motion and interactions on these dual component surfaces would be beneficial. Studies employing steady-state and transient optical polarization spectroscopy employing surface-immobilized fluorescent probe molecules are currently underway.<sup>11</sup>

Benzyl phenyl ether linkages are much more reactive than PPE linkages, and show significant thermal decomposition at temperatures as low as 275 °C. Our pyrolysis studies on  $\approx$ BPE revealed two competitive free radical decay pathways that follow the initial homolysis of the weak O-C bond that produces phenoxy and benzyl radicals.<sup>8</sup> The first is recombination of these radicals at phenoxy ring carbons to form hydroxydiphenylmethane isomers (Figure 4). This path appears to be enhanced compared with BPE pyrolysis in fluid phases as a consequence of the restrictions on diffusion experienced by the phenoxy radical. The second path

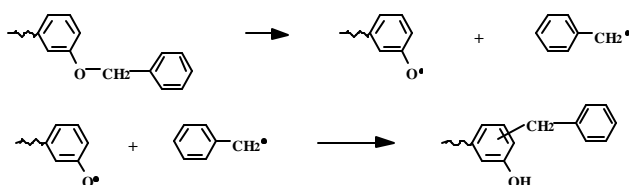


**Figure 4.** Recombination of surface-bound phenoxy and vapor-phase benzyl radicals to form hydroxydiphenylmethanes.

involves rearrangement of the intermediate  $\approx$ PhOCH•Ph radical, formed from radical hydrogen abstraction, by an O,C-phenyl shift. The rearranged radical then undergoes hydrogen abstraction to form silica-immobilized benzhydrol or hydrogen loss to form benzophenone (Figure 5). Interestingly, this rearrangement path had not been previously detected in the pyrolysis of fluid-phase BPE, yet under restricted diffusion conditions the selectivity for this rearrangement path relative to the recombination path was 1.0 at high

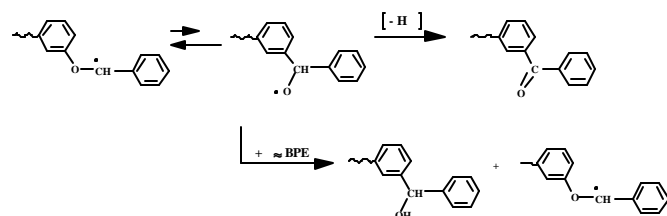


**Figure 5.** Rearrangement path for  $\approx$ BPE involving O,C-phenyl shift.

$\approx$ BPE surface coverages (0.24 mmol g<sup>-1</sup>), and 0.5 at low surface coverages (0.084 mmol g<sup>-1</sup>). This selectivity depended not only on surface coverage but also on the structure of spacer molecules, which can perturb both the hydrogen transfer step that forms  $\approx$ PhOCH•Ph and the O,C-phenyl shift. In the thermal processing of lignin, the aryl ether rearrangement pathway for BPE- and PPE-based structures generates ketone and aldehyde products that have potential commercial value. Increasingly improved knowledge of the fundamental pathways for their formation, and the pyrolysis conditions that increase or decrease their selectivity, could be important in development of advanced processes for recovering these valuable aromatic chemicals.

**Diphenylmethanes.** We showed above that thermal transformation of a model for the  $\alpha$ -O-4 aryl ether in lignin ( $\approx$ BPE) generates diphenylmethane linkages (Figure 4). Moreover, lignins modified by acidic or basic treatments as in pulping processes generates condensed structures containing diphenylmethane-type

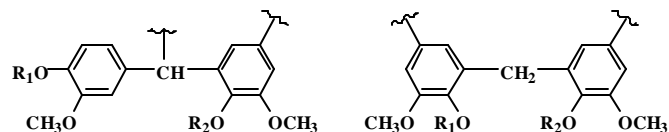


**Figure 6.** Examples of diphenylmethane-type condensed units in acid or base modified lignins.<sup>1b</sup>

linkages as illustrated in Figure 6.<sup>1b-d</sup> Thermochemical processing of these materials have the potential for PAH formation through cyclodehydrogenation reactions that form fluorene-based structures. We have been studying recently the potential for such PAH formation in the pyrolysis of simple diarylmethanes such as the silica-immobilized diphenylmethane ( $\approx$ DPM) shown in Figure 7.<sup>9</sup> At 400-425 °C,  $\approx$ DPM undergoes slow pyrolysis to form the products shown by a free radical pathway that is accelerated

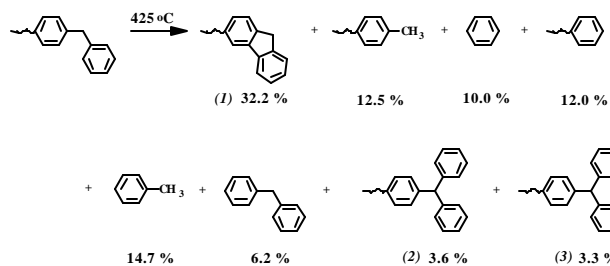


**Figure 7.** Pyrolysis of silica-immobilized diphenylmethane.

significantly in the presence of free radical sources. The cyclodehydrogenation process to form fluorene (**1**) is indeed observed to be important, and could occur at much lower temperatures for the highly substituted diphenylmethane structures found in lignin (Figure 6). Interestingly, the presence of a co-attached hydrogen donor molecule (tetralin) decreased the cyclodehydrogenation reaction (fluorene yield reduced 2.3-fold) but did not eliminate it. In contrast, fluorene formation has not been reported in fluid phase pyrolysis of DPM in the presence of tetralin or other hydrogen donors. One significant surprise was the formation of the triphenylmethanes, **2** and **3**, which have not been reported in the pyrolysis of DPM in fluid phases. The formation of these products resulted from a radical substitution process (Figure 8) promoted by the restricted mass transport on the surface. Radical substitution reactions resulting in diattached products such as **3** are representative of retrogressive cross-linking reactions that yield more refractory linkages. Similar cyclization and substitution reactions have been observed for other diarylmethanes,<sup>9</sup> although the product selectivity was found to depend on molecular orientation as well as the structure of spacer molecules.

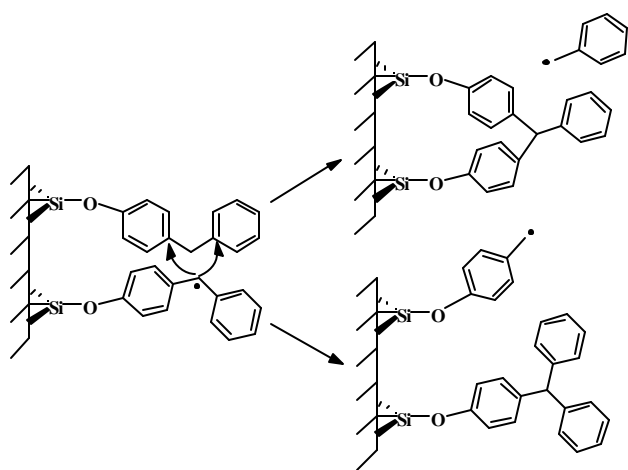
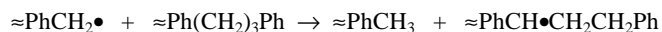


**Figure 8.** Radical displacement path leading to triphenylmethane formation.

**Oriented Hydrogen Transfer.** Our current research is addressing the question of whether molecular orientation can play a role in the rates of hydrogen transfer under diffusional constraints during thermochemical processing of fossil and renewable fuels. Efficient utilization of native hydrogen, or added hydrogen from donors, is critical in the thermochemical processing of these hydrogen deficient resources. Our earlier studies employed two component surfaces with 1,3-diphenylpropane (DPP) as a probe molecule,<sup>10</sup> a structural linkage which is also found in processed lignins.<sup>1c</sup> Pyrolysis of DPP in fluid phases occurs at reasonable rates at 375 °C by a free radical chain reaction to cleanly produce toluene and styrene.<sup>12,13</sup> This decomposition also occurred readily under surface-immobilized conditions, but the overall rate was extremely sensitive to the rate of the key hydrogen transfer propagation step on the surface.<sup>10</sup> The



hydrogen transfer was found to be very sensitive to the spatial separation of these species on the surface. Remarkably, we found that the presence of intervening spacer molecules that possess reactive benzylic C-H bonds can result in significant rate accelerations compared with  $\approx\text{DPP}$  surfaces containing aromatic spacers such as biphenyl and naphthalene. The rate acceleration was found to result

from a novel hydrogen transfer, radical relay process that is illustrated in Figure 9 for a  $\approx\text{DPM}$  spacer.

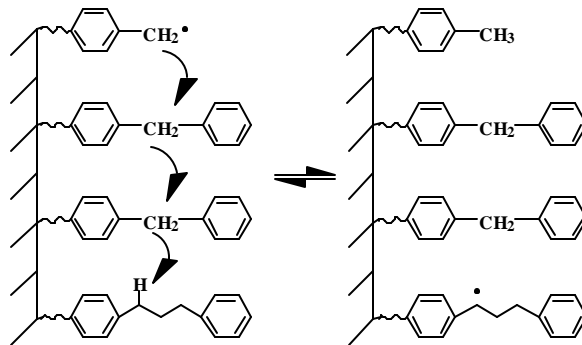


**Figure 9.** Hydrogen transfer, radical relay pathway.

This pathway was confirmed by deuterium labeling studies, and from correlation of the pyrolysis rate with the reported rates for hydrogen abstraction by benzylic radicals from the hydrogen donating spacer molecules employed.

We are now examining this hydrogen transfer pathway in more detail through the use of spacer molecules that have different orientations with respect to their attachment to the surface as illustrated in Figure 10 for the fluorene spacer.

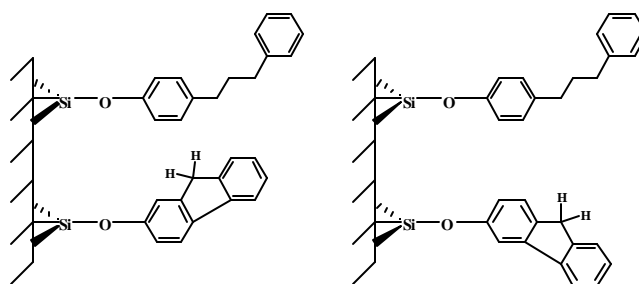


**Figure 10.**  $\approx\text{DPP}/\approx\text{2-FL}$  and  $\approx\text{DPP}/\approx\text{3-FL}$  surfaces synthesized to probe orientation effects of spacers on  $\approx\text{DPP}$  pyrolysis kinetics.

The synthesis of the 2-hydroxyfluorene precursor has been previously described.<sup>10</sup> We have now synthesized the 3-hydroxyfluorene precursor by a multi-step route that will be reported elsewhere. The  $\approx\text{DPP}$  samples shown in Figure 10 have now been prepared with a  $\approx\text{DPP}$  surface coverage of ca. 0.08 mmol g<sup>-1</sup> and the remaining available surface area containing the respective fluorene spacers. Initial pyrolysis results at 375 °C indicate that the  $\approx\text{DPP}/\approx\text{3-FL}$  pyrolysis rate is a factor of ca. 2.7 slower than the pyrolysis rate for  $\approx\text{DPP}/\approx\text{2-FL}$ . This rate decrease suggests that the fluorene spacer having benzylic hydrogens in a *para*-orientation with respect to the surface linkage is less effective at participating in the hydrogen transfer, radical relay process than the fluorene spacer having a *meta*-orientation. These preliminary findings are now being explored in more detail, and will be extended to other hydroaromatic spacers.

## Conclusions

Pyrolysis studies of silica-immobilized model compounds for structures in lignins are providing new molecular level insights into the potential impact of restricted mass transport on reaction pathways. In particular, radical rearrangement, cyclization, and

hydrogen abstraction pathways are sensitive to the structure, orientation, and spatial separation of molecules under diffusional constraints. For aryl ether models, radical rearrangement pathways give rise to new aromatic ketone and aldehyde functional groups that may have commercial value. On the other hand, thermochemical processing of lignins containing diphenylmethane-type linkages can lead to the unwanted formation of PAHs through cyclodehydrogenation reactions. An improved understanding of the role of restricted mass transport, steric effects of neighboring structures, kinetics of hydrogen transfer, etc. will be important for future progress in the thermochemical processing of lignin.

**Acknowledgment.** This research was sponsored by the Division of Chemical Sciences, Geosciences, and Biosciences, Office of Basic Energy Sciences, U.S. Department of Energy under contract DE-AC05-00OR22725 with Oak Ridge National Laboratory, managed and operated by UT-Battelle, LLC.

## References

- (1) *Lignin: Historical, Biological, and Materials Perspectives*; Glasser, W. G., Northey, R. A., Schultz, T. P., Eds.; American Chemical Society Symposium Series 742: Washington, DC, 2000. (a) McCarthy, J. L.; Islam, A. Chapter 1. (b) Lai, Y.-Z.; Xy, H.; Yang, R. Chapter 10. (c) Gargulak, J. D.; Lebo, S. E. Chapter 15. (d) Gratzl, J. S.; Chen, C.-L. Chapter 20.
- (2) *Developments in the Thermochemical Conversion of Biomass*; Bridgwater, A. V.; Boocock, D. G. B., Eds.; Blackie Academic: London, 1997.
- (3) Britt, P. F.; Buchanan, III, A. C.; Malcolm, E. A. *J. Org. Chem.* **1995**, *60*, 6523.
- (4) Britt, P. F.; Buchanan, III, A. C.; Cooney, M. J.; Martineau, D. R. *J. Org. Chem.* **2000**, *65*, 1376.
- (5) Cooney, M. J.; Britt, P. F.; Buchanan, III, A. C. *Prepr. Pap. - Am. Chem. Soc., Div. Fuel Chem.* **1997**, *42(1)*, 89.
- (6) Buchanan, III, A. C.; Britt, P. F. *J. Anal. Appl. Pyrolysis* **2000**, *54*, 127.
- (7) Britt, P. F.; Buchanan, III, A. C.; Malcolm, E. A. *Energy Fuels* **2000**, *14*, 1314.
- (8) Buchanan, III, A. C.; Britt, P. F.; Skeen, J. T.; Struss, J. A.; Elam, C. L. *J. Org. Chem.* **1998**, *63*, 9895.
- (9) Buchanan, III, A. C.; Britt, P. F.; Koran, L. J. *Prepr. Pap. - Am. Chem. Soc., Div. Fuel Chem.* **2001**, *46(1)*, 225.
- (10) Buchanan, III, A. C.; Britt, P. F.; Thomas, K. B.; Biggs, C. A. *J. Am. Chem. Soc.* **1996**, *118*, 2182.
- (11) Ivanov, I. N.; Dabestani, R.; Buchanan, III, A. C.; Sigman, M. E. *J. Phys. Chem. B* **2001**, *105*, 10308.
- (12) Poutsma, M. L.; Dyer, C. W. *J. Org. Chem.* **1982**, *47*, 4903.
- (13) Gilbert, K. E.; Gajewski, J. J. *J. Org. Chem.* **1982**, *47*, 4899.

## ENHANCED WOOD FUELS VIA TORREFACTION

Edward S. Lipinsky, James R. Arcate, and Thomas B. Reed

Innovative Thinking, Inc.  
6481 Bellbrook Place  
Worthington, OH 43085-2988

### Introduction

There is a pressing need for better biomass fuels. Raw biomass has a relatively low energy density, contains too much moisture, is too hygroscopic, can rot during storage, and is difficult to comminute into small particles. This paper presents a technology that has the potential to ameliorate many or all of these deficiencies. It is a form of thermal processing known as "torrefaction".

Torrefaction occurs during the heating of biomass between 200 C and 280 C in thermogravimetric analysis (1). Serious consideration of development of this process as a source of fuels, chemicals, and materials began with the work of Bourgeois in the 1980's (2). Pechiney used torrefied wood as a replacement for charcoal in production of metals from metal oxides (3). Work on related processes that are not directed to fuel and chemical products continues, especially in France and Finland (4,5).

Torrefaction achieves an equilibrium moisture content of 3%, reduction of mass by 20 to 30% (primarily by release of water, carbon oxides, and volatiles) while retaining 80% to 90% of the wood's original energy content as shown in Table 1 and 2. (2)

**Table 1. Characteristics of Torrefied Maritime Pine**

Species	Maritime Pine
Temperature reached (° C)	280
Yield (on bone dry wood)*	77%
Characteristics of torrefied woods	
High calorific value (bone dry)	
Kcal/kg	5,710
KJ/kg	23,900
Ashes %	
	0.55
Volatiles %	
	71.9
Fixed Carbon %	
	27.7
Elementary Analysis	
C %	59.7
H %	5.6
N %	0.25
O %	32.9

**Table 2. Mass & Energy Yields**

Species	Maritime Pine
Low calorific value of bone dry wood (kJ/kg)	19,150
Low calorific value of torrefied wood (kJ/kg)	22,600
Yield by weight %	77
Energetic Yield %	90.8

The lignocellulosic biomass feedstock is typically predried to 10% or less moisture content prior to torrefaction. Particle thickness plays an important role in torrefaction in that this parameter determines the duration of the process, given a specific heating rate. We believe that the reaction mechanisms and kinetics are different for thin (wood chips) and thick particles

(wood chunks). The chemical reactions that occur when reactive intermediates are trapped in a thick matrix differ from the situations in which products can escape and be swept away in a gas stream. The duration of torrefaction processing is adjusted produce friable, hydrophobic and energy-rich Enhanced Wood Fuels (EWF). The products of both types of reactions are hydrophobic, friable, and energy-rich fuels.

### Results and Discussion

**Chemistry.** The chemistry of torrefaction is influenced by many parameters, including: biomass composition; particle size; processing temperature and time; heating rate; and gas composition, pressure, and flow rate. In the temperature range of 220 C to 280 C, the major decomposition reactions concern hemicellulose. Cellulose also can undergo similar polymer restructuring. Cellulose and lignin also undergo depolymerization reactions, but to a lesser degree.

Commercially available dynamic simulation software (STELLA®, from High Performance Systems, Inc.) was employed to model the reactions of biomass. The model contains modules for hemicellulose, cellulose, lignin, and biomass. Here, we discuss the hemicellulose module of the model (Figure 1).

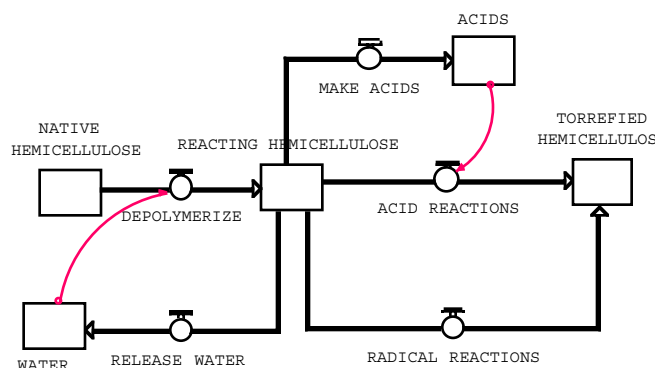


**Figure 1.** Dynamic simulation model of hemicellulose torrefaction.

The flow sheet shows stocks of hemicellulose, torrefied hemicellulose, water, and acids. The pipes show the flow of materials from starting material to products. The "wires" show transfer of information.

During thermolysis, native hemicellulose is partly depolymerized by hydrolysis and/or thermal chain scission to provide "reacting hemicellulose". This intermediate is decomposed by acid and radical reactions to yield many substances (e.g., furfural) that recombine to form torrefied hemicellulose. Water and acids are formed during the above reactions and are released into the reaction environment (6). Some of this water may be reused to depolymerize hemicellulose or to release acids from the hemicellulose by hydrolysis of acetate groups. Acids can also be formed by radical reactions.

The water and acids released by hemicellulose become available to depolymerize cellulose and lignin. Wooten (7) and Pastorova (8) have demonstrated that microcrystalline cellulose can form "disordered pyrolytic cellulose" that is a 3-dimensional polymer at about 270 C. If the cellulose is exposed to acids and radicals that originate with hemicellulose, even more degradation of cellulose would be expected. This disordered cellulose is thermostable and contains furan, aliphatic, and keto groups. Evans, et.al. have shown that lignin releases some small phenolic

fragments within the temperature range of torrefaction (9). There also are opportunities for grafting of torrefied hemicellulose onto cellulose and/or lignin. Thus, all of the lignocellulose polymers can participate in torrefaction.

**Process description.** Because water can play a significant role in torrefaction, the potential effects of added water (in the form of superheated steam or saturated steam) merit investigation. Figure 2 shows a generalized process schematic of such a process.

Raw lignocellulosic biomass is predried to less than 10% moisture using superheated steam (SHS). SHS has a much higher heat capacity than does hot air or nitrogen. Steam also provides an airless drying environment that reduces yield losses from oxidation.

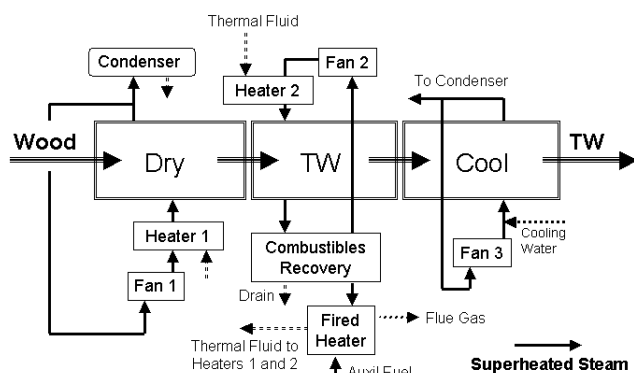


**Figure 2.** Enhanced Wood Fuels Production Process

Both batch and continuous reactors have been used to produce torrefied wood. We prefer a continuous reactor using superheated steam at atmospheric pressure to dry and torrefy the wood feed. Torrefaction is, on balance, endothermic and releases water, acetic acid, carbon dioxide, carbon monoxide, and other volatiles. This local cooling effect needs to be counteracted. The reaction temperature is closely monitored and controlled. To avoid possible runaway exothermic conditions the torrefaction temperature reaction will not be allowed to exceed 280 C.

Steam containing wood acids and other volatiles is vented from the reactor continuously. This stream is condensed for recovery of acids and combustible volatiles or for waste treatment and disposal purposes.

The EWF is cooled to a safe unloading temperature. The specific properties of the final EWF product may vary depending on the cooling procedure because the hot EWF contains free radicals (10).

EWF can be used in cofiring with coal in electric power plants. Alternatively, EWF can be used in manufacturing fuel pellets and briquettes. Densifying EWF will produce energy-rich, transportable fuels with good properties for outdoor storage.

**Cofiring with Coal at Power Plants.** Cofiring involves substituting biomass fuels for a portion of coal in an existing power plant furnace. This allows the energy in biomass to be converted to electricity with the high efficiency (in the 33% to 40% range) of a modern coal-fired power plant. Table 3 presents examples of various levels of EWF cofiring.

**Table 3.** Cofiring TW with Coal in PC Power Plants

EWF tonnes per year	GWh/year	Mwe @ 7000h
30,000	75	12
60,000	150	25
90,000	225	37
120,000	300	49

Compared to the coal it replaces, biomass reduces sulfur dioxide (SO<sub>2</sub>), nitrogen oxides (NO<sub>x</sub>), and net greenhouse gas emissions of CO<sub>2</sub>.

Cofiring EWF is more attractive than using raw biomass such as wood chips because EWF is friable and can be blended, pulverized and co-fired with coal. The capital and operating costs for separate biomass fuel feed and firing systems are avoided.

**Densification.** The mass density of EWF pellets is about 23kJ/Kg, compared with 19.3 kJ/Kg for conventional pine wood pellets. Densification of EWF to a volume energy density of about 18 GJ/m<sup>3</sup> can be attained by pelletization. Although this is less than coal (29 GJ/m<sup>3</sup>), it is 20% higher than commercial wood pellets. In addition, less than half as much electricity is consumed making EWF pellets. A study for the Pellet Fuel Institute (11) indicated that electricity costs are about \$10/ton of wood pellet product. These data are based on old experiments. There are methods for increasing the energy value and reducing further the energy costs of EWF pellets (12).

Densified EWF products have good prospects for use in pellet stoves in residential and commercial heating markets. The size of this market is more than 700,000 tons/year in the United States (13). EWF also could be briquetted or used to make HeatLogs® analogs. This segment of the domestic fuel market is larger than the pellet market. The fireplace log market has special requirements for sustained burning and flame quality because it is frequently a recreational fuel, rather than a utilitarian fuel.

## Conclusions

Torrefaction provides fuels that are rich in energy, low in moisture content, resistant to weathering, and easily pulverized or densified. Although these are good features, we must also consider the challenges that confront EWF developers.

The European pioneers in torrefaction have abandoned fuel markets and modified the process so that they can focus on furniture and construction markets. The first major **challenge** in development of EWF is to find and develop viable fuel markets. An example of a potentially viable opportunity is conversion of the wood pellet industry into a torrefied wood pellet industry. This is a matter of inserting torrefaction into an existing enterprise that already has a raw material supply, predrying equipment, and marketing channels. This is much cheaper than a “green field” venture. Another example is the cofiring of EWF with coal to improve environmental performance.

The thermal technology for torrefying biomass uses moderate temperatures in the range of 220 C to 280 C. Traditional torrefaction technology required many minutes for completion of the reactions. However, slowness is not an inherent feature of torrefaction. The major processing **challenge** is to create processes that reduce the processing time to a desirable degree. The superheated steam torrefaction process discussed here may be a successful example.

The chemical reaction mechanisms and kinetics that are at the foundation of torrefaction are complex and not well understood. The problems arise from the interaction of both acids and free radicals with the polymers that comprise lignocellulose. The major **challenges** here are to devise experiments that distinguish acid-catalyzed reactions from radical reactions and to

apply to torrefaction reactions some of the methods used in elucidating radical reaction pathways in hydrocarbon cracking. Modeling can help in thinking about the system, but usable experimental data are essential for progress in this activity.

## References

- (1) Gaur, S., and Reed, T., Thermal Data for Natural and Synthetic Fuels, Dekker, New York, 1998.
- (2) Bourgeois, J., and Guyonnet, R., in Bioenergy 84, Volume III, edited by H. Egneus, Elsevier, 1985, pp. 153-159.
- (3) Girard, P., and Shah, N., Recent Developments on Torrefied Wood, an Alternative to Charcoal for Reducing Deforestation. FAO/CNRE Workshop, Norway 1989, pp. 101-114.
- (4) Dirol, D., and Guyonnet, R., Report to 24<sup>th</sup> Annual Meeting of The International Research Group on Wood Preservation, Stockholm, 1993.
- (5) Viitaniemi, P.; Jamsa, S., Ek, P., Viitanen, H., U.S. Patent 5,678,324, October 21, 1997
- (6) Bourgeois, J. and Guyonnet, R., Wood Sci. and Tech., **22**, 143-155, (1988); and **23**, 303-310, (1989).
- (7) J. Wooten, et.al., Fuel Chemistry Division Preprints, **46** (1), 191 (2001).
- (8) I. Pastorova, et.al., Carbohy. Res., **248**, 151-165 (1993) and, **262**, 27-47 (1994).
- (9) Evans, R.A., Milne, T.A., Soltys, M.N., J. Anal. Appl. Pyrolysis **9** (1986) 207-236.
- (10) Shafezadeh, F., in Fundamentals of Thermochemical Biomass Conversion, ed. by Overend, Elsevier, New York, 1985, p.183-217.
- (11) NEOS Corporation., Wood Pelletization Sourcebook, 1995, available from Pellet Fuel Institute.
- (12) Reed, T. B., Trezek, G. and Diaz, L., in "Thermal Conversion of Solid Wastes", J. L. Jones and S. B. Radding, ACS Symposium Series 130, Was D.C. pp 169-177, 1980.).
- (13) Pellet Fuel Institute Annual Survey, 2000-2001 (available from Pellet Fuel Institute).

## EXHAUST EMISSIONS FROM A SI ENGINE FUELED WITH PYROLYSIS GAS

M. Ratcliff\*, C. Baca-Overly, S. Deutch, C. Feik, J. Graham and S. Phillips

National Renewable Energy Laboratory, 1617 Cole Blvd, Golden, Colorado, USA 80401

Fax: 303-384-6363; [matthew\\_ratcliff@nrel.gov](mailto:matthew_ratcliff@nrel.gov)

### Introduction

A 4-cylinder, 4-stroke, spark ignition (SI) engine of 2.5L displacement and 9.4 compression ratio was operated for over 100 hours on wood-derived pyrolysis gas to measure exhaust emissions and performance characteristics. The pyrolysis gas (15-16.5 MJ/Nm<sup>3</sup>) was produced from mixed hardwood and softwood pellets, in NREL's Thermochemical Process Development Unit (TCPDU) using a two-step, indirect gasification process [1]. A typical fuel gas composition is shown in Table 1. In addition, light gasifier "tar" that escaped the pyrolysis gas clean-up train was consumed as fuel. These "tar" components were principally benzene (~1 vol. %) and smaller amounts of toluene, naphthalene and related aromatics.

**Table 1. Pyrolysis Gas Composition from TCPDU in Volume %**

H <sub>2</sub>	CO	CH <sub>4</sub>	C <sub>2</sub> H <sub>4</sub>	C <sub>2</sub> H <sub>2</sub>	C <sub>2</sub> H <sub>6</sub>	CO <sub>2</sub>	N <sub>2</sub>
17.9	34.9	15.8	4.7	1.0	0.5	17.3	6.0

The manufacturer's rated output for the engine-generator on natural gas (~37 MJ/Nm<sup>3</sup>) was 17 kW. The engine-generator also achieved 17 kW on pyrolysis gas, albeit with slightly less stable performance. This is in contrast to spark ignition engines fueled with producer gas (5.5-7.0 MJ/Nm<sup>3</sup>), which typically must be derated 30-40% compared to natural gas [2]. At loads # 13 kW, the genset's performance on pyrolysis gas was as good or better than natural gas, as measured by the ability to maintain 60 ∓ 0.3 Hz.

### Results and Discussion

The regulated exhaust emissions from both natural and pyrolysis gas are compared in Figure 1, as a function of Lambda ( $\lambda$  = actual Air/Fuel ) stoichiometric Air/Fuel) at a load of 13 kW and ignition timing of 30° Before Top Dead Center (BTDC). NOx from natural gas peaked (44.3 lb/MWh) at  $\lambda$  = 1.10, then decreased with leaner air/fuel mixtures. The lean operating limit for natural gas (i.e. for a generator frequency = 60 ∓ 0.3 Hz) was  $\lambda$  = 1.18. At this setting, the CO and total hydrocarbon (THC) exhaust emissions were similar to those from pyrolysis gas. However, the NOx emitted from natural gas was 29.2 lb/MWh, in contrast to 382 lb/MWh from pyrolysis gas. There are three possible explanations for this large, fuel dependent, difference in NOx. Fuel-bound nitrogen in the wood, which produces NOx upon combustion, contributes to the total. However, given that the nitrogen content in the wood pellet feedstock was < 0.03 wt %, this can not explain a significant amount. Thermal NOx enhancement, due to higher localized flame temperatures within the combustion chambers, is another contributing mechanism. This hypothesis may be supported by the exhaust port temperature data. For the comparison in Figure 1, the average exhaust port temperature from natural gas at  $\lambda$  = 1.18 was 588°C; while the average was 592°C from pyrolysis gas at  $\lambda$  = 1.22. The slightly higher average exhaust

port temperature was measured despite the presence of ~17% CO<sub>2</sub> in the pyrolysis gas. The CO<sub>2</sub> would be expected to reduce the combustion and exhaust temperatures relative to natural gas, due to its high heat capacity. This is the key mechanism by which exhaust gas recirculation (EGR) affects NOx reductions in reciprocating internal combustion engines [3]. Finally, the prompt NOx mechanism may be the principal explanation for the higher NOx emissions from pyrolysis gas, due to the presence of ethylene and acetylene in the fuel, typically 5% and 1%, respectively. The prompt NOx chemistry depends on the presence of CH radicals, which may arise in significant amounts from cleavage reactions of unsaturated hydrocarbons [4].

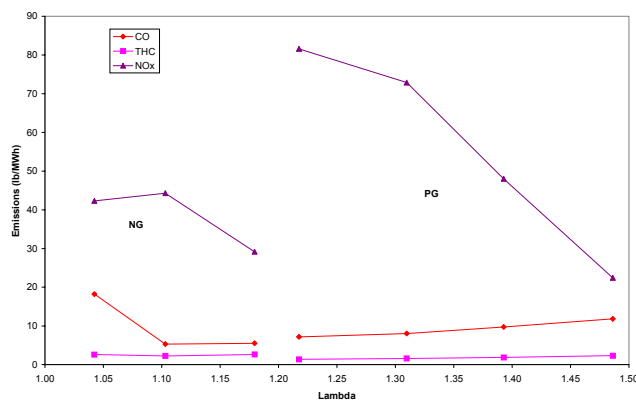


**Figure 1.** Regulated exhaust emissions from natural gas (NG) and pyrolysis gas (PG) at a load of 13 kW and ignition timing of 30° BTDC.

Figure 1 also shows that  $\lambda$  could be increased with pyrolysis gas to a lean operability limit of 1.49 (generator frequency = 60 ∓ 0.3 Hz), resulting in a NOx emission of 22.4 lb/MWh. At this condition, the averaged exhaust port temperature was 541°C, or 50°C lower than at  $\lambda$  = 1.22. Both CO and THC emissions from pyrolysis gas began to increase with increasing  $\lambda$ . This trend was expected, because unburned-fuel emissions increase as combustion temperatures decrease, or the engine enters lean-misfire conditions [5]. Because carbon monoxide is a major fuel component in pyrolysis gas, and CO oxidation kinetics are relatively slow, much of the CO in the exhaust should be considered to be unburned fuel.

In order to reduce NOx emissions, the limits of lean-burn operation and ignition timing were explored. Figure 2 shows NOx versus load curves from pyrolysis gas and natural gas. The top pyrolysis gas curve is from  $\lambda$  = 1.30, and 24° BTDC. Up to approximately 9 kW, the pyrolysis gas NOx emissions from this setting were very similar to the best natural gas results ( $\lambda$  = 1.03, 24° BTDC). At higher loads there was an increase in NOx compared to natural gas, despite the much leaner air-fuel mixture. The next lower pyrolysis gas curve in Figure 2 was obtained by optimizing the air-fuel ratio and ignition timing for each load tested. These data show that reducing NOx from pyrolysis gas combustion was most effectively done by lean operation, even when the ignition timing had to be advanced to maintain stable engine operation. The broad air flammability limits of pyrolysis gas are due to the presence of hydrogen in the fuel, as well as the relatively low concentration of nitrogen (compared to producer-gas). By exploiting this quality with lean-burn operation, we were able to achieve significantly lower, part-load NOx emissions using pyrolysis gas. Nevertheless, it appears that some form of exhaust after-treatment will be necessary

for both pyrolysis and natural gas fueled, spark ignition engine-generator systems, in order to achieve some existing and proposed NO<sub>x</sub> standards [6]. The “Lean-NO<sub>x</sub>” catalysts being developed for diesel engines may be ideal for pyrolysis gas, in order to achieve NO<sub>x</sub> standards and maintain high energy efficiency. However, those catalytic converters are not commercially available. Therefore, stoichiometric operation with conventional 3-way catalysts is the best approach.

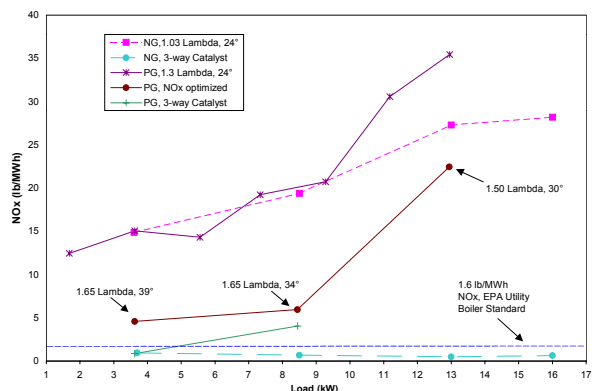


**Figure 2.** NO<sub>x</sub> emissions from pyrolysis gas and natural gas as a function of load, Lambda, ignition timing and 3-way exhaust catalyst.

At the bottom of Figure 2 is a two-point NO<sub>x</sub> line from pyrolysis gas fueled operation with a 3-way catalyst. Difficulties maintaining stoichiometric operation prevented collection of quality data, especially at higher loads. This was principally due to a lack of feedback air-fuel ratio control. The data presented suggest that NO<sub>x</sub> levels similar to those from natural gas with the 3-way catalyst (also shown in Figure 2) are possible using this strategy. A larger catalytic converter would perhaps be necessary, because of the higher raw NO<sub>x</sub> emissions from pyrolysis gas during stoichiometric operation. In either fuel case, a larger 3-way catalyst, or additional engine NO<sub>x</sub> control, such as EGR, would be required to meet present and future NO<sub>x</sub> standards for states such as Texas (0.14 lb/MWh in east Texas after January 1, 2005) [6].

At a given  $\lambda$ , NO<sub>x</sub> from pyrolysis gas fueling was higher than from natural gas. However, because of the ability to operate the engine at higher air/fuel ratios on pyrolysis gas at comparable outputs, the differences in NO<sub>x</sub> emissions between the two fuels can be negligible. Regardless, the lowest measured NO<sub>x</sub> value at a load of 9 kW is still an order of magnitude higher than proposed U.S. emissions standards for small generators. Further reductions in NO<sub>x</sub> emissions from SI engines will have to come from enhanced lean-burn performance and/or addition of exhaust after-treatment technologies. Alternatively, engines could run stoichiometrically with feedback control and a 3-way exhaust catalyst, as developed by the automotive industry.

## References

- 1) Ratcliff, M. A.; et. al. *Biosyngas Characterization Tests*, NREL/TP-510-31224. **1998**.
- 2) Shashikantha, Parikh, P. P. *Spark Ignition Producer Gas Engine and Dedicated Compressed Natural Gas Engine Technology Development and Experimental Performance Optimization*. SAE 1999-01-3515, **1999**.

- 3) Tomazic, D. *A Primer on Exhaust Gas Recirculation*. Diesel Progress. **October 2001**, 26-30.
- 4) Miller, J. A.; Bowman, C. T. *Prog. Energy Combust. Sci.* **1989**, 15, 287-338.
- 5) Abdel-Rahman, A.A. *Int. J. Energy Res.* **1998**, 22, 483-513.
- 6) *Air Quality Standard Permit for Electric Generating Units*. Air Permits Division, Office of Permitting, Registration & Remediation. Texas Natural Resource Conservation Commission. **2001**.

# FORMATION OF NITROGEN CONTAINING POLYCYCLIC AROMATIC COMPOUNDS FROM THE CO-PYROLYSIS OF CARBOHYDRATES AND AMINO ACIDS

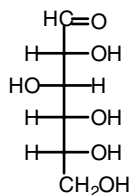
Phillip F. Britt, A. C. Buchanan, III, Clyde V. Owens, Jr., and J. Todd Skeen

Chemical Sciences Division  
Oak Ridge National Laboratory  
P.O. Box 2008, Oak Ridge, TN 37831-6197

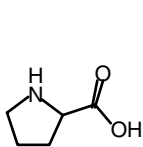
## Introduction

Utilization of biomass for fuel or energy production can reduce our dependence on fossil fuels, and reduce the emissions of CO<sub>2</sub> and other hazardous elements, such as sulfur, lead, and mercury, to the environment. However, pyrolysis, gasification, and combustion of biomass produces polycyclic aromatic hydrocarbons (PAHs),<sup>1</sup> which are environmental pollutants. Nitrogen-containing polycyclic aromatic compounds (N-PACs) can also be formed from pyrolysis of proteinaceous materials found in agriculture and forestry residues (1-25 wt% protein) and in animal waste and sewage (15-30 wt% protein).<sup>2,3</sup> To reduce the formation of PAHs and N-PACs from the thermal processing of biomass, more information is needed on the chemical reactions that lead to these compounds.

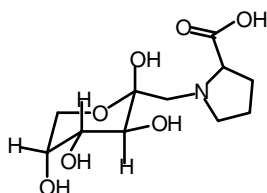
In this investigation, the formation of PAHs and N-PACs from the pyrolysis of amino acids and carbohydrates was studied. The low temperature reactions (<350 °C) between amino acids and carbohydrates have been extensively studied.<sup>4</sup> The non-enzymatic browning reaction (i.e., Maillard reaction) leads to a deterioration in the quality of food during storage and cooking (via formation of polymeric brown pigments and volatile compounds).<sup>5</sup> The Maillard reaction is also responsible for the formation of the aroma and flavor of tobacco smoke.<sup>6</sup> However, the high temperature pyrolysis of the intermediates in the Maillard reaction has not been investigated. In this study, the formation of PAHs and N-PACs from the independent pyrolysis of proline and glucose will be compared to pyrolysis of mixtures of proline and glucose and to the pyrolysis of (1-[2'-carboxy]pyrrolidinyl)-1-deoxy-D-fructose), the proline Amadori compound, which is a key intermediate in the Maillard reaction.



D-Glucose



Proline



1-[(2'-Carboxy)pyrrolidinyl]-1-deoxy-D-fructose

## Experimental

L-Proline (Acros), D-glucose (Acros), acetone (J&W Residue analysis) were used without additional purification. 1-[2'-carboxy]pyrrolidinyl]-1-deoxy-D-fructose was prepared as previously described.<sup>7</sup> Perdeuterated PAHs (phenanthrene-*d*<sub>10</sub> and 1,2-benzanthracene-*d*<sub>12</sub>) were obtained from Aldrich.

The flow pyrolysis procedure has already been described in detail and will be briefly reviewed.<sup>8</sup> The pyrolysis tube consists of three different sizes of quartz tubing fused together: a 12 in. by 3/4 in. o.d. tube (sublimation chamber) connected to a 19 in. by 0.354 in. o.d. 0.276 in. i.d. tube (the reaction chamber) which tapers to a 1/4 in. o.d. piece of tubing 2 in. long (exit to traps) which terminates with a o-ring

sealed ball joint (size 12/5). The pyrolysis tube was connected to two traps by ball joints cooled to 77K. The tip of the entrance tube for the second trap was ca. 1 in. deep into a loosely packed plug of clean glass wool. The glass wool trapped aerosol particles formed at high flow rates (>100 mL min<sup>-1</sup>). In a typical run, a quartz boat (1 in. x 5/8 in. x 3/8 in.) was charged with a known amount of substrate (typically 200 - 1200 mg) and placed in the 3/4 in. o.d. tube. A glass tube containing a fitting for the introduction of helium and an Ace-Thred adapter was connected to the pyrolysis tube via a 3/4 in. Cajon Ultra-Torr union. Gas flow was controlled by a MKS mass flow controller (either 200 or 1000 mL min<sup>-1</sup> ± 3% accuracy) and confirmed with a soap bubble meter on the exit of the pyrolysis apparatus (after the cold traps). The residence time in the furnace was calculated from the volume of the reactor (11 mL) in the hot zone (12 in. hot zone with temperature ±2.9 °C at 650 °C), the gas flow rate at room temperature, and a correction for the gas flow rate at the reaction temperature. The sample chamber was heated to 460 °C via an aluminum tube (2.4 in. o.d./2.1 in. i.d. x 6 in long) wrapped with heat tape. The temperature of the reaction chamber was monitored and controlled via two thermocouples next to the sample. The sample was pushed into the sublimation chamber by a glass rod, inserted through the Ace-Thred adapter with an O-ring seal, or by a thermocouple wrapped around the sample boat. The quartz pyrolysis tube was heated by a horizontally mounted three-zone Carbolite tube furnace. The pyrolysis tube was wrapped with a heating tape at the exit of the furnace and heated to ca. 200 °C to prevent condensation of the products. After the pyrolysis, both traps were washed with high purity acetone and the washings were combined (total volume 10-20 mL). Solutions of phenanthrene-*d*<sub>10</sub> and 1,2-benzanthracene-*d*<sub>12</sub> were added as standards, and the reaction mixtures were analyzed by GC-MS and quantitated by GC-FID (see below) or GC-MS with splitless injection.

Product analysis was performed on a Hewlett-Packard 5890 Series II gas chromatograph equipped with a flame ionization detector, and the identification of products was confirmed by comparison of retention times and mass spectral fragmentation patterns from authentic samples using a Hewlett-Packard 5972A/5890 Series II GC-MS (EI 70 eV). Both instruments were equipped with a J&W DB-5 5% diphenyl-95% dimethylpolysiloxane capillary column (30 m x 0.25 mm i.d. with 0.25 µm film thickness). The injector temperature was 280 °C, and the detector temperature was 305 °C. The oven was programmed with an initial temperature of 45 °C, and the temperature was ramped to 300 °C at 10 °C min<sup>-1</sup> and held for 20 minutes. The carrier gas, helium, was set at a constant flow rate of 1.0 mL min<sup>-1</sup>. Samples were injected four times onto the GC using a HP 7673 autosampler. Typical shot to shot reproducibility was ±3-5%. The products were quantitated by averaging the GC-FID output relative to the internal standards. Response factors were measured with authentic samples or estimated from measured response factors for structurally related compounds and based on carbon number relative to the internal standards (phenanthrene-*d*<sub>10</sub> or 1,2-benzanthracene-*d*<sub>12</sub>). The yield of PAHs was also determined by GC-MS analysis from calibration curves of the individual PAHs relative to the deuterated PAH standards in a concentration range of 0.5 to 20 µg mL<sup>-1</sup>. The limits of detection (LOD) for the PAHs depended upon the complexity of the reaction mixture, but the LOD was typically 20 µg g<sup>-1</sup> for GC-FID analysis and 0.2 µg g<sup>-1</sup> for GC-MS analysis with splitless injection.

## Results and Discussion

The pyrolysis of proline was initially investigated at 840 °C with a residence time of 10 s (longest possible residence time for the reactor used in this study) to compare the yield of products formed in

previous studies at 850 °C and 840 °C with estimated residence times of 30 s and 10 s, respectively.<sup>9,10</sup> In general, the yield of products agree with those previously reported, except the ratio of isoquinoline to quinoline is low (see Table 1). Isoquinoline has been reported to rearrange to quinoline at 850 °C with a residence time of 13 s, but the conversion was low (2.3%).<sup>11</sup> Thus, it is unlikely that isomerization of isoquinoline is important under these reaction conditions. The 1-[2'-carboxy]pyrrolidinyl]-1-deoxy-D-fructose (i.e., the proline Amadori compound) was pyrolyzed at 840 °C for 10 s, and the yield of phenanthrene and quinoline increased 12 fold and 9-fold, respectively compared to proline. A similar increase in the yield of phenanthrene and quinoline was observed in the pyrolysis of a 1:1 mixture (by wt) of glucose and proline. Clearly, there is a synergistic reaction between the glucose and proline to enhance the formation of PAHs and N-PACs compared to pyrolysis of the individual components.

**Table 1. Product Yields from the Pyrolysis of Proline, Glucose, and Proline Amadori Compound**

Compound	Proline <sup>9</sup>	Proline <sup>10</sup>	Proline <sup>a</sup>	Glucose <sup>a</sup>	Amadori <sup>a,b</sup>	Proline Glucose <sup>a,c</sup>
Temperature	850 °C	840 °C	840 °C	840 °C	840 °C	840 °C
Time	ca. 30 s	20 s	10 s	10 s	10 s	10 s
Products (mg/g)						
Pyrrole	38.7	27.2	38.9	-	6.7	3.0
Benzene	1.1	1.3	1.6	2.2	8.9	6.2
Benzonitrile	1.0	0.3	1.6	-	1.9	1.7
Quinoline	0.9	0.3	0.3	-	2.6	2.1
Isoquinoline	1.9	1.7	0.09	-	0.6	0.5
Phenanthrene	0.09	NR	0.05	0.10	0.6	0.3
Pyrene	0.09	NR	0.06	0.02	0.2	0.2

<sup>a</sup> This study <sup>b</sup> 1-[2'-carboxy]pyrrolidinyl]-1-deoxy-D-fructose. <sup>c</sup> 1:1 Mixture by weight.

The pyrolysis of the 1-[2'-carboxy]pyrrolidinyl]-1-deoxy-D-fructose, a 1:1 mixture of glucose and proline, glucose, and proline was investigated at 800 °C and 700 °C with a residence time of 1.0 s. For all substrates except proline, char was found in the reactor at 800 °C and in the sublimation boat. The yield of char in the sublimation boat for 1-[2'-carboxy]pyrrolidinyl]-1-deoxy-D-fructose, glucose, and the glucose:proline mixture was 15, 4, and <1 wt%, respectively. The yield (mg product per gram of substrate) of selected products from the pyrolysis of 1-[2'-carboxy]pyrrolidinyl]-1-deoxy-D-fructose is shown in Figure 1. A variety of one to five membered ring PAHs and cyano-substituted PAHs were detected in addition to N-PACs. Molecular ions were also found for products that appeared to be azapyrene (*m/z* 203), azachrysene (*m/z* 229), and azabenz[a]pyrene (*m/z* 253), but the identity of these products have not been confirmed. A similar slate of products was formed from the pyrolysis a 1:1 mixture of glucose and proline, and PAHs as large as benzo[a]pyrene (0.23 µg/g) and benzo[b,j,k]fluoranthrenes (combined yield 4.6 µg/g) were formed. Pyrolysis of proline or glucose at 800 °C for 1.0 s produced lower yields of PAHs and N-PACs compared to the Amadori compound as shown in Figures 2 and 3. Low yields of benzo[a]pyrene (0.81 and 0.70 µg/g), benzo[b,j,k]fluoranthrenes (0.24 and 2.1 µg/g), and benzo[a]anthracene (0.43 and 3.2 µg/g) were also found in the pyrolysis of proline and glucose, respectively.

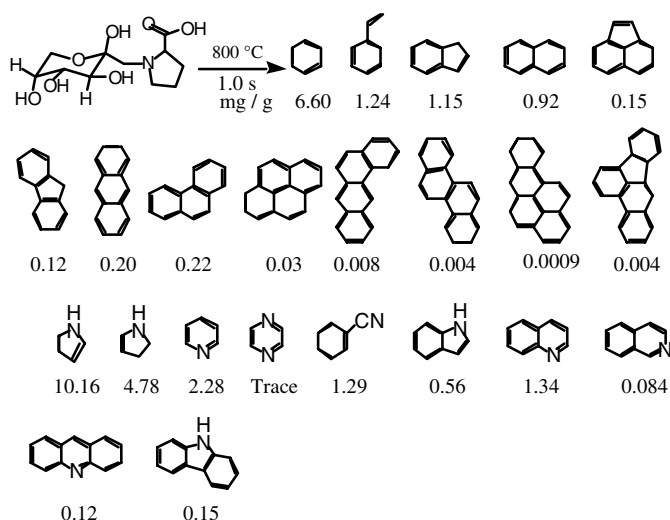


**Figure 1.** Selected products from the pyrolysis of 1-[2'-carboxy]pyrrolidinyl]-1-deoxy-D-fructose at 800 °C with a residence time of 1.0 s.

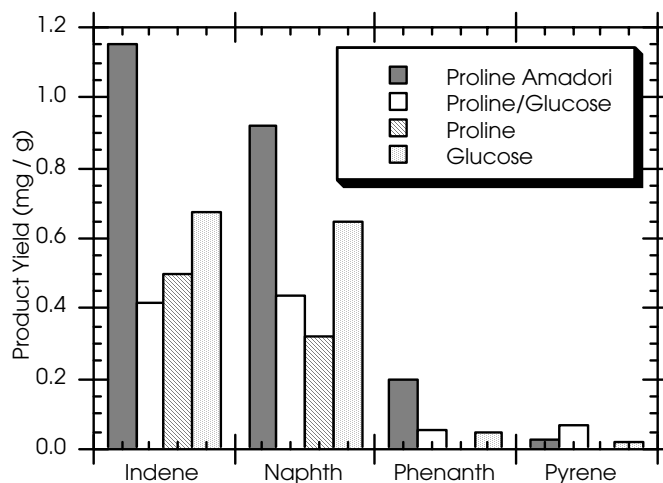


**Figure 2.** PAH yields from the pyrolysis of 1-[2'-carboxy]pyrrolidinyl]-1-deoxy-D-fructose (Proline Amadori), 1:1 mixture of proline and glucose, proline, and glucose at 800 °C with a residence time of 1.0 s. Naphth and Phenanth is naphthalene and phenanthrene.

Pyrolysis of proline at 700 °C with a 1.0 s residence time only produced single ringed compounds (pyrrole, benzene, styrene, and benzonitrile) and no multi-ringed aromatic compounds. Pyrolysis of 1-[2'-carboxy]pyrrolidinyl]-1-deoxy-D-fructose or a 1:1 mixture of proline and glucose produced significant yields of N-PACs as shown in Figure 4. N-PAC formation was clearly enhanced by the presence of glucose. PAH yields were also enhanced relative proline and glucose as shown in Figure 5.

## Conclusions

These experiments clearly showed that glucose increased the formation of N-PACs from the pyrolysis of proline at 700 to 840 °C. PAH yields were also enhanced compared to the independent pyrolysis of proline or glucose. The formation of N-PACs and PAHs from pyrolysis of additional amino acids and carbohydrates is currently under investigation.

**Acknowledgment.** The authors gratefully acknowledge the financial support from Philip Morris USA. CVO was supported by an appointment to ORNL Postdoctoral Research Associates program administered jointly by Oak Ridge Institute for Science and Education and Oak Ridge National Laboratory.

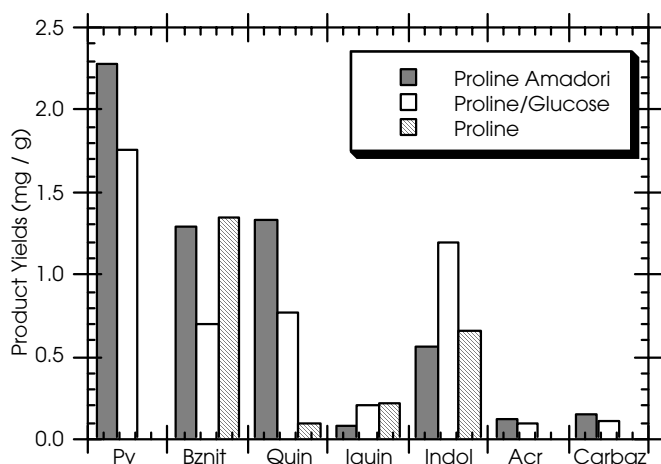


**Figure 3.** N-PAC yields from the pyrolysis of 1-[2'-carboxy]pyrrolidinyl]-1-deoxy-D-fructose (Proline Amadori), 1:1 mixture of proline and glucose, proline, and glucose at 800 °C with a residence time of 1.0 s. Products include pyridine (Py), benzonitrile (Bznit), quinoline (Quin), isoquinoline (Isoquin), indole, acridine (Acr), and carbazole (Carbaz).

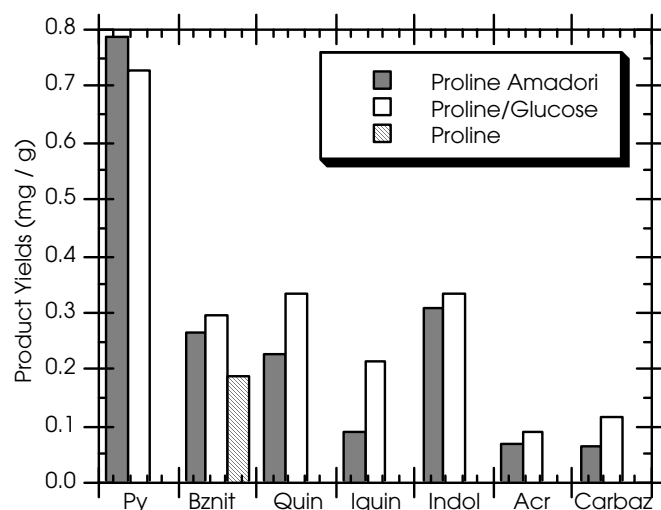


**Figure 4.** N-PAC yields from the pyrolysis of 1-[2'-carboxy]pyrrolidinyl]-1-deoxy-D-fructose, 1:1 mixture of proline and glucose, proline, and glucose at 700 °C with a residence time of 1.0 s. See Figure 3 for products.

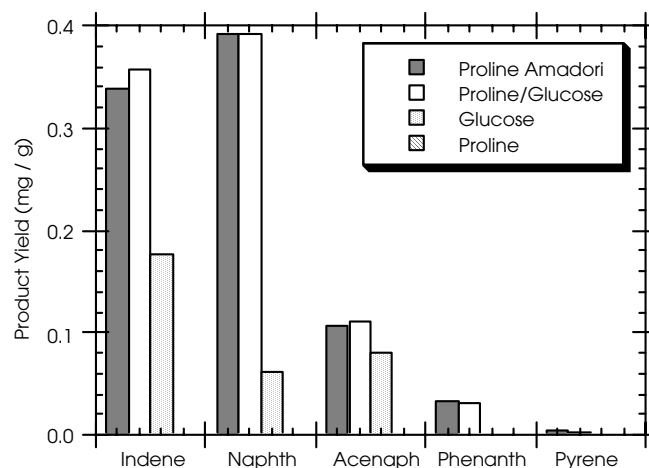


**Figure 5.** PAH yields from the pyrolysis of 1-[2'-carboxy]pyrrolidinyl]-1-deoxy-D-fructose, 1:1 mixture of proline and glucose, proline, and glucose at 700 °C with a residence time of 1.0 s.

## References

- (1) (a) *Developments in Thermochemical Biomass Conversion*; Bridgwater, A. V.; Boocock, D. G. B., Eds; Blackie Academics: London, 1997 and references therein. (b) Elliott, D. C. In *Pyrolysis Oils from Biomass: Producing, Analyzing and Upgrading*; Soltes, E. J., Milne, T. A., Eds.; ACS Symposium Series 376; American Chemical Society: Washington, DC, 1988; Chapter 6. (c) *Fundamentals of Thermochemical Biomass Conversion*; Overend, R. P., Milne, T. A., Mudge, L. K., Eds.; Elsevier: Essex, UK, 1985.
- (2) (a) Detroy, R. W. In *Organic Chemicals from Biomass*; Goldstein, I. S., Ed.; CRC Press: Boca Raton, FL, 1981; Chapter 3. (b) Barton, G. M. In *Organic Chemicals from Biomass*; Goldstein, I. S., Ed.; CRC Press: Boca Raton, FL, 1981; Chapter 11.
- (3) For examples see: (a) Patterson, J. M.; Chen, W.-Y.; Smith, W. T., Jr. *Tob. Sci.* **1974**, *18*, 99. (b) Elliott, D. C.; Sealock, L. J., Jr.; Butner, R. S. In *Pyrolysis Oils from Biomass: Producing, Analyzing and Upgrading*; Soltes, E. J., Milne, T. A., Eds.; ACS Symposium Series 376; American Chemical Society: Washington, DC, 1988; Chapter 17.
- (4) Huyghues-Despointes, A.; Yaylayan, V. A.; Keyhani, A. J. *Agric. Food Chem.* **1994**, *42*, 2519 and references therein.
- (5) (a) *The Maillard Reaction in Foods and Nutrition*; Waller, G. R.; Feather, M. S., Eds.; ACS Symposium Series 215; American Chemical Society: Washington, DC, 1983. (b) *Thermally Generated Flavors: Maillard, Microwave, and Extrusion Processes*; Parliament, T. H., Morello, M. J., McGorin, R. J., Eds.; ACS Symposium Series 543; American Chemical Society: Washington, DC, 1994.
- (6) Leffingwell, J. C. *Rec. Adv. Tob. Sci.* **1976**, *2*, 1.
- (7) Yaylayan, V. A.; Huyghues-Despointes, A. *Crit. Rev. Food Sci. Nutr.* **1994**, *34*, 321 and references therein.
- (8) (a) Britt, P. F.; Buchanan, A. C., III; Kidder, M. K.; Owens, C. V., Jr.; Ammann, J. R.; Skeen, J. T.; Luo, L. *Fuel* **2001**, *80*, 1727. (b) Owens, C. V., Jr.; Britt, P. F.; Buchanan, A. C., III *Prep. Pap.-Am. Chem. Soc. Div. Fuel Chem.* **2001**, *46*, 264.
- (9) Smith, W. T.; Haidar, N. F.; Patterson, J. M. *Tobacco Sci.* **1975**, *19*, 142.
- (10) Higman, E. B.; Schmeltz, I.; Schlotzhauer, W. S. *J. Arg. Food Chem.* **1970**, *18*, 636.

(11) Patterson, J. M.; Issidorides, C. H.; Papadopoulos, E. P.; Smith, W. T., Jr. *Tetrahedron Lett.* **1970**, 1247.

# FRACTIONAL PYROLYSIS OF BIOMASS FOR HIGH-VALUED PRODUCTS

F. A. Agblevor and S. Besler-Guran\*

Department of Biological Systems Engineering  
Virginia Polytechnic Institute & State University  
Blacksburg, VA 24061

\*New Jersey Department of Environmental Protection,  
Air Quality Management, Trenton, NJ.

## Introduction

Conventional rapid pyrolysis (RP) of biomass is a thermal treatment process in the absence of air, which produces solid, liquid, and gaseous products<sup>1-4</sup>. In these processes, the pyrolysis temperatures range from 450 - 600°C and vapor residence times are one to five seconds. In the RP process, liquid production is maximized at the expense of gaseous and solid products. The liquid product (bio-oil) is generally unstable, acidic, corrosive, viscous, and has high moisture content.<sup>5-6</sup> The poor stability of bio-crude oils is attributed to the char and alkali metals in the oil, which catalyze secondary reactions during storage. However, if the hot pyrolysis vapors are filtered to reduce the char content before condensation, the stability of the oil is improved considerably.<sup>1,5</sup>

Bio-crude oils are complex mixtures of carbohydrate and lignin thermal decomposition products, which cannot be used for most bio-based products and fuel applications except after considerable secondary processing. Catalytic studies of biomass pyrolysis products have focused on post pyrolysis catalysis to higher value products<sup>7,8</sup>, but most of these studies reported low yields of hydrocarbons, high coke/char yields and rapid deactivation of the catalysts. Fractional pyrolysis has not been reported.

Biomass feedstocks are composed of structural (lignin, cellulose, and hemicellulose) and non-structural (extractives) components, which have distinct chemical properties. It is conceivable to selectively convert the biomass constituents to a defined slate of chemicals and separate these products *in situ* (fractional pyrolysis) without necessarily going through secondary extraction and upgrading processes. Fractional pyrolysis is defined as a selective *in situ* conversion of biopolymers to desired products. This approach is aided by catalysts and can produce a narrow slate of pyrolysis products, which can be tailored to specific applications.

The goal of this research is to selectively convert biomass components *in situ* into suitable products using suitable catalysts and thus eliminating potential secondary processing steps. In this paper, we report the fractional catalytic conversion of the carbohydrate components of hybrid poplar wood into gaseous products and depolymerization of lignin into phenol, cresols, and catechols.

## Experimental

**Feedstock and Catalyst.** The feedstock used for this experiment was a hybrid poplar whole wood ground in a Wiley mill to pass a 1-mm screen. The moisture content of the feed was 5%. 200 g batches of a proprietary catalyst (VPISU-001) were used in each experiment.

**Fluidized Bed Pyrolysis.** The reactor consisted of a 50 mm schedule 40 stainless steel pipe, 500 mm high (including a 140-mm pre-heater zone below the gas distribution plate) and equipped with a 100- $\mu$ m porous metal gas distributor. The reactor was externally heated with a three-zone electric furnace. The biomass was conveyed by a twin-screw feeder into a compartment from where high-velocity nitrogen entrained the feed and carried it through a jacketed air-cooled tube into the fluidized bed. The pyrolysis temperature was maintained at 500°C and the apparent pyrolysis vapor residence time

was about 1 s. A typical run lasted for 2-3 h, and the feed rate was 100 g/h. Pyrolysis gases and vapors exiting the reactor passed through a heated hot gas filter unit to separate char/ash and any entrained catalyst. The pyrolysis liquids were collected in two condensers and an electrostatic precipitator (ESP). The amount of char/coke was determined by weighing the reactor/catalyst and hot gas filter before and after each run. No attempt was made to differentiate between the char and coke and no further analysis was done.

## Results and Discussion

**Pyrolysis Products.** During first half hour of pyrolysis, there was very little condensation of pyrolysis products. The absence of liquid condensate in any significant quantities suggested that during this phase the catalyst was extremely active and the major reaction was gasification. The material balances for two catalytic pyrolysis runs are shown in Table 1. Compared to rapid non-catalytic pyrolysis (RP), the total liquid yields were very low (30%), and the gas yields were very high (60%). The char/coke yields (11.5%) were comparable to those reported for conventional pyrolysis of hybrid poplar wood.<sup>2</sup>

Table 1. Material balance on catalytic pyrolysis of hybrid poplar (on as received basis).

Fractions	Run 1461-40 #4	Run 1461-42 #5		
Gas Yield (%)	60	55.0		
Total Liquids (%)	30.6	30.1		
Char/Coke (%)	11.5	11.9		
Total	102.1	97.0		
Liquid Fractions collected			Color	# Phases
Chilled Water Condenser (g)	19.9	18.9	Brown	1
Ice/Water Condenser (g)	14.7	16.8	Yellow	1
ESP (g)	25.7	25.3	Brown	1
Total Liquids (g)	60.3	61		
Total Biomass Pyrolyzed (g)	197	202		

About 90% by weight of the gaseous products was CO and CO<sub>2</sub> and the rest was a mixture of hydrocarbons. Butene was the most abundant hydrocarbon and in some cases constituted 30% of the total hydrocarbon products.

The liquids from the first condenser and the ESP were both brown, with extremely low viscosity. The liquids composition included almost exclusively phenolics (phenol, cresols, guaiacol, methyl-substituted phenols), small quantities of indene and substituted naphthalenes, with no detectable carbohydrate pyrolysis products. No benzene, toluene or xylenes were detected in any of the products. The elemental composition of the liquids had high carbon (71%) and relatively low oxygen content (21%) compared to non-catalytic pyrolysis oils. The HHV was consequently high (30.5 MJ/kg) compared to 23 MJ/kg for the non-catalytic pyrolysis oil. The liquid from the second condenser was light yellow, also had very low viscosity and appeared to be 95% water and 5% dissolved organics.

**Molecular Weight Distribution of Liquid Products.** Gel permeation chromatography (GPC) showed very low molecular mass distribution of the liquid products. The number average molecular weights (M<sub>n</sub>) of the liquids from the ESP and the chilled water

condenser were both 160 while the weight average molecular weight (Mw) were 215 and 220 respectively. These molecular weights are about half of those reported for phenol/neutral fraction from conventional rapid pyrolysis products (Mn = 290, Mw = 440) (Fig 1).

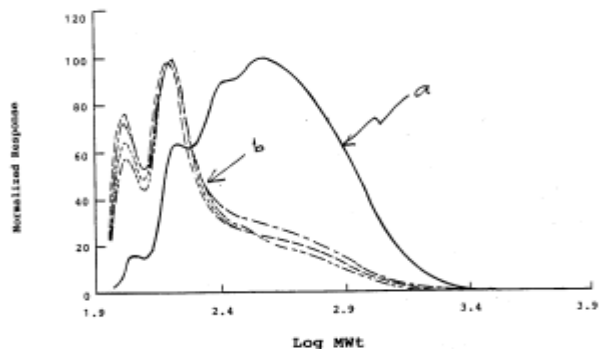


**Figure 1.** Molecular weight distribution of (a) phenol/neutral fraction extracted from sugar cane bagasse conventional rapid pyrolysis oils and (b) hybrid poplar catalytic pyrolysis liquids.

**Catalyst Activity.** The CO and CO<sub>2</sub> concentrations appeared to vary with time during the catalytic pyrolysis. The variation was probably due to catalyst deactivation. In these studies we attempted to monitor catalyst activity by following the variation in CO and CO<sub>2</sub> concentration in the gaseous product and compared CO/CO<sub>2</sub> ratio for the catalytic pyrolysis with a non-catalytic process carried out in a silica sand media. The CO/CO<sub>2</sub> ratio decreased with time and appeared to approach the value for non-catalytic pyrolysis (Fig 2). If we assume that this ratio is a true monitor of catalytic activity, then the catalyst was still active after three hours run albeit less active than the fresh catalyst.

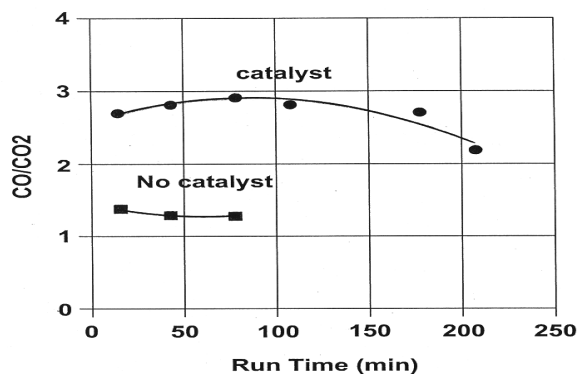


**Figure 2.** Variation of carbon monoxide and carbon dioxide during fractional and conventional pyrolysis of hybrid poplar wood

Under post-pyrolysis catalysis conditions, biomass feedstocks tend to produce very high coke yields, which rapidly deactivate the catalyst. The post-pyrolysis catalysis liquid products usually contain benzene, toluene, xylene, naphthalenes, substituted benzene, and naphthalenic compounds. On the contrary, in the catalytic pyrolysis, where the catalyst and the biomass feed were contacted, the catalyst was still active after 3 hours on steam and the product slate was quite different from that reported for post-pyrolysis catalysis. Coke formation seemed to be very low because the total yield of solids from the process was only 12%, which is equivalent to the coke yield alone from the post-pyrolysis catalysis runs. This could be attributed to the minimal secondary conversion of the primary lignin pyrolysis products

to hydrocarbons, which is mostly responsible for the coke formation and thus strongly contribute to the deactivation of the catalyst as observed in post-pyrolysis catalysis. Deactivation of the catalyst seems to be followed by a decrease in CO concentration in the product gas as shown in Fig 2.

Clearly in the fractional catalytic process appeared to be selective pyrolysis and gasification of the biomass components. The carbohydrate degradation products are more labile than the lignin degradation compounds and thus were rapidly converted into gases while the more refractory lignin-derived components mostly formed the liquids. The total liquid yield was 30% with a water fraction of 30-40%. This implies that the organic liquid yield was only 18-21%, which coincides with the lignin content of hybrid poplar wood. Thus, the catalytic pyrolysis appeared to favor production of modified liquid phenolics from the lignin fraction of the biomass while converting the carbohydrate fraction to gases. The presence of high proportions of cresols and dihydroxy phenols (catechol) suggested that demethylation, demethoxylation and cleavage of the lignin decomposition products occurred. As the catalyst slowly deactivated, also some carbohydrate pyrolysis products such as hydroxyacetaldehyde, ethanedial, and hydroxyacetone were not cracked and condensed with the aqueous phase in the chilled water condenser.

## Conclusions

We have demonstrated the concept of fractional pyrolysis of biomass. The most important factor is the choice of catalyst. By selecting a suitable catalyst, various components of the biomass feedstocks can be converted *in situ* into desirable products. In this work we showed that the lignin fraction of the biomass could be effectively converted into phenolics with low char yield when catalysis and pyrolysis reactions were performed simultaneously. Char yields for this process were similar to those obtained from conventional rapid pyrolysis. The molecular mass distribution of fractional catalytic pyrolysis process were about one half that obtained for phenol/neutral fraction in a conventional pyrolysis and there appeared to be considerable demethylation and demethoxylation reactions. The liquid product appeared to be stable with minimal repolymerization reaction.

## References

1. Aglevor F.A., Besler, S., Wiseloge, A.E. *Energy and Fuels*, **1995**, 9(4), 635-640.
2. Scott D.S., Piskorz, J. *Can. J. Chem. Eng.* **1982**, 60, 666.
3. Graham, R.G. and Bergougnou. *J. Anal. Appl. Pyrolysis* **1984**, 6, 95-135.
4. Diebold, J.P., Scahill, J. In *Pyrolysis Oils from Biomass*, Soltes, E.J. and Milne T.A., Eds. ACS Symposium Series 376; American Chemical Society, Washington DC. **1988**; pp 31-40.
5. Diebold, J.P. and Czernik, S. *Energy and Fuels* **1997**, 11(5), 1081-1091.
6. Aubin, H. and Roy, C. *Fuel Science International* **1990**, 8(1), 77-86.
7. Sharma, RK, Bakhshi NN., *Bioresour. Technol.* **1991**, 35(1), 57-66.
8. Horne, P.A. and Williams, P.T. *J. Anal. Appl. Pyrol.* **1995**, 34, 65-85.

# HEAT TRANSFER CONTROLLED PYROLYSIS OF CELLULOSICS

Eric M. Suuberg and Ivan Milosavljevic

Division of Engineering  
Brown University  
Providence, RI 02912 USA  
Tel. (401) 863-1420, Fax (401) 863-1157  
email: eric\_suuberg@brown.edu

## INTRODUCTION

The thermal decomposition of cellulosic solids has been extensively studied. There have been numerous reviews of various aspects of the problem (e.g., pyrolysis [1-3], modeling of combustion [4, 5]). In recent papers, we have described new results on the global kinetics of cellulose pyrolysis [6-8], suggesting that these are heating-rate dependent because of the role that mass transfer can play in the process [8]. There continues to be considerable debate regarding the kinetics of pure cellulose pyrolysis [e.g., 9,10]. When adding uncertainties regarding the role of transport processes [11] and secondary reactions, the modeling of the processes remains problematic. We have previously presented a number of results from a study in which the behavior of cellulose samples has been examined under simulated fire-level heat fluxes [12]. In this paper, further experimental results are considered.

The present study is concerned with bulk cellulose pyrolysis under conditions simulating those of a fire, but which are also relevant to any system in which cellulose undergoes pyrolysis. The experiments were carried out in an inert gas environment. The material studied here was "pure" cellulose, selected to produce "realistic", but highly reproducible samples. Samples were pressed to densities typical of those encountered with wood. There have been many other studies of cellulosic pyrolysis of large cellulosic particles [e.g., 12-25]. Some have noted a well-defined pyrolysis front [13-17] and a period of relatively constant mass loss rate [16, 17, 20, 23, 25], particularly with high imposed radiative fluxes. Generally, the data revealed a significant sensitivity to char thermal conductivity [21]. The effects of oxygen [19] and retardants [23] can also be significant in affecting observed behavior.

## EXPERIMENTAL

### Materials

The cellulose studied in this work was Whatman CF-11 powder, with an ash content of 0.009% and a moisture content of 7.68% (as-received). Powder samples were formed into pellets using an ordinary laboratory press, without any additives. Three different density samples were prepared:  $0.965 \pm 0.041$  g/cm<sup>3</sup>,  $0.691 \pm 0.035$  g/cm<sup>3</sup> and  $0.458 \pm 0.026$  g/cm<sup>3</sup>. These densities are comparable to those of woods ranging from softwoods to hardwoods. All pellets were 38 mm in diameter and had a thickness of up to about 10 mm.

### Radiative Pyrolysis Apparatus

The experimental setup has been described earlier [12]. Briefly, a nitrogen purged pyrolysis chamber houses the sample, whose front surface is heated by quartz lamps. The sample is held inside a ceramic insulator, placed atop an electronic balance. The two tungsten filament heaters supply a constant incident heat flux of 20-60 kW/m<sup>2</sup>, and deliver radiation in wavelength range simulating a flame at 1700 K. This is important because the wavelength range of the delivered radiation has a significant impact on the surface reflectivity [11]. Temperature measurements were made within the cellulose using chromel-alumel

thermocouples (0.5 mm diameter), positioned at different distances from the sample

## RESULTS AND DISCUSSION

### Influence of Sample Density on Mass Loss and Temperature Profiles

After turning on the radiant heaters, the sample mass was monitored continuously until a time at which no additional mass loss was observed. Figure 1 shows typical mass loss results for three different density samples, irradiated with a 40 kW/m<sup>2</sup> surface flux. An early heating period (< 500 s) involves little mass loss, except for a small amount of residual moisture. This is followed by active pyrolysis, indicated by the loss of sample mass as, approximately, a linear function of time during much of the period. This indicates a pyrolysis front moving with near-constant propagation velocity into the solid. The result seen here is consistent with those of many above-cited studies, involving constant (high) incident heat flux.

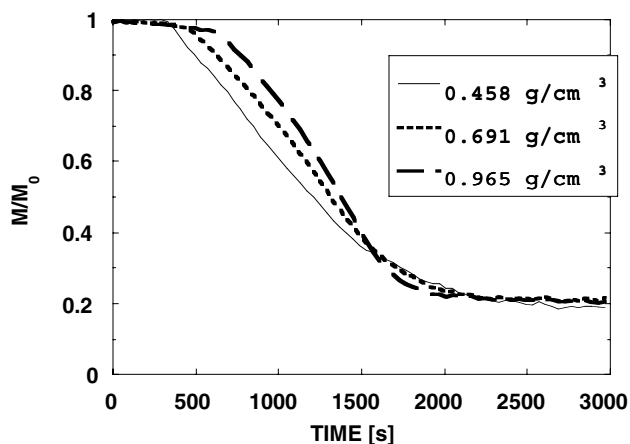


**Figure 1.** Fractional mass loss from cellulose of 0.458 g/cc (solid line) 0.691 g/cc (dotted line) and 0.965 g/cc (dashed line).

The point of pyrolysis onset depends on sample density. It can be seen from Fig. 1 that the lower the sample density, the earlier pyrolysis starts. The lower density sample behaves as a better "insulator". Its front surface temperature rises faster, which results in an earlier onset of pyrolysis.

The above explanation is made clearer by reference to the sample temperature profiles. Figure 2 shows the temperature history of different thermocouples within the highest density (0.965 g/cm<sup>3</sup>) samples, under the conditions as shown in Figure 1. The temperature profiles indicate clearly that the sample loses heat from its back face, and at the time the mass loss reaches near zero rate, a nearly constant temperature profile has been achieved throughout the sample. The final temperature of the back face of the sample is sufficiently low such that some further pyrolysis could be possible, if the temperature were to be raised. This fact should be noted in considering the long-time char yield of Fig. 1. Thus in any such bulk sample experiment, the char yield is operationally defined as the fractional mass left after the mass loss ceases under given conditions. It can, however, be seen from Fig. 1 that the char yield, about 20%, averaged over the entire sample,

is not a very strong function of initial sample density. The particular cellulose used here gives char yields of about 5% or less, when examined in an ordinary thermogravimetric experiment at comparable heating rates [7].

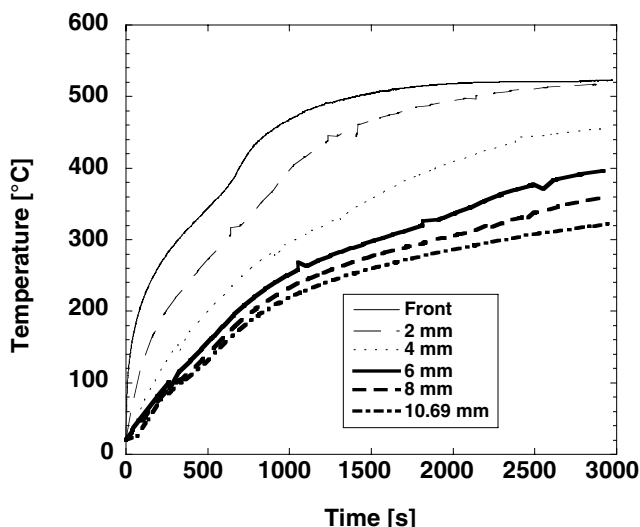


**Figure 2.** Temperature profiles in a 0.965 g/cc sample subject to a nominal surface flux of 40 kW/m<sup>2</sup>.

The effect of sample density on front and back surface temperatures is shown in Figure 3. The better the insulating properties of a sample, the larger the temperature gradient that it will support. These results confirm that sample conductivity increases with density, as has been independently shown [11].

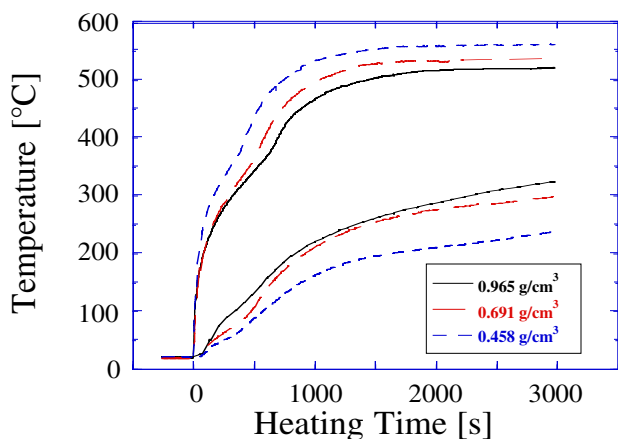


**Figure 3.** Sample front (top curves) and back face temperatures for nominal 40 kW/m<sup>2</sup> irradiation.

The front surface temperature-time profile always shows an inflection point at around the pyrolysis onset temperature. The reason for this is that as cellulose decomposes, material properties (surface emissivity and thermal conductivity) change [11], and a reaction endotherm occurs [7].

The mathematical modeling of this process has demonstrated that the actual absorbed surface fluxes are much lower than the nominal incident surface fluxes. When taking this into account, it is possible to model the propagation of the thermal wave implied in Figures 2 and 3 quite well. There are large contributions from reflective loss, convective loss, re-radiation and volatiles screening of the incident radiation. The endothermic nature of pyrolysis plays a relatively minor role in determining the thermal behavior.

Experimentally, the observed total mass loss behavior is quite similar in wood and cellulose. This is not particularly surprising, insofar as a conduction-limited pyrolysis process depends only upon the thermal conductivity and thermal diffusivity of the materials, which in this case are quite similar. Where the influence of the starting materials is strongest is in the nature of the volatile products.

The final char yield is a strong function of distance into the char pellet, despite the similarity of average yields at different densities (as noted in Fig. 1). This difference is only partly attributable to the temperature gradient noted above. There is an influence of in-depth cracking of volatiles. The char yield from within 2 mm of the surface was around 10%, whereas the yield near 4 mm was 20% and at 8 mm over 30%.

## References

1. Antal, M.J. Jr., in *Advances in Solar Energy*, (K. Boer and J. Duffie, Eds.), American Solar Energy Society, 1982, Vol.1, p. 61.
2. Antal, M.J. Jr., in *Advances in Solar Energy*, (K. Boer and J. Duffie, Eds.), American Solar Energy Society, 1985, Vol.2, p. 175.
3. Antal, M.J., Jr. and Varhegyi, G., *I&EC Res.*, 34:703-717 (1995).
4. Di Blasi, C., *Prog. Energy Comb. Sci.*, 19:71-104 (1993).
5. Ohlemiller, T., *Prog. Energy Comb. Sci.*, 11:277-310 (1985).
6. Milosavljevic, I., Suuberg, E.M., *I&EC Res.*, 34:1081 (1995).
7. Milosavljevic, I., Suuberg, E.M., *I&EC Res.*, 35:653 (1995).
8. Suuberg, E.M., Milosavljevic, I. and Oja, V., *26th Symp. (Int.) on Combustion*, The Combustion Institute, 1996, pp 1515-1521.
9. Reynolds, J.G., Burnham, A.K. *Energy and Fuels*, 11:88-97 (1997).
10. Gronli M, Antal MJ and Varhegyi G, *I&EC Res.* 38: 2238-2244 (1999).
11. Suuberg, E.M., Aarna, I., and Milosavljevic, I., in *Progress in Thermochemical Biomass Conversion*, A.V. Bridgwater, Ed., Blackwell Science, Oxford, UK, 2001, pp. 1246-1258.
12. Milosavljevic, I. and Suuberg, E.M., *ACS Div. Fuel Chem. Prepr.*, 37(4):1567-1571 (1992).
13. Kanury, M. A. and Blackshear, P.L., *Pyrodynamics* 4:285-298 (1966).
14. Blackshear, P.L., Jr., and Kanury, M.A., *10th Symp. (Int.) on Combustion*, The Combustion Institute, Pittsburgh, 1965, pp. 911-923.
15. Kanury, M.A., Blackshear, P.L., Jr. *Comb. Sci. Tech.*, 1:339-355 (1970).
16. Lee, C.K., Chaiken, R.F. and Singer, J.M., *16th Symp. (Int.) on Combustion*, The Combustion Institute, Pittsburgh, 1976, pp. 1459-1470.
17. Lee, C.K. and Diehl, J.R., *Comb. Flame*, 42:123-138 (1981).
18. Ohlemiller, T.J., Kashiwagi, T., Werner, K., *Comb. Flame*, 69:155-170 (1987).
19. Kashiwagi, T., Ohlemiller, T.J., Werner, K., *Comb. Flame*, 69:331-345 (1987).
20. Becker, H.A. and Phillips, A.M., *Comb. Flame*, 58:255-271 (1984).
21. Chan, W.-C., Kelbon, M., Krieger, B.B., *Fuel*, 64:1505 (1985).
22. Chan, W.-C., Kelbon, M., Krieger, B.B., *I&EC Res.*, 27:2261 (1988).
23. Chen, Y., Frendi, A., Tewari, S.S., and Sibulkin, M., *Comb. Flame*, 84:121-140 (1991).
24. DiBlasi, C., Gonzalez-Hernandez, E., Santoro, A., *I&EC Res.*, 39:873-882 (2000).
25. DiBlasi, C., Branca, C. and Santoro, A., in *Progress in Thermochemical Biomass Conversion*, A.V. Bridgwater, Ed., Blackwell Science, Oxford, UK, 2001, pp. 1143-1157.
26. Milosavljevic, I., Ph.D. Thesis, Division of Engineering, Brown University, 1994.

# HYDROGEN TRANSFER REACTIONS OF PHENOXY RADICALS STUDIED BY LASER FLASH PHOTOLYSIS TECHNIQUE

Reza Dabestani,\* Ilia N. Ivanov, Phillip F. Britt, Michael E. Sigman, and A. C. Buchanan, III

Chemical Sciences Division, Oak Ridge National Laboratory,  
Oak Ridge, TN 37831

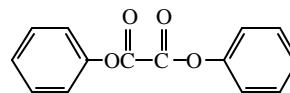
## Introduction

Aryloxy radicals are important intermediates in the thermal decomposition of lignin and low rank coals. Their rate of formation, termination, hydrogen abstraction, and addition (i.e. cross-linking) have a significant impact on the product yields and distributions. The Arrhenius parameters of hydrogen abstraction reactions of phenoxy radicals with substituted phenols and hydroperoxides have been reported.<sup>1</sup> However, there are only a few reports of Arrhenius parameters for hydrogen abstraction by phenoxy radicals from hydrocarbons. This is mainly due to the experimental challenges associated with the slow relative rates of hydrogen abstraction by phenoxy radical from hydrocarbons and the very rapid recombination rates of phenoxy radicals. In previous studies Britt et al.<sup>2</sup> have assumed that the Arrhenius parameters for hydrogen abstraction by phenoxy radicals from hydrocarbons are similar to that of benzyl radical. However, this does not take into account the well-known polar effects in free radical reactions.<sup>3</sup> Since hydrogen abstraction reactions of aryloxy radicals plays an important role in the processing of energy resources, such as lignin and low rank coal, we have undertaken this study to investigate the kinetics of hydrogen abstraction by phenoxy and substituted phenoxy radicals from hydrocarbons structures found in energy resources, such as toluene, diphenylmethane and fluorene. The data obtained from such studies will serve as a benchmark for thermochemical kinetic estimates on related systems.

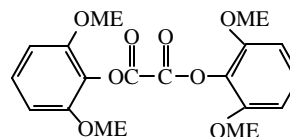
## Experimental

Diphenyl oxalate (DPO), di-(4-methoxy)-phenyl oxalate (PMPO), and di-(2,6-dimethoxy)-phenyl oxalate (DMPO) were synthesized (Scheme I) as precursors for this study using a literature method.<sup>4</sup> Laser flash photolysis set-up has been described elsewhere.<sup>5</sup> For the excitation light, 308 nm line of an excimer laser (Lambda Physik, 20 ns pulse width) or the third harmonic (355 nm, 5 ns pulse width) of a Minilite II ND:YAG (Continuum) was employed. The excitation beam was overlapped with the probe beam (450-W xenon) delivered to the sample at right angle to the excitation. Changes in the relative transmission of the probe beam, which was directed into the entrance port of a monochromator, as a function of time due to transient formation were detected by a photomultiplier tube (PMT) attached to the exit port of monochromator. The output of PMT was amplified by a two-stage amplifier and the signal was fed into a LeCroy 9354A transient digitizer for data acquisition. All digitized kinetic signals from the transient digitizer were fed to a GPIB board (National Instruments) and stored as ASCII files. The data were then transformed to time-resolved absorption spectra using Origin 6.0 software (Microcal). A thermostated cell holder was employed to study the effect of temperature on hydrogen abstraction rate for phenoxy radicals. For room temperature experiments, we used a flow cell to pump new solution into the cell for each laser shot to avoid interference from the excitation of products formed during the first laser pulse. For high temperature studies, solutions of the oxalates in dimethoxy ethyl ether with and without the hydrocarbon (H-donor, e.g. diphenylmethane, fluorene, etc.) were placed in a 1-cm quartz cell. After exposure to a single laser shot, the solution was discarded and replaced with a fresh solution, allowed to equilibrate to the desired temperature, then flashed. This procedure was repeated for all the kinetic data reported in this study. Purging of the samples with

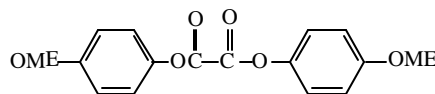
argon had no effect on the kinetics of the observed transients suggesting oxygen does not quench these transients.



Diphenyl Oxalate (DPO)



Di-(2,6-Dimethoxy)-Phenyl Oxalate  
(DMPO)



Di-(4-methoxy)-Phenyl Oxalate  
(PMPO)

## Scheme I

## Results and Discussion

Introduction of methoxy substituents into the phenoxy ring of DPO causes a red shifting of the absorption spectrum. Although DMPO contains two methoxy substituents in the *ortho*-position, the absorption spectra of PMPO which bears only one methoxy group in the *para*-position is considerably more red-shifted (~ 10 nm) than DMPO. Time-resolved transient absorption spectra of DPO, DMPO, and PMPO obtained at various time intervals after the laser pulse (308 nm) show the formation of a transient in the 300-450 nm region (due to phenoxy radical)<sup>6</sup> which slowly decays to produce a longer lived transient(s) with absorption in the 500-650 nm region. Because excited state lifetime of the initially formed triplet states is most likely in the pico-second time regime (which is outside of our time resolution limit), we only observe the appearance of phenoxy radical (us time domain) which absorb around 400 nm. The phenoxy radical can form from the breaking of carbon-oxygen bond in the triplet excited state of the oxalate. The observed red-shifting of the transient absorption, upon the addition of methoxy groups on the phenyl ring, further supports the notion that the observed transient is due to phenoxy radical formation.<sup>6</sup> Figure 1 shows the time-resolved transient absorption spectra of DPO obtained at 50 us time intervals after the laser pulse. The decay of the 395 nm peak with time is accompanied by the evolution of the 530, 560, and 600 nm peaks. Single exponential fit of both the rise for 560 nm peak (Fig. 2) and the decay for 395 nm peak (Fig. 3) gives a lifetime of 20 us.

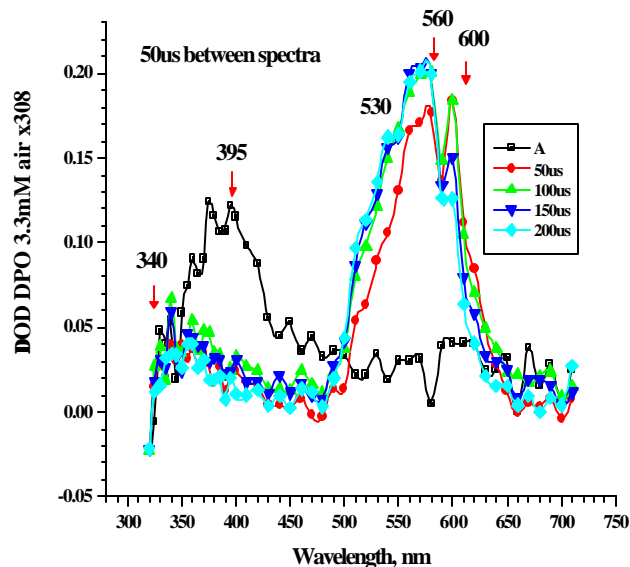


**Figure 1.** Time-resolved transient absorption spectra of DPO in air-saturated dimethoxy ethyl ether taken at 50 us time intervals after the 308 nm laser pulse.

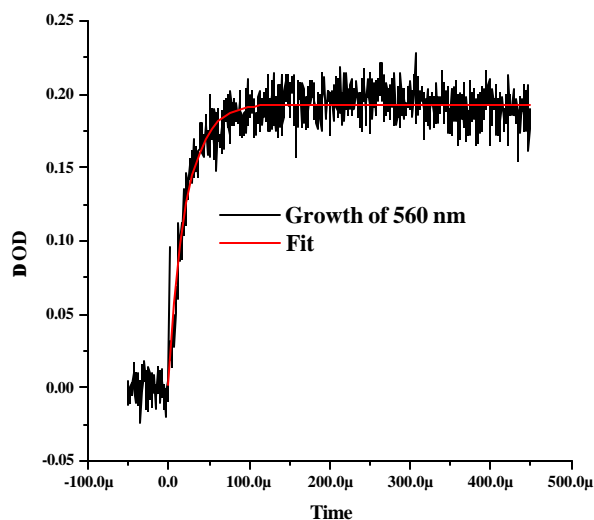


**Figure 2** Growth of the 560 nm peak with time and its single exponential fit observed for DPO in air-saturated dimethoxy ethyl ether.

Time-resolved transient absorption spectra of PMPO and DMPO show similar behavior, but are red shifted. The quenching of phenoxy radical by various hydrocarbons (e.g. diphenylmethane, fluorene, and toluene) is currently under investigation to obtain the rate constants for H-abstraction by phenoxy radicals. The rate constant for H-abstraction will be measured at various temperatures in order to determine the Arrhenius parameters. One of the limiting factors in such studies is thermal stability of the oxalate at higher temperatures. Thermal stability studies are currently being conducted on DPO, DMPO, and PMPO to determine the feasibility of using the laser

flash photolysis technique to study H-abstraction rates at higher temperatures. The results of this investigation will be presented at the meeting.

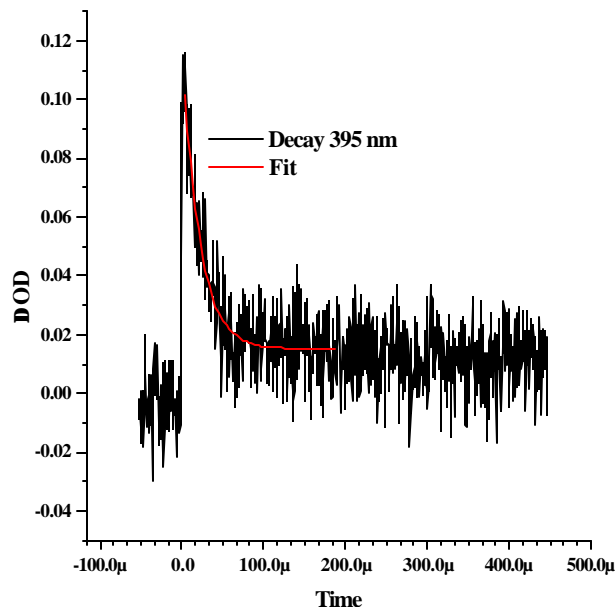


**Figure 3.** Decay profile for 395 nm transient and its single exponential fit observed for DPO in air-saturated dimethoxy ethyl ether.

## Conclusions

Laser flash photolysis of a number of light sensitive oxalates proceeds to produce the corresponding phenoxy radicals. Time-resolved transient absorption spectra of these oxalates show strong absorption around 400 nm in good agreement with the reported literature values. The initially formed transient (due to phenoxy radical) slowly decays to produce a new transient(s) with strong absorption in the 500-600 nm region. The nature and identity of the newly formed transient(s) is currently under investigation. Studies are also underway to determine the effect of concentration on the formation of new transient(s) and the rate constant for H-abstraction from hydrocarbons by phenoxy radicals.

## Acknowledgements

This research was sponsored by the Division of Chemical Sciences, Geosciences, and Biosciences, Office of Basic Energy Sciences, U. S. Department of Energy under contract DE-AC05-96OR22464 with Oak Ridge National Laboratory, managed by UT-Battelle for the Department of Energy. I. Ivanov is supported by the ORNL Postdoctoral Research Associates program, which is administered jointly by Oak Ridge Institute of Science and Education and ORNL

## References:

1. Denisov, E., *Handbook of Antioxidants*; CRC Press: Boca Raton FL, 1995; Chapter 3.
2. Britt, P. F.; Buchanan, A. C., III; Malcolm, E. A. *J. Org. Chem.* **1995**, *60*, 6523.
3. Minisci, F.; Fontana, F.; Recupero, F.; Bravo, A.; Agano, E.; Rinaldi, C.; Di Luca, M.; Grossi, F.; Bjorsvik, H-R. *J. Am. Chem. Soc.* **1999**, *121*, 7760.

4. Lahti, P. M.; Modarelli, D. A.; Rossitto, F. C.; Inceli, A. L.; Ichimura, A. S.; Ivatury, S. *J. Org. Chem.* **1996**, *61*, 1730.
5. Dabestani, R.; Higgin, J.; Stephenson, D.; Ivanov, I. N.; Sigman, M. E. *J. Phys. Chem. B* **2000**, *104*, 10235.
6. Das, P. K.; Encinas, M. V.; Steenken, S.; Scaiano, J. C. *J. Am. Chem. Soc.* **1981**, *103*, 4162.

# INFRARED LASER PYROLYSIS OF BIOMASS DERIVED CHARS

Andrew M. Herring, J.Thomas McKinnon, David E. Petrick,  
Jonathan Filley, Keith W. Gneshin and Bryan McCloskey

Department of Chemical Engineering  
Colorado School of Mines  
Golden, CO 80401-1887

## Introduction

Recent studies have attempted to rationalize a global pyrolysis mechanism for cellulose pyrolysis.<sup>1,2,3</sup> However, these mechanisms are based on the observation of stable species many seconds into the pyrolysis event. The observation and validation of the reactive intermediates generated in the first second or less of pyrolysis should enable a better understanding of the kinetics of the processes involved to be developed. The neutral species formed during this short time scale of reaction have been extensively studied by molecular beam mass spectroscopy, MBMS, from tube furnace pyrolysis of volatilized cellulose at increasing temperatures corresponding to primary pyrolysis and to secondary and tertiary cracking products.<sup>4,5</sup> The subsequent pyrolysis of cellulosic chars formed at different temperatures has also been studied<sup>6</sup> leading to the conclusion that these are predominantly aromatic at temperatures above 310°C.

Infrared laser heating of biomass samples allows very rapid temperature ramps to be achieved. Rapid heating in this way with a carbon dioxide laser has been used to both volatilize organic samples and for the generation of reactive intermediates for subsequent analysis.<sup>7,8</sup>

In this paper, we describe the identification by MBMS of both radical and molecular reactive intermediates as well as stable end products from the carbon dioxide laser pyrolysis of cellulose and charred cellulose at the site of irradiation. The temperature profiles of the cellulose char surface during laser pyrolysis have been characterized by both experiment and modeling. In general, only the surface of the solid is heated and the assumption is made that the off-gassed volatiles are not further heated. We are, therefore, able to determine the nature of the char from MBMS as well as the important intermediate radicals produced during rapid heating events.

## Experimental

All manipulations of char and laser pyrolysis experiments were performed under an inert atmosphere of helium, nitrogen or argon as explained below.

Avicel cellulose (Analtech), propargyl chloride (Aldrich) and 50% 1,5-hexadiyne in pentane (Alfa Aesar) were used as received without further purification. The cellulose was pelletized. Pellets were charred in a quartz tube furnace, the temperature of which was ramped from ambient to 375°C over 5 min, as measured by a thermocouple at the side of the pellet, in a flow of argon at 1.41 cm s<sup>-1</sup> for times up to 3 h. The pellets were then transferred to a sample post inside the MBMS combustion chamber such that the outside of the sample disc touched the nickel nozzle inlet of the MBMS.

The unpolarized 10.6 μm CO<sub>2</sub> laser radiation (Synrad, 65W Duo-Lase) was directed into the MBMS combustion chamber through an optical train giving a relatively large spot size of ca. 2 mm. In a typical experiment, a mass range 0 - 450 amu, was collected in two overlapping 250 amu segments at a scan rate of 0.5 s scan<sup>-1</sup>. 10 background spectra were collected before

irradiating the sample, for 3 s with laser radiation fluxes from 3.25 W to 13 W (5% to 20% of full power). The data reported are the average of at least 10 such experiments, the pellet being rotated between each, over at least two pellets. From these experiments, the error in the relative intensities is +/- 10%, data falling outside this range was rejected. Arbitrary intensity scales are presented throughout the paper as many factors, such as vacuum stage pressures, nozzle condition *etc.*, independent of the laser pyrolysis experiment influence the absolute intensities obtained. In some experiments, the pellet was rotated continuously while being irradiated; again the data reported are the average from more than one pellet.

## Results and Discussion

Figure 1 shows the laser pyrolyzed mass spectra of cellulose and cellulose charred at 375°C for various times, at 0.5s of a low powered laser pulse. All of the major products observed in Figure 1 for uncharred cellulose fall into the class of primary products of cellulose pyrolysis, that is, no secondary cracking in the gas phase is observed. We can therefore deduce that under these conditions, the products observed in this experiment using cellulose char, discussed below, are volatilized from the surface with no major contributions from gas phase cracking, due to the poor coupling of the infrared radiation with low concentrations of gas phase species.

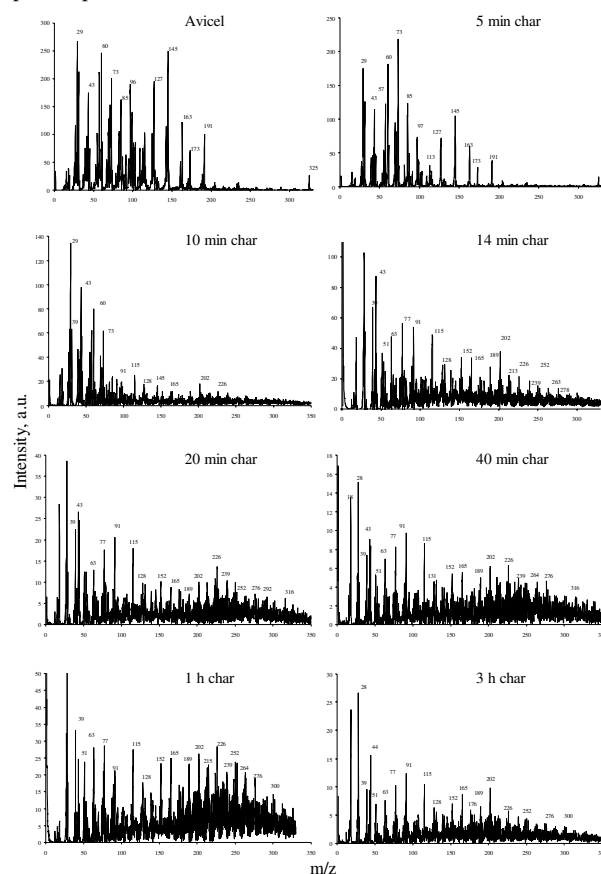


Figure 1. Mass Spectra of Avicel and 375°C charred Avicel at 0.5 s of a 3 s 10% laser power pulse..

After 10 min of charring, we begin to see peaks in the mass spectrum that we assign to polyaromatic hydrocarbons or their radicals, M-1. Some carbohydrate is present in this mass

spectrum. This is likely tar that has not yet left the char matrix, as irradiating at 13 W laser power for 0.5 – 1.0 s, an average temperature *ca.* 400°C higher than at 6.5 W, gives a mass spectrum with no *m/z* 60 or 73. At the higher laser power, all residual tar is flashed off.

From 14 min to 1 h of charring, the mass spectra obtained from the short time low power laser pyrolysis of char are all similar in that we observe predominantly PAH and little carbohydrate, **Figure 1**. The dominant masses larger than 77 can all be assigned to aromatic, PAH, or PAH radical species. The major trend observed with charring time is the molecular weight growth of the ions assigned to PAH and PAH radicals observed above *m/z* 202.

The analysis of trends involving the lower molecular weight fragment is a little harder to discern as many of these ions are also present in the mass spectrum of carbohydrate. Nevertheless, it is apparent that at early charring times the lower mass aromatic species, between *m/z*, 77 and 189 grow in and become constant after the intermittent charring times of 20 min. At this early time, 0.5 – 1.0 s, of the laser pulse the low molecular weight region of the spectrum is dominated by masses, *m/z* 29, 39 and 43. After a further second of irradiating, 1.5– 2.0 s, the dominant low molecular weight peaks are *m/z* 28, 39 and 44, data not shown. The maximum PAH we have observed in any of these experiments is *m/z* 376. After 3 h of charring the ions assigned to PAH larger than *m/z* 202 again diminish, but as stated earlier the smaller aromatic hydrocarbons maintain constant relative intensity, **Figure 1**.

We are observing the fragmentation of PAH moieties from the char surface by laser pyrolysis. These PAH molecules would not form in the gas phase except at very much higher temperatures (because bimolecular reactions will be slow) than we can achieve with our laser under these conditions.

It appears that the depolymerization and decomposition of the cellulose chain first produces smaller PAH up to a molecular weight of 202. These smaller PAH fragments then anneal into larger PAH as the charring process continues. The M-1 species are presumed to be the radicals produced during the laser pyrolysis event.

PAH typically give mass spectra with a dominating molecular ion. However, several of the masses correspond to M-1 ions and we believe that we are observing these PAH as radicals. Laser pyrolysis at 6.5 W, of char produces predominantly phenyl, 77, benzyl, 91, indenyl, 115, C<sub>13</sub>H<sub>9</sub>, 165, C<sub>17</sub>H<sub>11</sub>, 189 and C<sub>19</sub>H<sub>11</sub>, 239 radicals, M-1 rather than their parents, M, benzene, toluene, indene *etc.* Naphthalene, 128, acenaphthylene, 152, pyrene, 202, C<sub>18</sub>H<sub>10</sub>, 226, C<sub>20</sub>H<sub>12</sub>, 252 and higher molecular weight species appear as the molecular species. This implies that the larger PAH are rapidly stabilized shortly after the ablation process and that the smaller aromatic and PAH molecules are released as reactive radicals, with the exception of naphthalene, *m/z* 128.

The conclusion is that we are observing the molecular weight growth of the PAH moieties in the solid bulk with time as the cellulose is charred as has been observed previously. As the cellulose is charred for progressively longer times the PAH anneals into larger and larger PAH moieties that are cleaved from the char surface during the laser pyrolysis event. After 3 h of charring the PAH moieties have begun to anneal into intractable graphite like entities that cannot be cleaved by the laser, so we see a marked cut off of PAH above *m/z* 202 from the more mature cellulose char.

The largest peaks in the low mass region of the mass spectrum for charring times of 14 minutes to 1 h are *m/z* 18, 29, 39 and 43. Mass 18 is water and mass 39 corresponds to a common fragment ion, the cyclopropenyl cation, as well as an important PAH precursor, the propargyl radical. The mass spectra of medium to large PAH give a large peak corresponding to a molecular ion with very little fragmentation. This is not true of the smaller aromatic species, e.g. benzene has a *m/z* fragment 11% the intensity of its molecular ion. In order to begin to assign the peak at *m/z* 39 to either a fragment ion or as the propargyl radical we created a synthetic mass spectrum. Using the 16 most prominent peaks from mass 77 and above in the MBMS data of cellulose charred for 1 h at 375°C, **Figure 1**, we assigned each to a likely PAH molecule or molecules, using the parent neutral molecule for the PAH that appeared as radicals. The results showed that *m/z* 39, 51 and 63 are under represented in the synthetic spectrum. These ions are either fragment ions of compounds, whose molecular ions are under the threshold of the experimental data or ions produced by ionization of radicals formed from laser pyrolysis, such as propargyl. It is more plausible that a large proportion of the *m/z* 39 peak comes from the propargyl radical. Further evidence that the peak at *m/z* 39 is a radical comes from the fact that it is still present in an experiment in which the ionization potential of the mass spectrometer's ionizer was reduced to 13 eV, a level below the ionization potential of benzene.

Interestingly the peak at *m/z* 43 is also present in the low ionization potential experiment. The peaks at *m/z* 29 and 43 are commonly present in mass spectra as fragment ions of carbonyl compounds, such as acetaldehyde and hydroxyacetone. However, the mass spectra of these cellulose chars show little if any evidence of carbonyl compounds. We, therefore, assign the peaks at *m/z* 43 to the formylmethyl radical and *m/z* 29 to a fragment ion.

<sup>13</sup>C NMR analysis reveals a loss in intensity of the aromatic carbons as well as a smaller loss in intensity of the methyl peak upon laser irradiation. Interestingly there is little change in the intensity of the oxygen substituted aromatic carbons. This is either because the oxygenated PAH are intractable or that the irradiated, active char, which has lost its Ar-O moieties, form an equivalent amount of oxygenated PAH on exposure to air. These observations are consistent with our MBMS data where hydrocarbon PAH are the major species detected, with few contributions from oxygen substituted species. Presumably, the oxygenated aromatic species become intractable during the charring. <sup>13</sup>C NMR also shows that the number of carbons attached to hydroxyl increases dramatically and there is a slight increase in the number of carbonyl groups in the irradiated char. In keeping with our model of bond cleavage from the char surface, we would expect laser pyrolysis to generate an extremely active char. As these chars were exposed to air for some time before the NMR measurements were performed it is assumed that atmospheric, water and oxygen have quenched the radical ends to form hydroxyl and carboxyl functionalities. It should be noted that a large proportion of the char is probably not molecular and is presumably graphitic in nature.

## Conclusions

We propose that charred cellulose has a network of small, up to molecular weight 202, PAH fragments between aliphatic hydroxyl linkages. When such a moiety is irradiated, formylmethyl radical is produced with either a PAH radical, as shown here, or a PAH neutral and a surface radical end. Upon

further charring, water is lost to give PAH moieties separated by olefinic linkages. When these moieties are irradiated, propargyl radical is liberated with again either a PAH radical or a surface radical end. On still more severe charring, the olefinic linkages become incorporated into the PAH. Both the hydroxy methyl and propargyl radical forming pathways postulated to occur during laser heating, probably occur in the maturing char, although more slowly to give the PAH, larger than molecular weight 202, in the solid bulk.

#### **Acknowledgement.**

We would like to thank Philip Morris, USA for financial support of this work.

#### **References**

1. Brown A.L., Dayton D.C. and Daily J.W., *Energy Fuels*, **2001**, *15*, 1286.
2. Antal, Jr., M.J., Várhegyi G. and Jakab E., *Ind. Eng. Chem. Res.*, **1998**, *37*, 1267.
3. I. Milosavljevic, V. Oja and E.M. Suuberg, *Ind. Eng. Chem. Res.*, **1996**, *35*, 653.
4. Evans R.J. and Milne T.A., *Energy Fuels*, **1987**, *1*, 123.
5. Park, B.-I., Bozzelli J.W., Botty M.R., Bernhard M.J., Mesuere K., Pettigrew C.A., Shi J.-C. and Simonich S.L., *Environ. Sci. Technol.*, **1999**, *33*, 2584.
6. Pastrorov I., Botto R.E., Arisz P.W. and Boon J.J., *J. Carbohydr. Res.*, **1994**, *262*, 27.
7. Tripathi A., Vaughn C.L., Maswadeh W. and Meuzelaar H.L.C., *Energy Fuels*, **1999**, *13*, 984.
8. Zhan Q., Zenobi R., Buseck P.R. and Teerman S., *Energy Fuels*, **1997**, *11*, 144.

# INVESTIGATION OF THE GAS-PHASE PYROLYSIS OF LIGNIN MODEL COMPOUNDS BY MOLECULAR BEAM MASS SPECTROMETRY

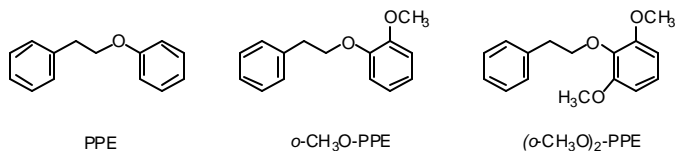
Phillip F. Britt,<sup>1</sup> A. C. Buchanan, III,<sup>1</sup> Robert J. Evans,<sup>2</sup>  
Michael Looker,<sup>2</sup> and Mark R. Nimlos<sup>2</sup>

<sup>1</sup>Oak Ridge National Laboratory, P.O. Box 2008,  
Oak Ridge, TN 37831

<sup>2</sup>National Renewable Energy Laboratory, 1617 Cole Blvd., Golden,  
CO 80401

## Introduction

The production of fuels and chemicals from the thermochemical processing of biomass depends on an understanding of the complex pathways and underlying mechanisms.<sup>1</sup> Unfortunately, the reaction pathways that lead to the complex array of products are still not resolved, and there is little insight into controlling product selectivity. To gain fundamental mechanistic insight into the pyrolysis of lignin, a major component of biomass,<sup>2</sup> our research has focused on the pyrolysis of model compounds that contain key structural elements found in native lignins.<sup>3-5</sup> The flash vacuum pyrolysis of lignin model compounds containing the  $\beta$ -O-4 linkage, which is the dominant linkage in lignin, has been reported.<sup>4,5</sup> These studies provided insight into the primary gas-phase reaction that occurs at 500 °C under low concentration conditions that favor unimolecular reactions. The reaction pathways were significantly more complex than expected, and the dominant reaction was C-O homolysis followed by intramolecular hydrogen abstraction, 1,2-phenyl shift, and/or  $\beta$ -scission of subsequent radicals to form stable products. In this study, the fast pyrolysis of lignin model compounds was investigated at atmospheric pressure in a stream of helium with real time sampling of the products by mass spectrometry. Under these reaction conditions, bimolecular reactions can compete with the unimolecular reactions for the formation of products. In this investigation, the pyrolysis of phenethyl phenyl ether (PPE) and its methoxy derivatives, *o*-CH<sub>3</sub>O-PPE and (*o*-CH<sub>3</sub>O)<sub>2</sub>-PPE, was studied at 500 – 650 °C with residence times of 0.3 and 0.6 s.



## Experimental

The synthesis of the model compounds has been previously described.<sup>3,5</sup>

The study of pyrolysis by MBMS has been described previously.<sup>6,7</sup> All reactions were carried out at atmospheric pressure in a quartz tube reactor from 500 °C to 650 °C. A schematic diagram of reactor coupled to a molecular-beam mass spectrometer sampling system is shown in Figure 1. The quartz reactor consisted of inner and outer tubes, with pyrolysis occurring in the inner tube and the outer tube providing additional helium flow to satisfy the demands of the MBMS. The length of the inner tube from the sample to the end was 37 cm while the length of the mixing regime was 13 cm. A reactor with a spiral reaction section was used, so longer length and higher gas linear velocities could be achieved, which improved the flow characteristics. A fraction of the sweep gas (He) was introduced into the reactor through a side port where samples were inserted to facilitate sample introduction.

A sample (1-10 mg) contained in a quartz holder, or "boat", was inserted into flowing, preheated helium carrier gas. The carrier gas was introduced through the ends of inner and outer tubes and vapors exiting from the pyrolysis reactor (inner tube) were diluted with neat carrier gas in the outer tube. The hot gases exiting the reactor are expanded through an orifice on the apex of a sampling cone into the stage one vacuum at 40 mtorr. The pressure difference is sufficient for free-jet expansion, which quenches the products and allows the full range of products, including light gases, high-molecular-weight

compounds, and reactive products, to be simultaneously sampled and analyzed. A molecular beam, collimated through a second expansion, enters an ion source, where approximately 17 eV electron impact ionization is used to form ions. The ionization voltage was adjusted to minimize fragmentation of the lignin model compounds while maintaining good sensitivity. The gas phase residence time is defined as the time in the pyrolysis (inner) tube and in the mixing region of the outer tube. The flow rate of carrier gas in the inner tube was varied from 500 mL/min to 2000 mL/min, keeping total flow rate (inner and outer flow) constant at 10,000 mL/min. This varied the residence time from 0.3 s to 0.6 s.

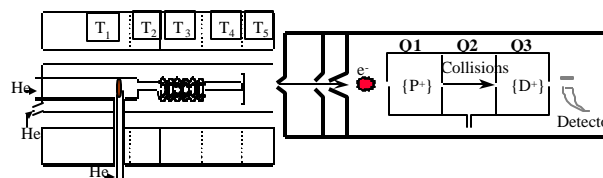
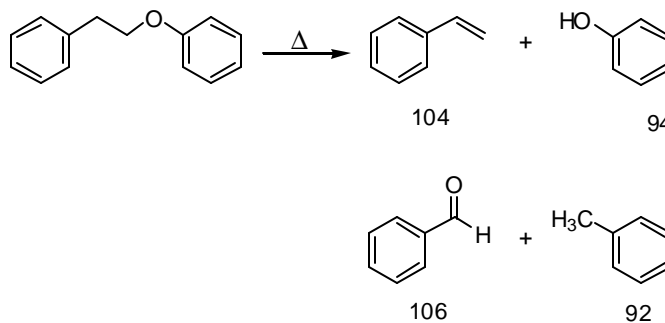


**Figure 1.** Tubular gas phase pyrolysis reactor coupled to a molecular beam mass spectrometer sampling system.

## Results and Discussion

The liquid and gas phase pyrolysis of PPE has been studied at low temperatures (330 – 425 °C).<sup>3</sup> Decomposition proceeds by a free radical chain pathway to produce two sets of products: styrene plus phenol and benzaldehyde plus toluene, in a ratio of 3:1, respectively, at 375 °C. In the FVP of PPE at 500 °C (ca. 0.3 s residence time, 0.9% conversion), the dominant reaction was C-O homolysis, which produced styrene and phenol (which accounted for 97% of the products).<sup>5</sup> Homolysis of the C-C bond, to produce toluene and benzaldehyde, was a minor reaction.



The pyrolysis MBMS of PPE was run at 500, 550, 600 and 650 °C with residence times of 0.3 and 0.6 s. As the temperature and residence time increased, the dominant products that appeared in the mass spectrum were styrene ( $m/z$  104) and phenol ( $m/z$  94) with very small amounts of toluene ( $m/z$  92) and benzaldehyde ( $m/z$  106). This product slate is very similar to that found in the FVP experiments. The mass spectrum of the reaction mixture at 600 °C and a residence time of 0.6 s is shown in Figure 2. Benzene ( $m/z$  78) can arise from the decomposition of benzaldehyde (confirmed by independent pyrolysis) and is observed as a mass spectral fragmentation product. The  $m/z$  at 105 is from fragmentation of the PPE, which decreases in intensity as the molecular ion ( $m/z$  198) decreases. Thus, the pyrolysis MBMS experiment gives primarily unimolecular products and little bimolecular reactions. However, small quantities of additional products are formed with  $m/z$  154, 168, and 180 that appear to be coupling products from the radicals formed in the reaction (phenoxy, benzyl, and phenyl, from decomposition of benzaldehyde to form biphenyl, dibenzofuran, and stilbene), but they also could arise from surface catalyzed reactions. Attempts to increase the yield of these products by addition of a free radical

initiator, such as benzyl phenyl ether, were unsuccessful. Thus, the origin of these products is still under investigation.

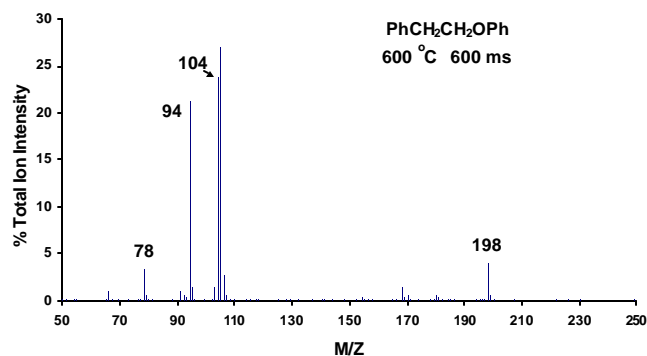
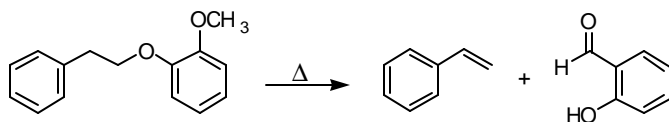


**Figure 2.** Average spectra of products detected by MBMS from the pyrolysis of PPE at 600 °C and a residence time of 0.6 s.

The pyrolysis MBMS of *o*-CH<sub>3</sub>O-PPE was run at 500, 550 and 600 °C at residence times of 0.3 and 0.6 s. The mass spectrum from a run at 500 °C and a residence time of 0.3 s is shown in the Figure 3. The mass at *m/z* 228, 124, and 105 are from mass spectrometer fragmentation of the starting material (see Figure 3), and there is little thermal decomposition of the material. At 600 °C with a residence time of 0.6 s, all the starting material is consumed (see Figure 4) indicating that the *o*-methoxy derivative is more reactive than PPE. The dominant products arise from C-O homolysis and form styrene and hydroxybenzaldehyde (*m/z* 122). Guaiacol (*m/z* 124) was a minor product in the reaction. Independent pyrolysis of guaiacol at 600 °C indicated that it was not stable under these reaction conditions but formed catechol (*m/z* 110) as the major product and small amounts of hydroxybenzaldehyde and phenol. Independent pyrolysis of hydroxybenzaldehyde at 600 °C produced small amounts of phenol (*m/z* 94). Small amounts of toluene and *o*-methoxybenzaldehyde (*m/z* 138) were also found which arise from C-C homolysis.



The major products are very similar to those formed in the FVP of *o*-CH<sub>3</sub>O-PPE at 500 °C indicating that unimolecular reactions are dominant. *o*-Hydroxybenzaldehyde is formed by C-O homolysis to give the *o*-methoxyphenoxy radical, intramolecular hydrogen abstraction to form *o*-hydroxyphenoxy radical, 1,2-phenyl shift to form *o*-hydroxybenzyloxy radical followed by β-scission of hydrogen. In solution phase at lower temperatures, bimolecular hydrogen abstraction is the dominant reaction and two sets of products are formed: guaiacol plus styrene, and toluene plus *o*-methoxybenzaldehyde, in a 3:1 ratio (at 375 °C).

The FVP of (*o*-CH<sub>3</sub>O)<sub>2</sub>-PPE produced a complex set of products.<sup>5</sup> Surprisingly, the dominant product was *o*-cresol (24 mol%), 2,6-dimethoxyphenol (13 mol%), and styrene (22 mol%). These products were formed by C-O homolysis followed by hydrogen abstraction, rearrangement, and β-scission reactions. The mass spectra of the products detected by MBMS from the pyrolysis of (*o*-CH<sub>3</sub>O)<sub>2</sub>-PPE at 600 °C and a residence time of 0.6 s is shown in Figure 5. The spectrum is surprisingly simple (compared to the FVP results). The dominant products appear to be styrene (*m/z* 104), cresol (*m/z* 108), *o*-hydroxybenzaldehyde (*m/z* 122), and benzene (*m/z* 78). Independent pyrolysis of 2,6-dimethoxyphenol at 600 °C produced a complex set of products with *m/z* 138, 126, 124, 110, 108. This indicates that 2,6-dimethoxyphenol is not a major primary product since its major decomposition products are not observed to a significant extent. More studies are needed to determine the origin of

these products. As a consequence of the decomposition and mass spectral fragmentation of the products, it is difficult to determine the primary and secondary products. Thus, the data will be analyzed by multivariate factor analysis to determine which masses (i.e., products) are correlated.<sup>8</sup> Results from this data analysis will be presented and the mechanisms of the decomposition of these lignin model compounds will be discussed.

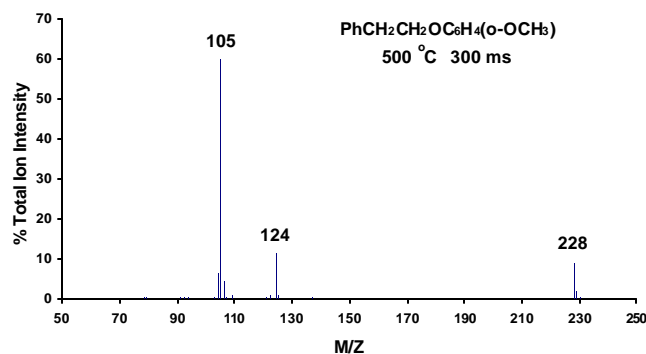


**Figure 3.** Average spectra of products detected by MBMS from the pyrolysis MBMS of (*o*-CH<sub>3</sub>O)-PPE at 500 °C.

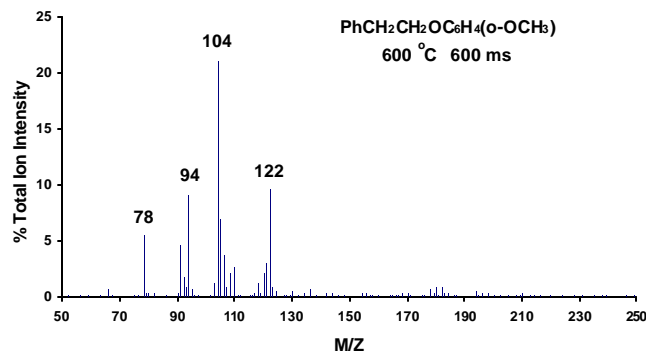


**Figure 4.** Average spectra of products detected by MBMS from the pyrolysis *o*-CH<sub>3</sub>O-PPE at 600 °C and 0.6 s residence time.

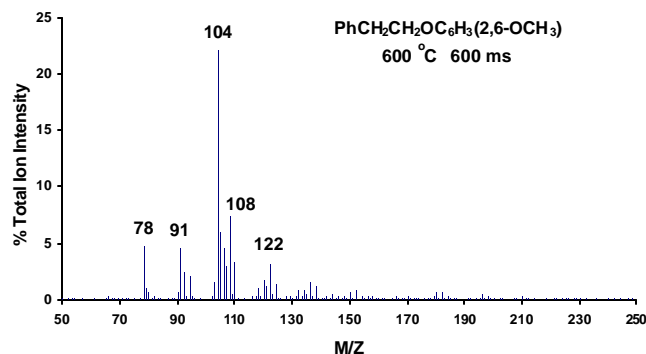


**Figure 5.** Average spectra of products detected by MBMS from the pyrolysis *o*-CH<sub>3</sub>O-PPE at 600 °C and 0.6 s residence time.

**Acknowledgement.** This research was sponsored by the Division of Chemical Sciences, Geosciences, and Biosciences, Office of Basic Energy Sciences, U.S. Department of Energy under contract

DE-AC05-00OR22725 with Oak Ridge National Laboratory, managed and operated by UT-Battelle, LLC. The authors also acknowledge the financial support from Philip Morris USA.

#### References

- (1) *Developments in Thermochemical Biomass Conversion*; Bridgwater, A. V.; Boocock, D. G. B., Eds; Blackie Academics: London, 1997.
- (2) Gargulak, J. D.; Lebo, S. E. Commercial Use of Lignin-Based Materials. In *Lignin: Historical, Biological, and Materials Perspectives*; Glasser, W. G.; Northey, R. A.; Schultz, T. P. Eds.; ACS Symposium Series 742; American Chemical Society: Washington, DC, 2000, pp 304-320.
- (3) Britt, P. F.; Buchanan, A. C., III; Malcolm, E. A. *J. Org. Chem.* **1995**, *60*, 6523.
- (4) Cooney, M. J.; Britt, P. F.; Buchanan, A. C., III *Prepr. Pap. - Am. Chem. Soc., Div. Fuel Chem.* **1997**, *42*, 89.
- (5) Britt, P. F.; Buchanan, A. C., III; Cooney, M. J.; Martineau, D. *R. J. Org. Chem.* **2000**, *65*, 1376.
- (6) Evans R.J.; Milne, T.A. *Energy & Fuel* **1987**, *1*,123
- (7) Shin, E-J.; Nimlos, M. R.; Evans, R. J. *Fuel* **2001**, *80*, 1697.
- (8) For an example see: Shin, E.-J.; Nimlos, M. R.; Evans, R. J. *Fuel* **2001**, *80*, 1681.

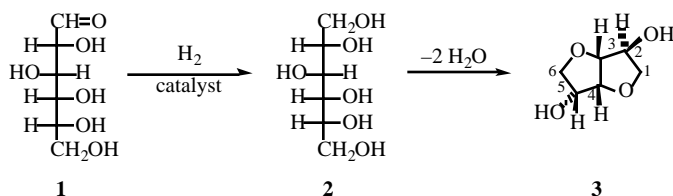
# ISOSORBIDE ESTERS: ENANTIOPURE ALCOHOLS DERIVED FROM GLUCOSE

Walter S. Trahanovsky and Yu Wang

Department of Chemistry  
Iowa State University  
Ames, IA 50011

## Introduction

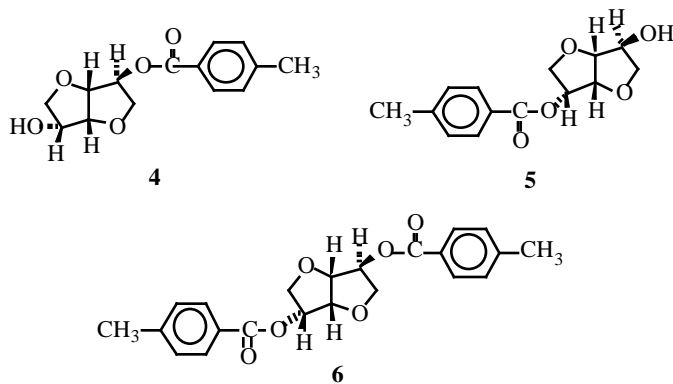
The catalytic hydrogenation of glucose (**1**) produces sorbitol (**2**)<sup>1</sup> which can be easily converted to enantiopure isosorbide by dehydration.<sup>2</sup> Isosorbide (**3**) has two hydroxy groups, one *exo*



(the 2-OH) and one *endo* (the 5-OH). Conversion of one of the hydroxy groups to an ester gives rise to a large class of enantiopure chiral alcohols. Enantiopure chiral alcohols have been used as chiral auxiliaries in asymmetric synthesis.<sup>3</sup> Moreover, the carboxylic acid portion of the ester can have other functional groups and this allows the synthesis of polyfunctional compounds that could function as complexing agents.

We have undertaken a study of the esterification of isosorbide (**3**) with the goals of a) determining how to effectively and efficiently prepare the *exo* and/or *endo* esters and b) developing convenient spectroscopic methods to determine whether the *exo* or the *endo* hydroxy group has been esterified.

Our first objective was to make and to fully characterize a pair of *exo* and *endo* esters of isosorbide (**3**). In this paper we report the preparation and characterization by <sup>1</sup>H and <sup>13</sup>C NMR spectroscopy of the mono *exo*- (**4**), the mono *endo*- (**5**), and the di (*para*-methylbenzoates of isosorbide (**3**).



## Results

Esters **4**, **5**, and **6** were prepared from isosorbide (**3**) and either *para*-methylbenzoic acid or its acid chloride. The esters were purified by column chromatography and the <sup>1</sup>H and <sup>13</sup>C NMR spectra of the esters were obtained. The chemical shifts of the <sup>1</sup>H and <sup>13</sup>C NMR data for these esters are presented in Tables 1 and 2.

Table 1. The <sup>1</sup>H NMR Chemical Shifts of Esters **4**, **5** and **6** (in CDCl<sub>3</sub>).

	<b>4</b>	<b>5</b>	<b>6</b>
H <sub>1<i>exo</i></sub>	4.171	4.016	4.116
H <sub>1<i>endo</i></sub>	4.130	3.982	4.106
H <sub>2</sub>	5.465	4.375	5.474
H <sub>3</sub>	4.633	4.454	4.667
H <sub>4</sub>	4.722	4.983	5.054
H <sub>5</sub>	4.354	5.395	5.412
H <sub>6<i>exo</i></sub>	3.938	3.946	4.038
H <sub>6<i>endo</i></sub>	3.618	3.921	4.022
H <sub>aromatic</sub> <sup>a</sup>	7.58	7.60	7.61
H <sub>CH<sub>3</sub></sub>	2.417	2.417	2.410
			2.421

<sup>a</sup> center of aromatic signals

Table 2. The <sup>13</sup>C NMR Chemical Shifts of Esters **4**, **5** and **6** (in CDCl<sub>3</sub>).

	<b>4</b>	<b>5</b>	<b>6</b>
C <sub>1</sub>	73.96	75.78	70.4
C <sub>2</sub>	78.91	76.53	78.3
C <sub>3</sub>	85.99	88.56	86.4
C <sub>4</sub>	82.3	80.94	81.3
C <sub>5</sub>	73.84	74.58	73.5
C <sub>6</sub>	72.64	71.04	74.3
C <sub>CO</sub>	165.82	166.24	166.03
			165.67
C <sub>aromatic</sub>	133.6 <sup>a</sup>	134.7 <sup>a</sup>	133.7 <sup>b</sup>
C <sub>CH<sub>3</sub></sub>	165.82	166.24	166.03
			165.67

<sup>a</sup> center of 4 signals

<sup>b</sup> center of 8 signals

## Discussion

The reaction of isosorbide (**3**) with *p*-methylbenzoyl chloride in pyridine gives all three esters, the mono *exo* (**4**), the mono *endo* (**5**), and the di (**6**). All three esters can be purified by column chromatography. The dominant mono ester is the *endo* isomer **5**.

The *exo* ester **4** is the dominant isomer when isosorbide (**3**) is allowed to react with *p*-methylbenzoic acid in the presence of dicyclohexylcarbodiimide. This is consistent with the report by Cekovic and Tokic who used this method to synthesize the isosorbide (**3**) mono *exo* benzoate.<sup>4</sup>

The <sup>1</sup>H NMR data of esters **4**, **5**, and **6** show that the proton on the carbon atom bearing the hydroxy group shifts downfield by *ca.* 1 ppm when converted to the ester. Changes of the other proton signals and of the <sup>13</sup>C signals are relatively small. The changes we observed in the <sup>1</sup>H NMR spectra of esters **4**, **5**, and **6** are consistent with the <sup>1</sup>H NMR spectrum of the benzoic acid mono *exo* ester of isosorbide (**3**) reported by Cekovic and Tokic<sup>4</sup> (the isomeric *endo* mono ester or the diester of benzoic acid is not described in this report).

## Experimental

**Preparation of mono *endo*- (**5**) and di (*para*-methylbenzoates of Isosorbide.** A 50-mL, round-bottomed flask equipped with a stir bar was charged with 0.3 g (2 mmol) of isosorbide (**3**) and 0.5 g of dry pyridine. The reaction was heated to 90 °C for 20 min and then *p*-methylbenzoyl chloride (0.67 g, 4 mmol) was added to the solution. The reaction was allowed to stand for 20 h. The mixture was treated with 2M HCl until the pH of the solution reached 1. The acidified mixture was extracted

three times with 5-mL portions of ethyl acetate. The organic layers were combined and dried over anhydrous MgSO<sub>4</sub>, and the mixture was filtered. The solvent was removed under reduced pressure. A white solid (657 mg) was obtained. After recrystallization from toluene, white needle-like crystals (126 mg) were obtained, mp = 145-152 °C. Analysis of its <sup>1</sup>H NMR spectrum showed it to be the mono *endo* ester (**5**). After evaporating the solvent of the mother liquor, ethyl ether was added to dissolve the white solid which remained. The solution was cooled with ice. White needle-shaped crystals (300 mg) was obtained, mp = 102.0-102.5 °C. Analysis of the <sup>1</sup>H NMR, <sup>13</sup>C NMR, IR, and cosy spectra of these crystals showed it to be the di ester (**6**).

When the reaction was repeated but with a reaction time of only 3 h, a mixture of all three esters was obtained: mono *exo* (**4**), mono *endo* (**5**), and di (**6**). All three esters can be separated by column chromatography. The major mono ester was the *endo* isomer (**5**).

**Preparation of mono *exo-para*-Methylbenzoate of Isosorbide (**4**).** A 50-mL, round-bottomed flask equipped with a stir bar was charged with 0.29 g (2 mmol) of isosorbide (**3**), 0.3 g (2.2 mmol) of *p*-methylbenzoic acid, and 5 mL of CH<sub>2</sub>Cl<sub>2</sub>. The solution was cooled to 0 °C and 454 mg (2.2 mmol) of dicyclohexylcarbodiimide, and 2.44 mg (0.02 mmol) of 4-dimethylaminopyridine were added with stirring. The reaction was allowed to stand at room temperature for 5 h. The mixture was filtered to remove N,N-dicyclohexylurea. The filtrate was washed with 2 mL of H<sub>2</sub>O, and then 2 mL of 5% aqueous AcOH. The washed organic layer was dried over anhydrous MgSO<sub>4</sub> and the mixture was filtered. The solvent was removed under reduced pressure to yield 379 mg white crystals, mp = 155.0-155.5 °C. Analysis of this product's <sup>1</sup>H NMR spectrum showed it to be the mono *exo*-ester (**4**). The ester can be purified by column chromatography

**Acknowledgement.** The authors would like to thank the Iowa Energy Center for financial support of this research.

## References

- (1) Noller, C. R. *Chemistry of Organic Compounds*. W. B. Saunders Company, Philadelphia, 1965, p. 434.
- (2) (a) Jasinski, W.; Ropuszynski, S. *Przegl. Nauk. Inst. Technol. Org.*, Tworzyw Sztucznych Politech. Wroclaw, 1973, 12, 3-29. (b) Fleche, G.; Huchette, M. *Starch/Staerke* **1986**, 38, 26.
- (3) (a) March, J. *Advanced Organic Chemistry*, 4<sup>th</sup> ed; John Wiley & Sons, 1992, p. 843. (b) Tamion, R.; Marsais, F.; Ribereau, P. and Queguiner, G. *Tetrahedron: Asymmetry* **1993**, 4, 1879.
- (4) Cekovic, Z.; Tokic, Z. *Synthesis* **1989**, 8, 610.

# LEVOGLUCOSAN PYROLYSIS

Mark R. Nimlos and Robert J. Evans

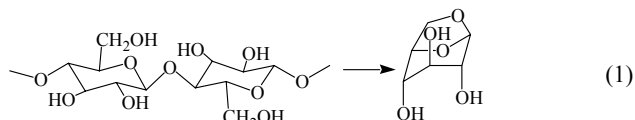
National Renewable Energy Laboratory  
1617 Cole Blvd.

Golden, Colorado 80401

Email: mark\_nimlos@nrel.gov

## Introduction

Levoglucosan 1,6-anhydro- $\beta$ -D-glucopyranose is known to be an important intermediate in the pyrolysis of cellulose, but little is known about its subsequent thermal degradation. Levoglucosan is formed in high yields (up to 60 %) by the pyrolytic unzipping of cellulose.



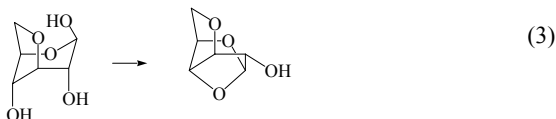
## Section of cellulose Levoglucosan

In a study of the thermal degradation of levoglucosan (600°C residence time = 8 min.), Shafizadeh and Lai<sup>1</sup> measured small molecular products such as 2-furaldehyde, 2,3-butanedione, pyruvaldehyde, acetaldehyde and glyoxal. They attempted to identify reaction mechanisms for the degradation of levoglucosan through radioactive labeling (<sup>14</sup>C) of the 1,2 and 6 carbon of levoglucosan and measurements the incorporation of this radioactivity into the pyrolysis products. Based upon earlier work by Gardiner<sup>2</sup> on cellulose pyrolysis, Shafizadeh and Lai proposed that levoglucosan is initially converted to 3,6-anhydro-D-glucose.



## 3,6-anhydro-D-glucose

Gardiner's work<sup>2</sup> also showed that this product can be thermally converted into 1,4:3,6-dianhydro-D-glucose.



## 1,4:3,6-dianhydro-D-glucose

Recently Li *et al.*<sup>3</sup> measured the evolution of CH<sub>2</sub>O, CO and CO<sub>2</sub> from the thermal degradation of levoglucosan using gas phase infrared (IR) spectroscopy. Finally, we have measured the global kinetics of the pyrolysis of levoglucosan using molecular beam mass spectrometry.<sup>4</sup>

Here we will report some of our work on the pyrolysis of levoglucosan in which we measure products by matrix isolation IR spectroscopy. Our studies are aided by electronic structure calculations (B3LYP/cc-pVDZ), which will allow us to accurately estimate reaction energies and occasionally reaction barriers. These values will be essential for estimating reaction kinetics.

## Experimental

Pyrolysis experiments are conducted in flowing argon in a two-stage alumina tubular reactor (1 cm ID) and the products are deposited on a cold (8 K) salt window at the tip of cryostat. Levoglucosan is volatilized in the first stage of the reactor (resistively heated with nichrome wire) and pyrolyzed in the second stage

(resistively heated with tungsten wire). The maximum practical temperature for the second stage is roughly 1200 °C. We estimate that the pressure in the reactor is about 100 mtorr and the residence time is about 1 ms. The levoglucosan is fed into the first stage of the reactor in a quartz boat that is fastened to the end of a thermocouple. The temperature of the sample is controlled so that sufficient levoglucosan is volatilized but so that the concentration is low enough that bimolecular reactions are minimized and good isolation is obtained. Once a sample has been deposited, IR absorption spectra are recorded using a Nicolet Magna 550 spectrometer.

## Results and Discussion

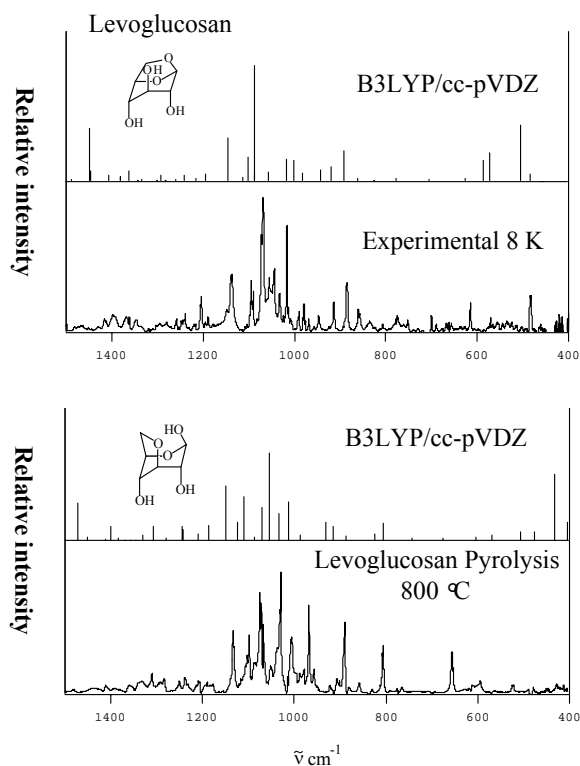


**Figure 1** Matrix isolation IR spectra of levoglucosan (top half) and its pyrolysis products (bottom half). The top experimental spectrum of levoglucosan is compared to that computed with B3LYP/cc-pVDZ calculations. In the bottom half, the measured spectrum is compared to the calculated spectrum of 3,6-anhydro-D-glucose.

**Figure 1** shows the matrix isolation infrared absorption spectra of a typical pyrolysis experiment involving levoglucosan. The top half of the figure compares the experimentally measured IR spectrum of levoglucosan with the IR spectrum calculated using B3LYP/cc-pVDZ. The experimental spectrum was collected by heating the levoglucosan to about 60 °C as measured by the thermocouple near the sample boat. At this temperature the vapor pressure of levoglucosan<sup>5</sup> is about 10<sup>-5</sup> torr and a mixing ratio with the argon of about 1/10,000. The calculated spectrum is uncorrected and was obtained using the Gaussian98 program suite<sup>6</sup> running on a SGI super cluster at the National Center for Supercomputing Applications. The B3LYP technique has been shown<sup>7</sup> to produce reasonable frequencies and IR intensities. Since the calculated transitions are harmonic frequencies, they are typically shifted to a higher energy than the experimentally observed transitions by roughly 3%. As can be seen from this figure, the fit of the calculated spectrum to the experimental spectrum is good.

The bottom half of **Figure 1** shows the experimental spectrum obtained when the second stage of the reactor is heated to 800 °C, while the sample is held at 60 °C in the first stage. The observed spectrum contains only gas phase pyrolysis products as well as some remaining levoglucosan, which has been subtracted from the spectrum presented in the figure. Since the concentration of the levoglucosan is low, this spectrum contains products that are primarily a result of unimolecular decomposition of levoglucosan. We tested this by changing the vaporization temperature and thus, the concentration of the levoglucosan. We saw no change in the IR spectrum when the concentration was lowered.

The infrared spectrum that we obtain by pyrolyzing levoglucosan at 800 °C is suggestive of that calculated for 3,6-anhydro-D-glucose. This calculated spectrum is shown in the bottom half of **Figure 1**, above the experimental spectrum. As can be seen there is a good fit of most of the features to this calculated spectrum to the experimental spectrum. There is an intense peak at 1075 cm<sup>-1</sup>, which may result from 1,4:3,6-dianhydro-D-glucose. Our calculations show that this molecule should have two intense transitions at 1068 cm<sup>-1</sup> and 1103 cm<sup>-1</sup> (harmonic frequencies). Further evidence for the formation of these two molecules lies in the fact that no IR transitions were observed in the region from 1650 cm<sup>-1</sup> to 1850 cm<sup>-1</sup>. Elimination of water or formaldehyde should result in intense peaks in this region. The absence of intense transitions in this region suggests that the products are unsaturated.

**Calculations of Reaction Pathways** In order to investigate possible decomposition pathways for levoglucosan further, we used density functional theory (B3LYP) to estimate reaction energies for some like decomposition reactions. This technique has an RMS accuracy of about 3 kcal mol<sup>-1</sup> compared to the G2 set of molecules.<sup>8</sup> Figure 2 shows the relative energies of some of the potential products from the unimolecular decomposition of levoglucosan and their calculated energies. These will be discussed below.

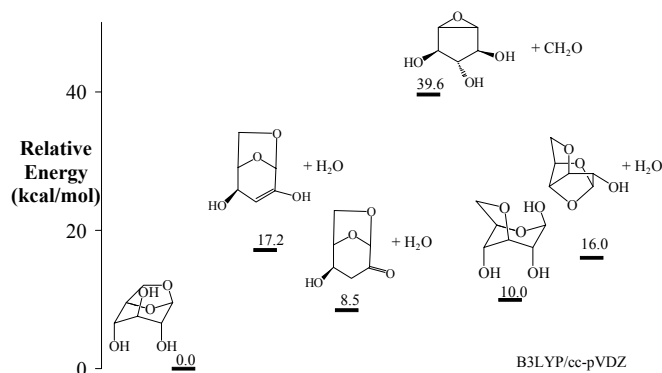
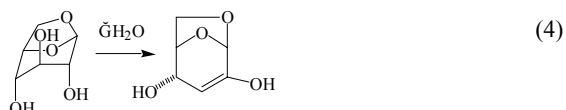


**Figure 2** Calculated relative energies of different products from the pyrolysis of levoglucosan.

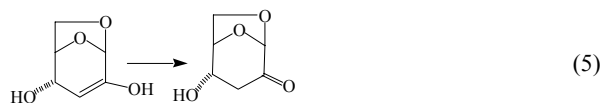
Homolytic bond dissociation in levoglucosan will not be important under typical pyrolysis conditions because the bond strengths are too high. The weakest bonds are the C–O ether bonds which will have bond energies<sup>9</sup> of about 82 kcal mol<sup>-1</sup>. With a large pre-exponential factor of 10<sup>15</sup> s<sup>-1</sup>, which is typical for bond scissions, the rate constant for these reactions at 600°C would be smaller than 10<sup>-6</sup> s<sup>-1</sup>. This is much smaller than the observed global rate constant (0.45 s<sup>-1</sup>) for levoglucosan destruction.<sup>4</sup>

Concerted reaction mechanisms are more likely. Dehydration of the alcohol groups to form alkenes is an example of this type of reaction. Loss of water from levoglucosan can result in the formation

of a vinyl alcohol. For example, loss of the OH from the number 3 carbon can form the following vinyl alcohol.

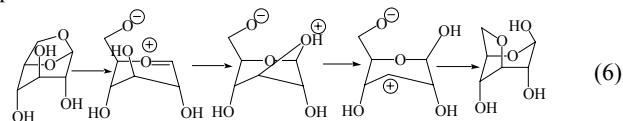


We calculate a reaction enthalpy for reaction (4) of  $\Delta_{\text{react}}H_{298\text{ K}} = 14.0$  kcal mol<sup>-1</sup>. The same reaction enthalpy is calculated for loss of the OH from the number 2 carbon, suggesting that all of the possible dehydration reactions involving the three OH groups in levoglucosan have a similar reaction enthalpy. We have conducted an exhaustive study of these types of dehydration reactions using electronic structure techniques<sup>10</sup> and found that the reaction barriers are about 69 kcal mol<sup>-1</sup>. Vinyl alcohols formed by dehydration reactions such as are shown in reactions (4) are likely to be quickly followed by enol-keto tautomerizations such as



We calculate a reaction enthalpy of  $\Delta_{\text{react}}H_{298\text{ K}} = -12.6$  kcal mol<sup>-1</sup> a reaction barrier of 56.2 kcal mol<sup>-1</sup> for this type of reaction. From the computed barriers and vibrational frequencies, we obtain a rate constant of about 10<sup>-4</sup> s<sup>-1</sup> (at 600°C) for reaction (4) and 10<sup>0</sup> s<sup>-1</sup> (at 600°C) for reaction (5). Since the first rate constant is low compared to the global rate constants for levoglucosan (0.45 s<sup>-1</sup>),<sup>4</sup> reactions (4) and (5) should not be important. Indeed we do not observe IR transitions for these products.

We are considering a mechanism for (2) and (3) involving an oxonium ion. For instance, reaction (2) may involve the following steps.



Our calculations suggest that formation of the oxonium ion, the first intermediate in (6), may require less than 50 kcal mol<sup>-1</sup>. This could make reaction (2) possible under pyrolysis conditions. Furthermore the anhydro product from reaction (3) may be formed directly from this oxonium ion.

#### Acknowledgement

We would like to acknowledge the support of Phillip Morris and Mohammad Hajoligol the National Center for Supercomputer Applications (NCSA Grant # CHE-980028N).

#### References

- Shafizadeh, F.; Lai, Y. Z. *J. Org. Chem.* **1972**, *37*, 278.
- Gardiner, D. *J. Chem. Soc. C* **1966**, 1473.
- Li, S.; Lyons-Hart, J.; Banyasz, J.; Shafer, K. *Fuel* **2001**, *80*, 1809.
- Shin, E.-J.; Nimlos, M. R.; Evans, R. J. *Fuel* **2001**, *80*, 1697.
- Oja, V.; Suuberg, E. M. *J. Chem. Eng. Data* **1999**, *44*, 26.
- Gaussian 98 (Revision A.1x), Gaussian, Inc., Pittsburgh PA, 2001.
- Koch, W.; Holthausen, M. C. "A Chemist's Guide to Density Functional Theory," 2<sup>nd</sup> Edition, Wiley, New York, 2001.
- Foresman, J. B.; Frisch, A. E. "Exploring Chemistry with Electronic Structure Methods," 2<sup>nd</sup> Ed. Gaussian, Inc, Pittsburg, 1995.
- Benson, S. W. "Thermochemical Kinetics," 2<sup>nd</sup> Ed., Wiley, New York, 1976.
- Nimlos, M. R.; Blanksby, S. J.; Evans, R. J. *J. Anal. Applied Pyrol.* Submitted.

# LIQUID SMOKE: PRODUCT OF HARDWOOD PYROLYSIS

*S. Ramakrishnan, Patrick Moeller*

Hickory Specialties, Inc, 1619 Service Merchandise Blvd, Brentwood  
-TN-37027, U.S.A

## Introduction

Liquid smoke compositions are obtained from pyrolysis of hardwood. These solutions are used to impart flavor, color, texture and in certain cases provide enhanced shelf life for food products. The constituents of liquid smoke are obtained from thermal degradation reactions of cellulose, hemicellulose and lignin. More than four hundred compounds have been detected in wood smoke.<sup>1</sup> In order to express the composition from an application stand point, the compounds in liquid smoke have been lumped together as three functional groups: carboxylic acids, phenols, and carbonyls. Cellulose and hemicellulose degradation are the primary sources of carbonyls and carboxylic acids, while phenols are obtained from lignin pyrolysis. In addition to these functional classes, there are other products like alcohols, lactones, and hydrocarbons.

The main variables that control liquid smoke product yield and characteristics are temperature, rate of heat transfer, particle size, atmosphere of pyrolysis, vapor and particle residence times, and composition of biomass. The developments related to control of these variables for improved product and process capabilities have resulted in several patents and publications over the last two decades in the field of liquid smoke. The difference in heat transfer rates results in different product yields. Rapid heat transfer rates are associated with fast pyrolysis systems.<sup>2</sup> Further liquid smoke flavors with different attributes can be made by varying the feedstock.<sup>3</sup> Experiments were done in a bench scale reactor system under conditions of slow pyrolysis. The characteristics of liquid obtained from such bench scale experiments were compared with commercial product.

## Experimental

### Bench-scale Pyrolysis of Dried Saw-dust Under Atmospheric Conditions:<sup>3</sup>

Dried mixed hard wood saw-dust (150 gm, 8 % moisture) was weighed into a 4-inch diameter, 14 inch long laboratory size quartz rotary kiln and placed in a heated tube furnace. The reaction tube was rotated, so as to mimic the industrial process of a horizontal rotary kiln. The vapors from pyrolysis were then condensed in two vertical condensers in series. The first condenser was held at 65 °C and the second was held at 5 °C. The non-condensable vapors were then passed through filters for removing any aerosols, before being vented off. The liquids collected in the condensers were weighed. The test time was dependent on the time required for the char bed to attain the desired bed temperature. The test was stopped when gas evolution was not observed at the desired char bed temperature.

### Analysis of Aqueous Condensate:<sup>3</sup>

The condensates were diluted with water, and analyzed for their overall composition for acid and phenol content.<sup>4</sup> The procedures used for composition analysis were those used in the liquid smoke industry. The acid content was determined by titration and expressed as percentage acetic acid. The phenols were determined by colorimetric methods using 2,6-dimethoxy phenol (Aldrich Chemical Co., U.S.A) as standard.<sup>3</sup> In this procedure liquid smoke solutions and standard solutions are complexed with 2,6-dichloroquinine-4-chloroimide (Aldrich Chemical Co. U.S.A) in a borate buffer solution at a pH of 8.3. The reaction is allowed to proceed for 30 minutes at room temperature. The color of the resulting complex is measured at 580

nm. The performance characteristics for the ability of carbonyls in liquid smoke to react with proteins was measured by staining index.<sup>3</sup> This index is obtained by measuring the net absorbance of a reacted sample of glycine and liquid smoke at 440 nm in a glacial acetic acid solution.<sup>3</sup>

## Results and Discussion

The product yields from bench scale experiments at various temperatures are presented in table 1.

**Table 1. Hardwood Saw-dust Pyrolysis Product Yields from Bench scale Experiment:**

Temperature °C	Liquid yield (%)	Char yield (%)
350	45.7	37.5
400	51.5	28.8
475	59.6	22.8
600	54.7	18.9

The yield values indicate an increase in liquefaction type reactions with increasing temperature. For similar temperatures, higher liquid and lower char yields are obtained from fast pyrolysis type process. The mechanisms involved in the degradation process of the saw dust components to various products have been presented by various researchers.<sup>4,5,6</sup> The composition analysis of the aqueous fraction from bench scale experiments for liquid smoke type characteristics are presented in table 2.

**Table 2. Composition Analysis (range) for Aqueous Fraction from Bench Scale Pyrolysis Experiments**

Temperature range °C	400 –600°C
Acidity %	6.1 – 7.2
Phenol (mg/ml)	9.9 – 11.1
Stain index	69.6 – 81.5

The composition analysis indicates an increase in smoke components in the aqueous fraction with increase in temperature. In a traditional liquid smoke manufacture saw-dust is pyrolyzed in temperature ranges of 350-600°C, under atmospheric pressure conditions. The vapors from pyrolysis are condensed and contacted with water. The aqueous condensate is allowed to settle for a period of ten to fourteen days. During this period, an insoluble organic fraction referred to as tar separates out. This fraction carries with it particulates and PAH compounds that are generated and condensed during the manufacturing process. The benzo(a)pyrene content of the resulting aqueous smoke is less than 2ppb. PAH characterization of liquid smoke can be done by HPLC –fluorescence spectroscopy or GC-MS.<sup>7</sup> A typical liquid smoke product from slow pyrolysis has the following average composition<sup>4</sup>: acidity =10.8%, phenol = 17.8 mg/ml, stain index =91.6. The acid and phenol concentration in liquid smoke indicate the flavor strength. The stain index value, provides information on the reactivity of the carbonyl compounds in liquid smoke towards non-enzymatic maillard type browning reactions with amino acids when applied on protein substrates. Thus it is observed that the aqueous extract from bench scale experiments have characteristics similar to a commercial liquid smoke product.

## Conclusion:

The similarities in compositional analysis data from bench scale experiments and commercial product indicate suitability of the bench scale experiments to study biomass pyrolysis chemistry for liquid smoke manufacture. Liquid smoke, a product of the biomass pyrolysis provides a safe alternative to food processors over conventional smoke houses. The clean up steps used in the manufacturing process makes it a safe ingredient.

References:

- (1) Maga, J.A. *Smoke in Food Processing*; CRC Press: Boca Raton, FL 1988
- (2) Graham, R.J.; Bergougnou, M.A., *Journal of Analytical and Applied Pyrolysis* **1984** (6), 95-135.
- (3) Moeller, P.W.; Ramakrishnan, S., *U.S. Patent 6214395* **2001**.
- (4) Mark R. Nimolos; Eun -Jae Shin; Alex L. Brown; Robert J. Evans, John W. Daily, *Prep. Pap.-Am. Chem.Soc., Div Fuel Chem* **2001**, 46 (1) 185.
- (5) Evans R.J.; Thomas A. Milne, *Energy Fuels* **1987**, 1, 123
- (6) Jan Piskorz; Desmond Radlein, *Journal of Analytical and Applied Pyrolysis* **1986** (9), 121-137.
- (7) Mario Dolores Guillen, Patricia Sopelana, Aranzazu Partearroyo., *J. Agri. Food Chem.*, **2000**, 48, 126.

## New Chemicals and Polymers from Renewable Resources

Joseph J. Bozell, Stephen Kelley, Wanxuan Kang, Darrin Miller, and Mark Davis

National Renewable Energy Laboratory  
1617 Cole Boulevard  
Golden, CO 80401

### Introduction

Biochemical pathways offer a rich source of new biomass derived building blocks. For example, the well known citric acid cycle is the central process in cellular respiration, and proceeds through 2-ketoglutaric acid (2-KGA) as a key intermediate. In most organisms, 2-KGA is a relatively transient intermediate in the metabolic process. However, some organisms do not possess a complete cycle, and stop at 2-KGA, allowing it to accumulate. Certain bacteria have been described as useful for the production of 2-KGA.<sup>1</sup> In addition, 2-KGA is an intermediate in the fermentative production of MSG, a large scale commercial bioproduct.<sup>2</sup> We wish to describe our preliminary results in the use of 2-KGA as a monomer in the production of new polyesters, and as a starting material for the synthesis of new renewables based chemical building blocks.

### Experimental

**Materials and Methods.** All reagents were commercially available and used as received. GPC was carried out using 3 columns (300 x 7.8 mm each, Polymer Laboratories) connected in series, containing polystyrene-divinylbenzene copolymer gel (10  $\mu\text{m}$  diameter particles) with nominal pore diameters of  $10^4$ ,  $10^3$ , and 50  $\text{\AA}$ . The samples (about 50  $\mu\text{g}$  sample/injection) were eluted with HPLC grade THF, at a flow rate of 1.0 mL/minute and were monitored by UV (220-400 nm) and RI. The columns were calibrated with polystyrene standards ranging in molecular weight from 580 to  $2 \times 10^6$  (Polymer Laboratories).  $M_n$  and  $M_w$  were calculated using PL Caliber GPC/SEC Software (Polymer Laboratories). Glass transition temperatures ( $T_g$ ) were measured on a DSC instrument (TA Instruments), using the transient method between -100 and 200°C at a scanning rate of 20°/min.  $T_g$  was designated as the temperature at half height of the transition shift. Variable amplitude cross polarization  $^{13}\text{C}$ NMR spectra were taken using a 2ms contact pulse ramped 1dB and a 1s recycle delay time. Single pulse  $^{13}\text{C}$  spectra were acquired using a 90° tip pulse and a 50 sec recycle delay time. For the single pulse experiments, the longest relaxation times were measured to be 10s using an inverse recovery pulse sequence.

**General procedure for the production of 2-KGA based polyesters.** 2-KGA (1 eq) was mixed neat with the diol components (1.01 eq) and 1% p-TsOH. The mixture was heated for three sequential 24h periods, first at 105°C, then 130°C, and finally 150°C.

### Background

The use of renewable raw materials as feedstocks for chemical production is continually suggested as offering several advantages over conventional petrochemical feedstocks, including a lowered demand for diminishing crude oil supplies, greater sustainability of the raw material source, the ability to recycle  $\text{CO}_2$ , the security of domestic feedstock supplies, and a source of new, structurally interesting building blocks with new properties and applications.<sup>3</sup>

Yet, despite these advantages, the huge majority of chemicals in the marketplace is not biomass derived. Although there are a few large scale examples of renewables based industrial production (the corn wet milling industry, production of EtOH, or the pulp and paper industry),<sup>4</sup> most chemical production is still based on petrochemicals.

Frequently, the dearth of renewables in the chemical feedstock stream is blamed on cost. Biomass based materials are normally assumed to be more expensive to use than existing petrochemicals. However, a closer examination indicates that cost is not nearly as large an issue as is commonly assumed. Many of the chemical building blocks available from biomass can be obtained at costs that are very competitive with existing building blocks in the chemical industry. Moreover, even the primary raw materials can be competitive on both an energy and weight basis when raw material costs are considered. Other factors, such as processing, collection, or transportation may be important, but are frequently minimal in comparison to the raw material costs.<sup>5</sup>

Other issues have been seen as hindrances to the existence of a large scale biobased products industry. In a very broad sense, either a petrochemical based industry or a biomass based industry faces issues of supply, separation, and conversion. To a first approximation, issues of supply and separation are solved for both the biomass and petrochemical industry. In contrast, processes for raw material or building block conversion are significantly better understood for petrochemical based starting materials. Many of these processes are highly efficient, and proceed in very high yield. Many of the products can be made from several different routes. Importantly, most of these processes are thoroughly understood at the molecular level. The amazing process control that is the hallmark of many industrial processes is achieved through a deep understanding of discrete chemical mechanism of transformation. Most of these features are not well developed in the biobased products industry.

Accordingly, we have been investigating new methodology to improve the technology available for the conversion of renewable building blocks into chemicals. This investigation includes the identification of new building blocks, and new synthetic methodology to convert these building blocks into chemicals. We have recently started to investigate production of new polymeric materials based on the synthetic roadmap shown in **Figure 1**.

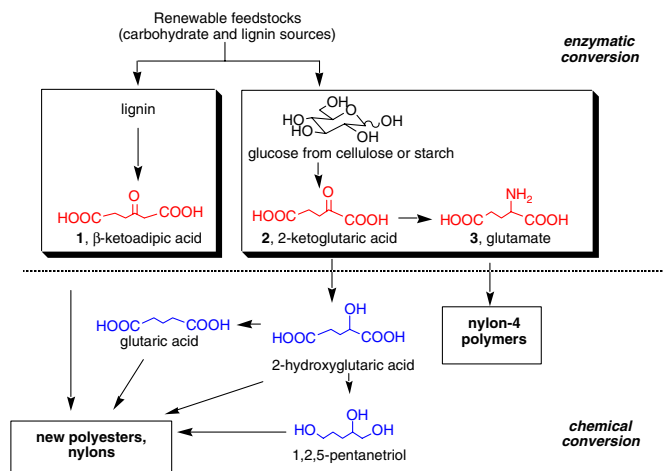


**Figure 1.** Reaction matrix for 2-KGA and derivatives

### Results and Discussion

The renewable raw materials used for this scheme are carbohydrates, leading to 2-KGA or glutamic acid, available through bioprocessing.<sup>6</sup> Importantly, these initial building blocks can be converted into an even larger family of renewables based materials through simple chemical transformations. Our initial investigation has looked at the use of these materials in the production of renewables based polyesters (**Figure 2**).

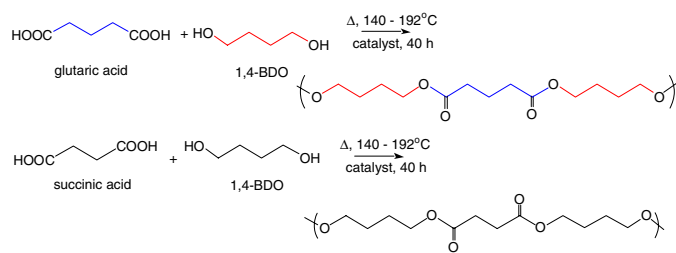


**Figure 2.** Production of linear polymers

Reaction of glutaric acid with 1, 4-butanediol between 140 – 190°C in the presence of catalytic p-TsOH results in the formation of a clear, light yellow rubbery material, presumably with the linear structure shown. Substitution of succinic acid as the diacid component leads to a stiffer material. We have carried out a number of polymerizations under these conditions, varying both the diacid and diol component, and find that we can produce polymers with reasonable molecular weights ( $M_w$  ~20,000 – 40,000;  $M_n$  ~10,000 – 20,000).

Substitution of the diacid component with 2-KGA introduces some profound changes in the polymerization process. The presence of the 2-keto group would be expected to introduce new electronic and structural variations in the process, leading to differences in reactivity. For example, the conditions initially used for production of the linear polymers of **Figure 2** lead to formation of dark intractable materials when 2-KGA is reacted with 1,4-butanediol. We have found that a three stage process (see Experimental Section) is much more effective for production of polymers based on 2-KGA (**Figure 3**).

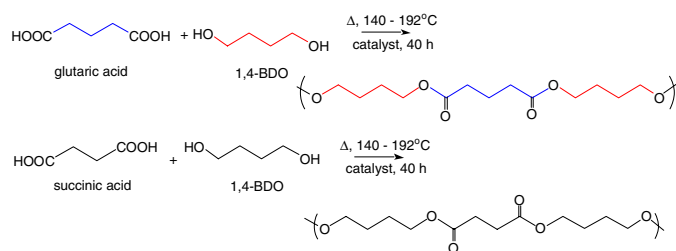


**Figure 3.** Polyester formation from 2-KGA and possible crosslinking mechanism

Changing the diol component from 1,4-butanediol to 1,3-propanediol leads to a stiffer material. As with the linear polymers, the molecular weights of these materials are also reasonable. Further heating of these materials to 165°C for several days results in a steady increase in the  $T_g$ .

In contrast to the initial linear polymers, polyesters based on 2-KGA become insoluble after heating for about 5 hours, indicating the presence of a crosslinking process. Several possible mechanisms to account for this crosslinking are possible, each centering upon a proposed initial reaction between the keto group of 2-KGA and the diol component of the polymerization.<sup>7</sup> We have investigated this reaction by solid state NMR, and observe a fairly smooth transition with time from the starting monomeric components to a crosslinked material that gives signals consistent with this mechanism. We have also tried to identify the initial reactions of the polymerization process by studying the solution esterification of 2-KGA with n-BuOH. Preliminary results indicate that the BuOH component shows little preference for one acid group over the other.

Finally, we have been studying the chemical conversion of 2-KGA into other building blocks (**Figure 4**) and find that some simple

transformations can lead to a much wider family of starting monomers for chemical production. Future work will include incorporation of these monomers into new renewables based polymeric materials.

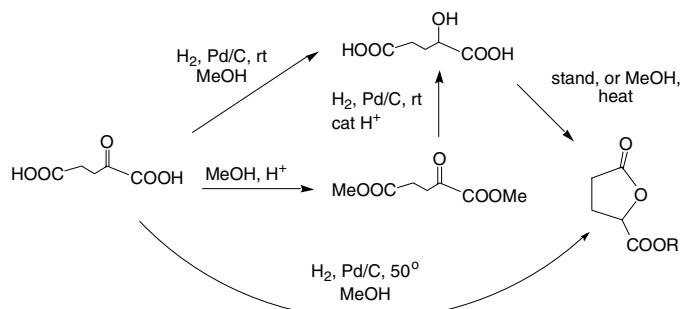


**Figure 4.** Transformations of 2-KGA into additional building blocks

## Conclusions

Renewable feedstocks derived from well known biochemical pathways can be useful building blocks in the production of new materials. 2-KGA forms novel crosslinked polyesters upon reaction with diols. Future work will expand this process to a wider range of monomers and polymers.

**Acknowledgement.** This work was supported by the NREL Director's Discretionary Research and Development program.

## References

- (1) Katagiri, H., Tochikura, T., Imai, K., *Bull. Agr. Chem. Soc. Japan*, **1957**, 21, 210.
- (2) 3 billion lb/yr of MSG is produced worldwide at a cost of \$0.75 - 0.80/lb; Bizzari, S., Janshekar, H., Yoneyama, M., *Chemical Economics Handbook*, July 2000, p. 543.6000.
- (3) *Chemicals and Materials from Renewable Resources*, Bozell, J. J., ed., ACS Symposium Series, **2001**, 784.
- (4) Several good smaller scale examples of commercial renewables based bioprocesses exist, but at a scale much smaller than a typical petrochemical based process; Wilke, D., *Appl. Microbiol. Biotechnol.*, **1999**, 52, 135.
- (5) Lynd, L. R. Wyman, C. E. Gerngross, T. U. *Biotechnol. Prog.*, **1999**, 15, 777.
- (6) We are also studying the  $\beta$ -ketoacid pathway, a process used by many organisms for the metabolism of aromatic compounds, and a possible route for the use of lignin as a renewable feedstock. This path provides  $\beta$ -ketoacidipic acid, which will be described in future publications; Harwood, C. S., Parales, R.E., *Annual Rev. Microbiol.*, **1996**, 50, 553
- (7)  $\beta$ -Keto acids form hydrates, and undergo condensation; Cooper, A. J. L., Ginos, J. Z., Meister, A., *Chem. Rev.*, **1983**, 83, 321.

# Production of ethyl esters from crude soybean oil: Optimization of reaction yields using a 2<sup>3</sup> experimental design and development of a new analytical strategy for reaction control.

Zagonel, G. F., Peralta-Zamora, P. G. and Ramos, L. P.\*

Research Center in Applied Chemistry (CEPESQ), Department of Chemistry, Federal University of Paraná – P. O. Box 19.081 – Curitiba, Paraná, Brazil – 81531-990 – fax (55) (41) 361-3186; phone (55) (41) 361-3175 – lramos@quimica.ufpr.br

## Introduction

In Brazil, as in many other countries, the first oil crisis in 1973 led to political initiatives to allocate funds for the development of alternative motor fuels. Initially, this program dealt with various types of raw materials and studied different conversion technologies to produce different liquid fuels from renewable resources (*e.g.*, ethanol). In all of its diversity, this broad national program also included efforts to develop vegetable oils and their derivatives for fuels applications. Indeed, this research area received governmental funding up to 1985, when it was discontinued from a general perception that the cost of making biofuels such as biodiesel from vegetable oils would always be greater than the products derived from the already well established petroleum chemistry and technology (MIC, 1985).

In recent years, ever since the Middle East crisis initiated a new cycle, the concept of producing biofuels from renewable resources regained international attention. In a direct attempt to contribute to this process, several projects were initiated in our country to evaluate the production of biodiesel from agro-commodities available nationwide, that is, ethanol and vegetable oils. In this work, the production of ethyl esters from crude soybean oil has been optimized and new analytical methods for process control have been designed to facilitate the *in situ* evaluation of reaction yields.

## Experimental

**Synthesis.** The optimization study developed herein was based on an experimental design in which three process parameters were assessed in two levels (2<sup>3</sup> experimental design): the ethanol:oil molar ratio used for transesterification (6:1 to 10:1), the concentration of the alkaline catalyst (KOH, 0.2 to 0.6% in relation to the oil mass) and the reaction temperature (40 and 70°C). A further expansion of the experimental design was performed at 40°C, with the ethanol:oil molar ratio ranging from 6:1 to 14:1, whereas the KOH concentration varied from 0.2 to 1% (Zagonel, 2001).

**Methods.** The reaction yields were initially monitored by size exclusion chromatography (SEC) and, at the latter stage of the project, by Fourier-transformed infrared spectroscopy (FTIR) (Zagonel, 2001). This method was successfully used to develop a mathematical model which could easily predict *in situ* reaction yields, thus allowing for a direct monitoring of conversion rates inside the transesterification vessel. Development and validation of the proposed model was carried out by multivariate analysis and the data was treated by principal component analysis and partial least squares regression.

**Size exclusion chromatography** was carried out using a Shimadzu LC10AD workstation provided with a SIL10A autosampler

and detection by differential refractometry (RID10A). Samples placed in THF were filtered through a Teflon membrane with a pore size of 0.45 µm and analysed using a series of one guard column and two Tosoh TSK-GEL columns (TSK 2000HXL and TSK 1000HXL). Tetrahydrofuran (THF) was used as the eluting solvent at a flow rate of 1 mL.min<sup>-1</sup>. A minimal of three analyses were carried out for each replicate and calibration was based on injection of external standards including ethyl oleate and mono, di and triolein.

**FTIR spectroscopy.** Standards (3 to 30 mg/mL) and reaction aliquots were also analysed by Fourier-transformed infrared spectroscopy (FTIR) using a Reagen KBr cell for liquid samples. The FTIR spectra were collected using a Bomem FTIR MB-100 spectrophotometer within the region of 500 to 4000 cm<sup>-1</sup>, with a resolution of 4 cm<sup>-1</sup>, 32 scans and triangular apodization.

## Results and Discussion

The optimal conditions for the one-step transesterification of crude soya oil with ethanol, in which an actual ester yield of 95% was obtained, were: ethanol:oil molar ratio of 12:1, KOH concentration of 0.8% in relation to the oil mass and reaction temperatures of 40°C. These conditions were shown to be adequate for the transesterification of used cooking oil as well, and a first scale up experiment, carried out by a factor of 50 in relation to the bench scale, was also proven perfectly feasible. Lower molar ratios were also proven adequate when reaction times longer than 1 h were used.

Four replicates were carried out at the center point of the experimental design to validate the analytical data generated throughout its execution. The relative standard deviation of the process, including all steps ranging from sampling to SEC analysis, was shown to be only 1.6%. Hence, the overall trends demonstrated by the experimental data were considered of sufficient statistical significance to back-up the proposed conclusions and process recommendations.

In respect to the experimental design, there was a certain limitation in increasing both the ethanol:oil molar ratio and the concentration of the alkaline catalyst (KOH) for further increases in reaction yield. Also, for reactions carried out for more than 20 minutes, temperatures above 40°C were detrimental to the amount of ester produced. In this regard, since the reaction was always carried out in one single step, it seemed that yields could be increased if a two-step transesterification strategy is included, probably using lower ethanol:oil molar ratios.

The FTIR model developed in this work to follow up *in situ* reaction yields was proven very useful and much more effective than traditional methods such as gas-liquid, size exclusion (SEC) and reverse-phase chromatography. The model matched almost perfectly the experimental data obtained by SEC, with a R<sup>2</sup> of 0.984 (Figure 1). This is certainly one outstanding achievement because both methods, regardless of differences in their principles, provided almost identical reaction yields for most of the time in which the reaction was followed.

The ethyl esters produced in this work were proven very appropriate for fuels applications. Tests were recently conducted in stationary diesel engines and the results were very promising in both fuel performance and emissions. Longer field tests, similar to those previously done in Curitiba (PR) with methyl esters produced from soybean oil (B20 mixtures), are solely awaiting for a greater local availability of this biofuel, which is now being synthesized in amounts by far below the least requirements for field trials. Therefore, viability

of the process is still depending upon a reasonable scale up to a pilot plant level, whereby a suitable cost assessment should indicate how far are we from implementing this process in our country.

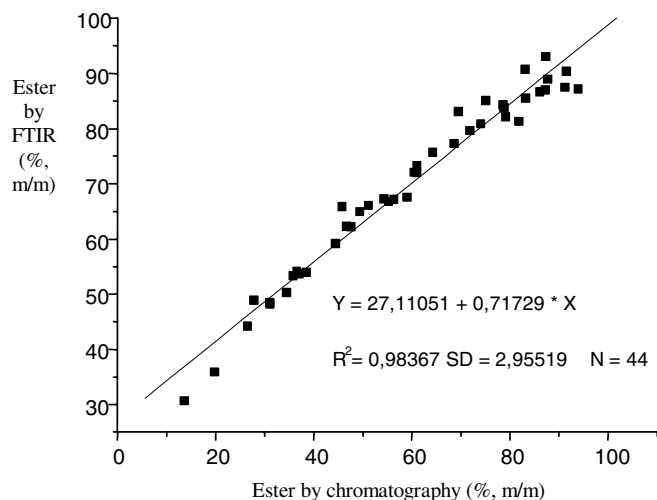


**Figure 1.** Correlation among reaction yields obtained by infrared spectroscopy and size exclusion chromatography

### Future Perspectives

Biodiesel is, by many, one almost irresistible alternative to diesel oil since many environmental as well as social and economic benefits would readily arise from its utilization in both transportation and energy generation. In Brazil, there has been an increasing interest in developing such an alternative but the economics of producing biodiesel from vegetable oils have always been negative. However, several factors are indicating that changes are just around the corner. These include the severe retraction recently observed in the soybean oil market, the competition of the soybean oil with vegetable oils derived from other sources (e.g., rapeseed, sunflower, palm, dendê and others), the recent decline in exportation of the edible oil to Asian markets such as China, and the several consecutive annual records recently attained in soybean production in Brazil (with the concomitant increase in productivity as well).

To our knowledge, only five Brazilian institutions are now directly involved with biodiesel: The State University of Santa Cruz (Ilhéus, BA), The COPPE School of Engineering (Rio de Janeiro, RJ), The Tecnology Institute of Paraná (TECPAR, Curitiba, PR), The National Institute of Technology (INT, Rio de Janeiro, RJ) and our institution. Some local representatives of the private sector are also investigating this new business opportunity, such as Risotolândia Indústria e Comércio de Alimentos Ltda. and the State Association of Sugar and Alcool Producers (ALCOPAR, Curitiba, PR), among others. Therefore, there is an increasing perception that biodiesel will soon become competitive and its use in replacement to diesel oil will increase steadily (Chang *et al.*, 1996; Ma and Hanna, 1999; Zagonel and Ramos, 2001). However, cost barriers among with powerful lobbies are still dominating the area and only a strong political support from all Brazilian soybean producers to these new market opportunities will possibly overcome these barriers (Ramos, 2000). Besides, how could biodiesel be produced if no oil is available to do so? Therefore, the future of biodiesel (and its environmental benefits) in Brazil now resides with the farmers and their sight to the immediate needs of our economy and/or society.

**Acknowledgement.** The authors acknowledge the collaboration of Prof. José Carlos Laurindo, as well as to the technical and financial support of Risotolândia Indústria e Comércio de Alimentos Ltda., Alcopar, Abiove, Imcopa Indústria e Comércio de Óleos Vegetais SA, Fundação Araucária e Instituto de Tecnologia do Paraná (Tecpar).

### References

1. Ministério da Indústria e do Comércio, MIC; *Produção de Combustíveis Líquidos a Partir de Óleos Vegetais*. Secretaria de Tecnologia Industrial, Coordenadoria de Informações Tecnológicas, Brasília, DF, Brasil, **1985**
2. Zagonel, G. F., *Obtenção e Caracterização de Biocombustíveis a partir da Transesterificação Etilica de Óleo de Soja*, Mestrado (M.Sc.), Programa de Pós-graduação em Química, Universidade Federal do Paraná, **2001**
3. Zagonel, G. F.; Ramos, L. P. - *Revista de Química Industrial* **2001**, 717, 17-26
4. Ramos, L. P. - In: *Anais do Congresso Tecnologia e Competitividade da Soja no Mercado Global*; Cuiabá, MT, August 28-30, **2000**, p. 111-113.
5. Ma, F.; Hanna, M. A. - *Biores. Technol.* **1999**, 70, 1-15
6. Chang, Y. Z. D., Gerpen, V. H. J., Lee, I., Johnson, A. L., Hammond, G. E., Marley, J. S. - *J. Am. Oil Chem. Soc.*, **1996**, 73, 1549-1555.

# PRODUCTION OF HYDROGEN BY CO-REFORMING BIOMASS PYROLYSIS LIQUIDS AND NATURAL GAS

S. Czernik, R. French, C. Feik, E. Chornet

National Renewable Energy Laboratory  
1617 Cole Blvd., Golden, Colorado, USA 80401

## Introduction

At present, hydrogen is produced almost entirely from fossil fuels such as natural gas, naphtha, and coal. We believe that in the future biomass can become an important sustainable source of hydrogen. As a renewable resource, it has an advantage of low environmental impact (almost zero net CO<sub>2</sub> emissions) compared to that for fossil fuels. However, the price of hydrogen obtained by direct gasification of lignocellulosic biomass is at least three times higher than that for hydrogen produced by steam reforming of natural gas [1]. Over the last several years we have been developing a method for producing hydrogen from biomass [2-4] and concluded that only a hydrogen/co-products strategy could compete with the cost of the commercial hydrocarbon-based technologies.

The proposed process combines two stages: fast pyrolysis of biomass to generate bio-oil and catalytic steam reforming of the bio-oil to hydrogen and carbon dioxide. This concept has several advantages over the traditional gasification/water-gas shift technology. First, bio-oil is much easier to transport than solid biomass and therefore, pyrolysis and reforming can be carried out, if needed, at different locations. A second advantage is the potential production and recovery of higher-value co-products from bio-oil. For example, the lignin-derived fraction can be separated from bio-oil and used as a phenol substitute in phenol-formaldehyde adhesives while the carbohydrate-derived fraction is catalytically steam reformed to produce hydrogen. Assuming that the phenolic fraction could be sold for \$0.44/kg (approximately half of the price of phenol), the estimated cost of hydrogen from the proposed process would be \$7.7/GJ [5], which is at the low end of the current selling prices.

The yield of hydrogen that can be produced from biomass is relatively low, 12-14% based on the biomass weight. It is even lower when only the carbohydrate-derived bio-oil fraction undergoes reforming while the lignin part is used for other applications. At present, the amount of biomass-derived liquids available for reforming is rather limited but a viable way to increase the production of hydrogen in a biomass-based plant could be co-reforming of pyrolysis liquid with natural gas. This approach, similar to co-firing of biomass with coal for power generation, would add environmental benefits to the traditionally fossil-based technology. The objective of this work was to investigate the co-reforming process and validate the concept.

## Experimental

C11-NK catalyst obtained from Süd-Chemie, Inc. was ground to the particle size of 300-500  $\mu$  and used for co-reforming in the 2"-diameter fluidized bed reformer system that was described in our earlier paper [4]. Bio-oil used for this study was generated from pine sawdust using the NREL fast pyrolysis vortex reactor system. The oil comprised 47.7% carbon, 7.4% hydrogen, and 44.8% oxygen with a water content of 26.7%. It was separated into aqueous (carbohydrate-derived) and organic (lignin-derived) fractions by adding water to the oil at a weight ratio of 1.5:1. The aqueous fraction contained 20.0 wt.% organics and 80.0% water and consisted of 11.8% carbon, 9.6% hydrogen, and 78.6% oxygen. Natural gas from the public utility was compressed and

fed to the fluidized bed reformer at the rate of 0.75 L<sub>STP</sub>/min, while the pyrolysis liquid feed rate was 2 g/min. The reactor operated at 850°C with a methane-equivalent gas hourly space velocity  $G_{CH_4}HSV$  of app. 1000 h<sup>-1</sup> and a molar steam-to-carbon ratio of 4.6. The test was carried out for 56 hours alternating between the co-reforming and the bio-oil-only reforming. The concentration of major gas components as a function of time is shown in Figure 1.

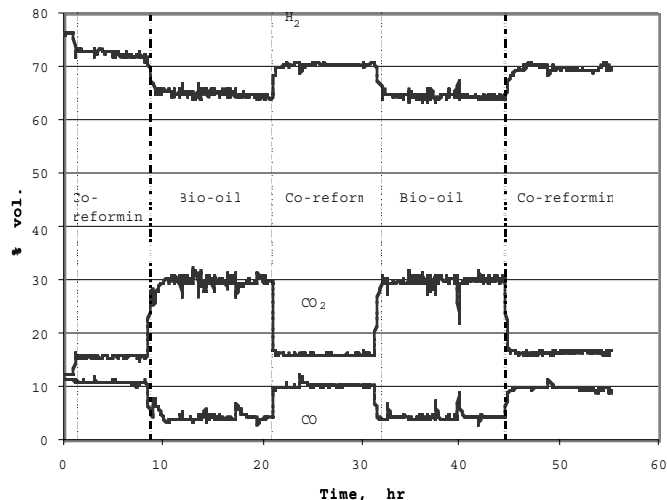


**Figure 1.** Composition of gas obtained from reforming of bio-oil and from co-reforming of bio-oil with natural gas.

The gas composition was almost constant during the stages of reforming and co-reforming, though a small decrease in hydrogen and increase in methane concentration were observed between the first and the second co-reforming cycle. Interestingly, co-feeding of natural gas helped maintain and restore the catalyst activity that was slowly declining during reforming the bio-oil fraction. An evidence of the catalyst deactivation is a sharp increase in methane concentration that was observed at the beginning of the second and third cycles of co-reforming but significantly decreased after 0.5-1 hour (Figure 2).

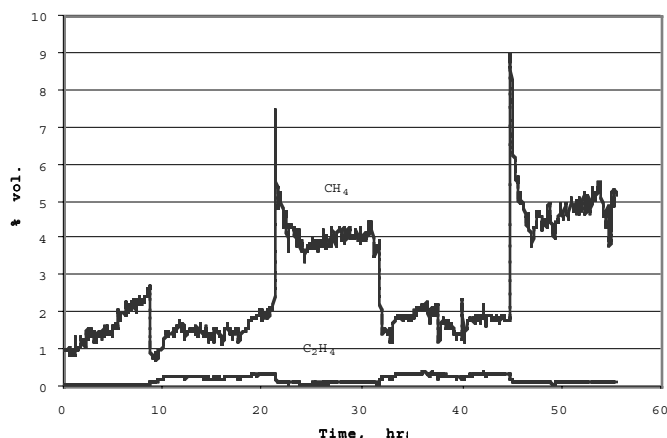


**Figure 2.** Concentration of hydrocarbons in the gas obtained from reforming of bio-oil and from co-reforming of bio-oil with natural gas.

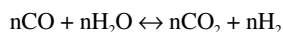
## Discussion

We believe that the mechanism of metal-catalyzed reforming of oxygenated organic molecules is similar to that proposed for hydrocarbons [6]. Dehydrogenation of the organic molecules adsorbed on the metal (nickel) sites produces hydrogen and smaller organic fragments that react with hydroxyl groups migrating from alumina sites to form first intermediate compounds and, eventually, carbon oxides. The above main processes are accompanied by side reactions leading to the formation of carbon deposits on the catalyst surface. This unwanted effect is enhanced by higher non-saturation, molecular weight, and aromaticity of the organic molecules [7]. Biomass-derived liquids are on one hand more reactive than hydrocarbons because they already have some carbon-oxygen bonds. On the other hand, they show greater tendency to form carbon deposits because of the large size of certain molecules (oligomeric carbohydrates and phenols) and thermal instability leading to carbonization at elevated temperatures.

The overall steam reforming of any oxygenated organic compound proceeds according to the following reaction:



Because of the excess steam used in the process, at least a part of carbon monoxide undergoes a consecutive water-gas shift reaction:



Thus the maximum yield of hydrogen that can be obtained by reforming/water-gas shift (corresponding to the complete conversion of organic carbon to  $CO_2$ ) equals  $2+(m-2k)/2n$  moles per mole of carbon in the feed material. During reforming of the bio-oil fraction the yield of hydrogen was initially 82% then decreased to 75% of the stoichiometric potential. For co-reforming the hydrogen yield was about 85% of the theoretical maximum (Figure 3). These values could increase by additional 10% if a secondary water-gas shift reactor followed the reformer. During co-reforming, 23-26% of the hydrogen was generated from bio-oil and 77-73% from natural gas.

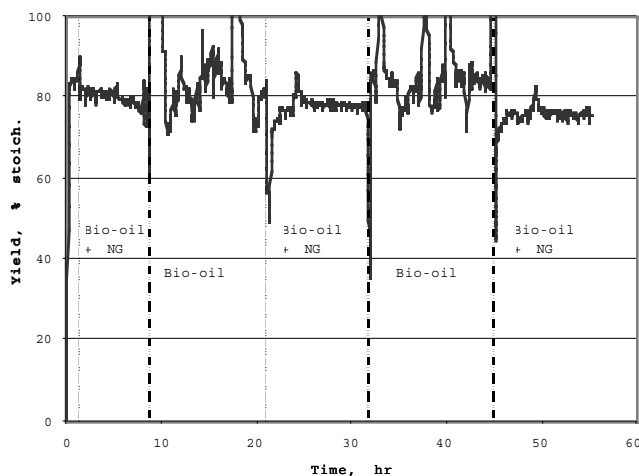


**Figure 3.** Yield of hydrogen obtained from reforming of bio-oil and from co-reforming of bio-oil with natural gas.

The decrease in the yield of hydrogen was a consequence of the declining conversion of methane that was initially 92.5% then decreased to 80% at the end of the test. All these clearly show

a gradual loss of activity of the catalyst. We believe (though we do not have direct evidence) that the catalyst deactivation progressed because of two types of reactions: formation of carbon deposits on the catalyst surface and oxidation of nickel due to a high excess of steam ( $S/C=13$ ), which was used for bio-oil reforming to remove those deposits. During co-reforming, the steam excess was much lower and the hydrogen production was greater, which prevented oxidation of the catalyst and slowed down the deactivation.

## Conclusions

The technical feasibility of co-reforming bio-oil and natural gas has been demonstrated. Co-reforming can be an attractive opportunity that enhances the flexibility of the biomass-to-hydrogen process.

**Acknowledgement.** The authors are thankful to the U.S. Department of Energy Hydrogen Program for financial support of this work

## References

- (1) Spath, P.; Lane, J.; Mann, M.; Amos, W., *Update of Hydrogen from Biomass – Determination of the Delivered Cost of Hydrogen*. NREL Milestone Report, April 2000.
- (2) Wang, D.; Czernik, S.; Montané, D.; Mann, M.; Chornet, E., *I&EC Research*, **1997**, 36, 1507-1518.
- (3) Wang, D.; Czernik, S.; Chornet, E., *Energy & Fuels*, **1998**, 12, 19-24.
- (4) Czernik, S.; French, R.; Feik, C.; Chornet, In *Advances in Hydrogen Energy*, Gregoire-Padró, C. and Lau, F., Eds., Kluwer Academic/Plenum Publishers, pp. 87-91.
- (5) Mann, M.; Spath, P.; Kadam, K., In *Proceedings of the 1996 U.S. DOE Hydrogen Program Review*, NREL/CP-430-21968, pp. 249-272.
- (6) Ross, J.R.H., Steel, M.C.F., Zeini-Isfahani, A., *J. Catal.*, **1978**, 52, 280.
- (7) Trim, D.L., *Catal. Today*, **1997**, 37, 233.

# PYROLYSIS OF $\alpha$ -AMINO ACIDS

Ramesh K. Sharma, W. Geoffrey Chan, Jeffrey I. Seeman<sup>1</sup>, and  
Mohammad R. Hajaligol\*

Philip Morris USA, Research Center  
P. O. Box 26583, Richmond, VA 23261  
<sup>1</sup>Saddle Point Frontiers, Richmond, Virginia

## Introduction

Amino acids are important constituents of most biomass. Pyrolysis of amino acids produces a complex slate of products.<sup>1-5</sup> Of particular interest among the pyrolysis products are the polycyclic aromatic compounds (PAC) which include polycyclic aromatic hydrocarbons (PAH) and nitrogen containing polycyclic aromatic compounds (N-PAC). Patterson et al.<sup>1</sup> pyrolyzed lysine, leucine and tryptophan and found that the total PAC yield was maximum at 850°C. Higman et al.<sup>2</sup> pyrolyzed proline at 840°C and observed pyrrole, indole, pyridine, isoquinoline, quinoline and picoline as products. Smith et al.<sup>3</sup> pyrolyzed valine, aminobutyric acid, and proline and observed nitriles, quinoline and isoquinoline at 850 °C. Yoshida and Matsumoto<sup>4</sup> observed the formation of amino- $\beta$ -carbolines from tryptophan at 550 °C. Recently, Chiavari and Galletti<sup>5</sup> reported the main products from pyrolysis of amino acids in a CDS Pyroprobe 100 at 600 °C for 5 s. Despite these studies, there is no detailed study on the effect of temperature and residence time on the product distribution.

In this work, the formation of PAC from pyrolysis of asparagine, proline, and tryptophan was studied under various pyrolysis conditions. The results were analyzed to determine the major product components and the effect of pyrolysis conditions and the structure of amino acid on the PAC yields.

## Experimental

Pyrolysis experiments were performed in a quartz reactor in two ways.<sup>6</sup> In the first case, the amino acid was pyrolyzed in a single zone reactor at 300 °C to collect LTT (low temperature tar) and LTC (char). A sample of 200 mg of amino acid was used and pyrolyzed for 60 minutes. The LTT was collected on a Cambridge pad. The pad was extracted with methanol. The LTC was then pyrolyzed further at 625 °C for 60 min to collect HTT (high temperature tar) and HTC (char). In the second case, a two-zone reactor was used and the LTT and HTT leaving the first zone were pyrolyzed further in the second zone at 720-920 °C. The final tars, LTFT (low temperature final tar) and HTFT (high temperature final tar) from LTT and HTT, respectively, were collected similarly. Only the runs with a residence time of 1370 ms in the second zone are discussed in this paper. Helium was used as carrier gas at 120 cm<sup>3</sup>/min. The LTT, HTT, LTFT, and HTFT were analyzed by chromatography/ mass spectrometry (GC/MS).

## Results and discussion

**Asparagine.** The overall material balance from pyrolysis of asparagine showed that, at 300 °C, the yield of LTT was negligible but the yield of LTC was 64%. The yields of HTT and HTC were 12% and 23% of initial weight of asparagine. The HTT consisted mainly of maleimide and succinimide with yields of ca. 8 and 48 mg/g of asparagine. Indole and a methylindole were also observed in low yields. Chiavari and Galletti<sup>5</sup> reported maleimide and succinimide from pyrolysis of asparagine at 600 °C.

No LTFT was obtained from asparagine. The yields of a few major PAC in HTFT are shown in **Figure 1**. At 700 °C, succinimide was the major component of HTFT. Both maleimide and succinimide decreased at high temperature. The yield of maleimide passed

through a maximum at 770 °C. At 870 °C and above, the yields of two- to four-ring N-PAC, such as a naphthalene carbonitrile, pyrrolicarbazole, a benzoquinoline, and azapyrene, were significant. Most other N-PAC, including fluorene carbonitrile, and anthracene carbonitrile, were formed in relatively low yields. Among the PAH, the highest yield was of phenanthrene followed at high temperature by pyrene. The formation of PAH indicates a complete loss of nitrogen from the initial products of pyrolysis.

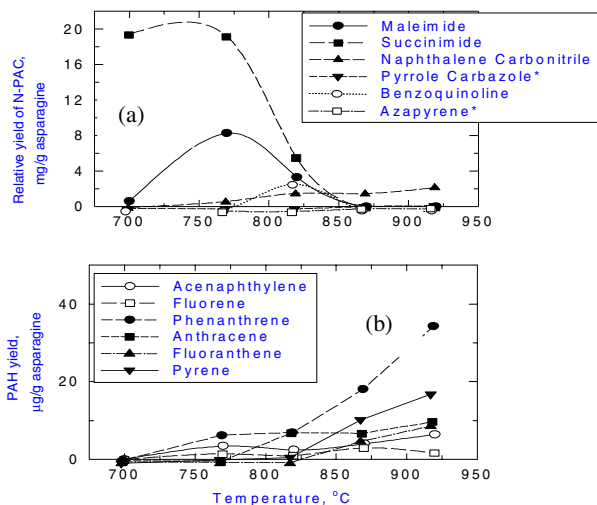


**Figure 1.** Effect of temperature on the yields of major N-PAC (a) and PAH (b) from the gas phase pyrolysis of HTT from asparagine at 700-920 °C.

**Proline.** Proline was completely converted into volatile products at 300 °C, with a LTT yield of ca. 80%. The LTT consisted mainly of 2,5-diketopiperazine. No HTT or HTFT was obtained.

The yields of some of the major components of LTFT are presented in **Figure 2**. Above 820 °C, both N-PAC and PAH were observed. Carbonitriles were the main components of the N-PAC fraction. The yield of acridine passed through a maximum at 870 °C. The yields of fluorene carbonitrile, anthracene carbonitrile, and azapyrene increased sharply with temperature above 820 °C. At 920 °C, methylbenzonitrile was absent from the products. Indole, quinoline, benzenecarbonitrile, phenylpyridine, naphthalene carbonitrile, benzoquinoline, fluorene imine, phenanthridine, carbazole, acenaphthopyridine, indenoisoquinoline, pyrrolicarbazole, and cyanopyrene were also observed. Among the PAH, phenanthrene was the major component at all the temperatures. Benzo[a]pyrene was observed only at 920 °C. Other PAH, such as naphthalene, biphenyl, ethenylanthracene, methylanthracene, phenylanthracene, benzo[a]fluorene, methylpyrene, benzo(ghi)fluoranthene, and isochrysene were also observed. The yields of acenaphthylene, fluorene, and anthracene either decreased or leveled off at high temperatures. This could be due to their growth into larger PAH. The formation of PAH from proline has also been reported earlier in the literature.<sup>2,3</sup> Smith et al.<sup>3</sup> also reported the formation of butadiene at 650 °C. Thus, the PAH in this study, may have formed via butadiene and related low molecular weight olefins.

**Tryptophan.** The yields of LTT and LTC from tryptophan were 15% and 56% whereas those of HTT and HTC were ca. 11% and 14%, respectively. The LTT contained indole, a methyl indole, norharman, harman and other indole derivatives, such as indoleethanamine and indoleacetonitrile. Ethylindole and dimethylindole were also observed in low yields. The HTT contained similar components but the yields of indole and substituted indoles were lower while those of the harmans were slightly higher. Other two- and three-ring PAC, such as quinoline and carbazole or azafluorene were also observed in small yields in the HTT. Some of these products have been reported earlier.<sup>5,7</sup>

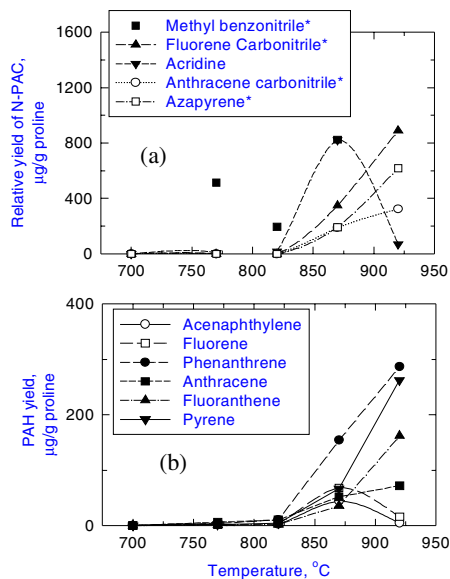


**Figure 2.** Effect of temperature on the yields of major N-PAC (a) and PAH (b) from the gas phase pyrolysis of LTT from proline at 700-920 °C.

No PAH were observed in the LTFT and HTFT from tryptophan. The constituents of LTFT and HTFT ranged from N-heterocycles to three-ring N-PAC (benzo[a]carbazole and anthracenamine). For both LTFT and HTFT, the yields of indole and skatole decreased as the temperature was increased until they were completely destroyed above 850 °C (**Figure 3**). The temperature had only a small effect on the yields of norharman and harman, although above 820 °C the yields decreased. Whereas harman was completely absent in the product at 920 °C, the yield of norharman remained significantly high even at 920 °C. Essentially similar observations were made by Kleinbauer and Rabache.<sup>7</sup> Harman and norharman were observed in the product even at 250 °C and the yield of norharman decreased slowly at high temperatures whereas the yield of harman decreased sharply. The nearly similar trends in the yields of norharman and harman in this study suggested that the norharman/harman ratio did not vary dramatically with temperature, except at high temperatures. The yield of quinoline remained relatively low at all temperatures. The yields of three-ring N-PAC, benzocarbazole and anthracenamine, became significant only at 920 °C. In the case of HTFT, the yield of carbazole also became significant at high temperatures suggesting that it is one of the end products of the pyrolysis of tryptophan. In addition to the components shown in

**Figure 3**, the product also contained cyanocarbazole, indenoisoquinoline, benzo[a]phenazine, benzo[a]acridine and other products.

### Conclusions

The results from the three amino acids showed that the amino acids pyrolyzed differently. The N-PAC from asparagine and proline were mainly aromatic carbonitriles and three- and four-ring azarenes. Asparagine and proline also formed PAH, although the yields of PAH were low compared to the yields of N-PAC. In contrast, tryptophan did not form any PAH but it formed  $\beta$ -carbolines and indoles even at low temperatures. The pyrolysis mechanisms may be governed by the structure of the amino acid.

**Acknowledgements.** The authors are grateful to the Philip Morris USA management for the support of this research.

### References

1. Patterson, J.M.; Baedecker, M.L.; Musick, R.; Smith, Jr., W.T. *Tob. Sci.* **1969**, 13, 26.
2. Higman, E.B.; Schmeltz, I.; Schlotzhauser, W.S. *J. Agric. Food Chem.* **1970**, 18, 636.
3. Smith, W.T.; Haidar, N.F.; Patterson, J.M. *Tob. Sci.* **1975**, 19, 142.
4. Yoshida, D.; Matsumoto, T. *J. Agric. Biol. Chem.* **1979**, 43(5), 1155.
5. Chiavari, G.; Galletti, G.C. *J. Anal. Appl. Pyrol.* **1992**, 24, 123.
6. McGrath, T.; Sharma, R.; Hajaligol, M. *Fuel* **2001**, 80, 1787.
7. Kleinbauer S.; Rabache, M. *Sci. Alim.* **1990**, 10, 417.

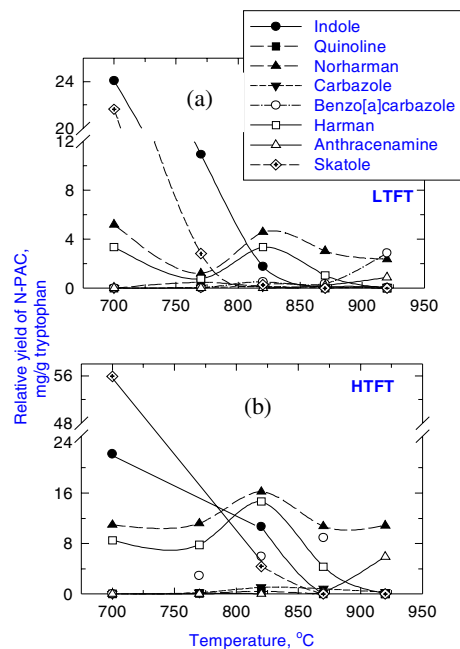


**Figure 3.** Effect of temperature on the yields of major N-PAC from the gas phase pyrolysis of LTT (a) and HTT (b) from tryptophan at 700-920 °C.

## Substituent Effects in the Pyrolysis of Lignin Model Compounds

Michelle K. Kidder, Phillip F. Britt, and  
A. C. Buchanan, III

Chemical Sciences Division  
Oak Ridge National Laboratory  
P.O. Box 2008, MS-6197  
Oak Ridge, Tennessee 37831-6197

### Introduction

Lignin is the second most abundant natural biopolymer found in vascular plants and a potential source for renewable chemicals and fuel. Lignin is also a byproduct from pulping processes in paper mills, and over 975 million solid tons of liginosulfonate are produced each year.<sup>1</sup> However, lignin is underutilized because the decomposition of the polymeric structure yields crude mixtures of products and bio-oils that are highly oxygenated and typically need to be upgraded before it can be used. As a consequence of the poor quality of the bio-oils, a large fraction of lignin is burned. Thus, more control is needed over the depolymerization of this complex heterogeneous polymer into higher valued products. Our goal is to provide a better understanding of the chemical reactions that occur during the thermal processing of lignin, to control the product selectivities and yields.

The dominant backbone unit of the lignin structure is the  $\beta$ -O-4 linkage (47-60%). The simplest model of the  $\beta$ -O-4 linkage is phenethyl phenyl ether (PPE). Recently, our group studied the decomposition of PPE, in the gas and liquid phases, to clarify the primary reaction pathways.<sup>2</sup> This study resolved that PPE decomposed by a free radical chain pathway rather than a concerted retro-ene reaction<sup>3</sup> that was previously proposed. The free radical chain pathway also explained the formation of two previously unreported primary products, toluene and benzaldehyde, which were formed in a 1:1 ratio and accounted for 25% of the product mixture. These products were formed by hydrogen abstraction at the  $\beta$ -carbon, followed by 1, 2-O, C-phenyl shift and  $\beta$ -scission as shown in Figure 1.

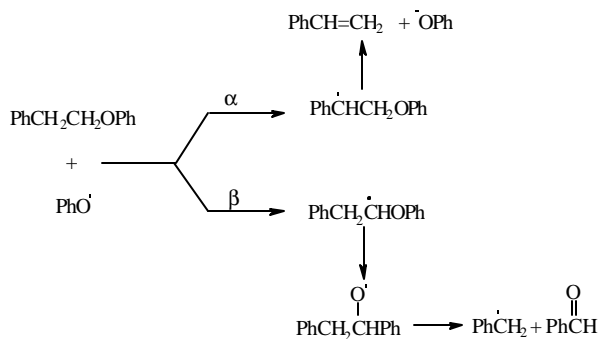


**Figure 1.** Hydrogen abstraction reactions in the free radical decomposition of PPE.

To determine if this free radical chain pathway occurs for substituted PPE's, a systematic study of the impact of substituents on the thermal decomposition of lignin model compounds was initiated. As a consequence of the complexity of the reaction mixtures and the reactivity of the products, the thermolysis was studied in the liquid phase with biphenyl as a solvent to minimize secondary reactions of the primary products. This study will focus on the impact of substituents on the rate of decomposition and selectivity of hydrogen abstraction at the  $\alpha$  and  $\beta$ -positions, which is determined by the ratio of products formed from the subsequent reactions (see Figure 1).

Unfortunately, a substituent can affect many steps in a reaction. For example, an *o*-methoxy substituent is predicted to weaken the  $\beta$ -O-4 linkage (hence accelerate the rate of decomposition), alter the selectivity of hydrogen abstraction at the  $\alpha$  and  $\beta$ -position (which will alter the product distribution) and alter the rate of 1, 2-O, C-phenyl shift. Thus, a systematic study of the impact of substituents on the rate of decomposition and product selectivity is needed to unravel the substituent effect on the reaction steps. This investigation will focus on oxygen containing substituents and the compounds to be studied are shown in Figure 2.

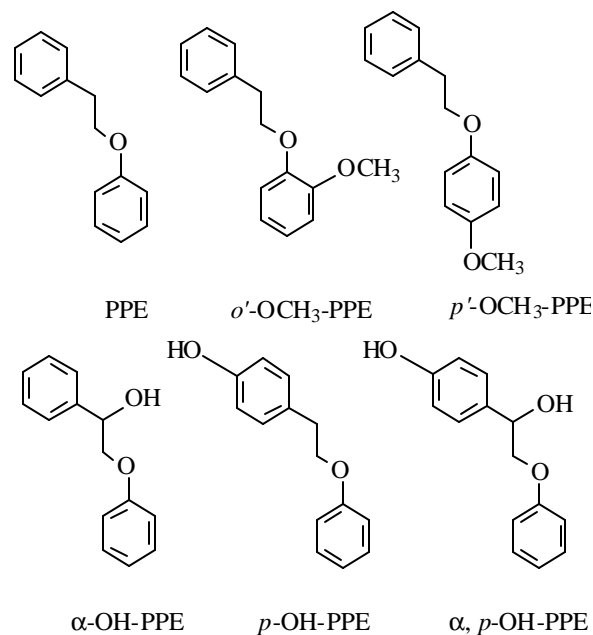


**Figure 2.** Substituted PPE compounds investigated.

### Experimental

**Materials.** Standards were purified to > 99.9% by GC analysis. Biphenyl was purified by recrystallization from ethanol. Cumene is purified by fractional distillation and 2, 5-dimethylphenol was recrystallized from ethanol. Benzyl phenyl ether (Aldrich) did not require further purification.

The synthesis and purification of PPE (99.9% pure by GC),<sup>2</sup>  $\alpha$ -OH-PPE (99.9%),<sup>4</sup> *o*'-OCH<sub>3</sub>-PPE (99.6%),<sup>5</sup> *p*-OH-PPE (99.9%),<sup>6</sup> has been previously reported. The procedure for the synthesis of *p*'-OCH<sub>3</sub>-PPE (99.9%) was similar to *o*'-OCH<sub>3</sub>-PPE, except that *p*-methoxyphenol was used rather than guaiacol. The procedure for the synthesis of  $\alpha$ , *p*-OH-PPE (99.4%) was similar to that for  $\alpha$ -OH-PPE, except a benzyl protected *p*-hydroxyacetophenone was used as the starting material.

**Thermolysis procedure.** Pyrex tubes with an internal volume of ca. 3.1 mL were washed with detergent then rinsed extensively with distilled water, acetone, CH<sub>2</sub>Cl<sub>2</sub>, and ethanol and dried in an oven at 120 °C. The tubes are cooled under argon and loaded with the ca. 30.0 mg of the substituted ether and diluted 8-fold with biphenyl. The tubes were connected to a high vacuum line via Swagelok fittings with Teflon ferrules, degassed by a minimum of three freeze-pump-thaw cycles and sealed at < 2.5 x 10<sup>-5</sup> Torr. The tubes were placed into a boat (2.54 cm x 35.6 cm) beside a RTD thermocouple, and slid into the center of a Carbolite three-zone furnace (45 cm x 3.8 cm i.d.) where the temperature was maintained within  $\pm 1^\circ\text{C}$  of the setpoint. Sample heat up times were ca. 3 minutes.

At the end of the reaction time, the tubes were removed from the oven, cooled to room temperature and frozen in liquid nitrogen. The tubes were opened and the samples dissolved in the minimum amount of high purity acetone (EM Scientific, Omni Solve, typically 200  $\mu\text{L}$ ),

and the standards (cumene, dimethylphenol and benzyl phenyl ether) were added in acetone.

**Analytical Methods.** Product analysis was performed on a Hewlett-Packard 5890 Series II gas chromatograph equipped with a flame ionization detector, and the identification of products was confirmed by comparison of retention times and mass spectral fragmentation patterns with authentic samples using a Hewlett-Packard 5972A/5890 Series II GC-MS (EI 70 eV). Both instruments were equipped with a J&W DB-5 5% diphenyl- 95% dimethylpolysiloxane capillary column (30 m x 0.25 mm i.d. with 0.25  $\mu$ m film thickness). The injector temperature was 280  $^{\circ}$ C, and the detector temperature was 305  $^{\circ}$ C. The oven was programmed with an initial temperature of 45  $^{\circ}$ C, and the temperature was ramped to 300  $^{\circ}$ C at 10  $^{\circ}$ C/min and held for 20 minutes. The carrier gas, helium, was set at a constant flow rate of 1.0 mL/min.

Samples were injected four times onto the GC using a HP 7673 autosampler. The products were quantitated, and the data was averaged using the GC-FID output relative to the internal standards. Typical shot to shot reproducibility was  $\pm 2\%$ . Response factors were measured with authentic samples or estimated from measured response factors for structurally related compounds and based on carbon number relative to the internal standards. Reaction mixtures were also silylated to the trimethylsilyl ether derivatives with *N,O*-bis(trimethylsilyl)trifluoroacetamide in pyridine (1:2) to determine if the products contained an alcohol functional group. Conversion calculations were based on the recovered products and the charge of the substituted PPE. The rate of reaction was calculated from the conversion over the corrected reaction time.

## Results and Discussion

Thermolysis of the substituted PPE model compounds was run at 345  $^{\circ}$ C diluted in biphenyl (8-fold) and the reaction time was varied to keep the conversion low (<10%) so the primary products could be observed. Products from the reactions were consistent with the free radical chain mechanism proposed for PPE (see Figure 1). The selectivity for products formed from hydrogen abstraction at the  $\alpha$ - and  $\beta$ - carbons is referred to as  $\alpha/\beta$  selectivity. The selectivity is calculated from the products containing ( $C_6 + C_8$  fragments)/ $C_7$  fragments for the PPE backbone. By the reaction stoichiometry, the ratio of the number of moles of  $C_6$  fragment (analogous to PhOH in PPE), to the  $C_8$  fragment (analogous to PhCH=CH<sub>2</sub> in PPE and products derived from PhCH=CH<sub>2</sub>) and the  $C_{7Tol}$  to  $C_{7Ald}$  (analogous to PhCH<sub>3</sub> and PhCHO respectively) should be unity if all the primary and secondary products are taken into consideration. The  $C_6/C_8$  and the  $C_{7Tol}/C_{7Ald}$  balances for the liquid phase runs and their mass balances will be discussed on an individual basis for the substituted PPE's.

All runs were made in duplicate, and their rates, selectivities and product distributions were in excellent agreement ( $\pm 10\%$ , unless otherwise noted) between the runs. For PPE, the mass balance was 99.7%, and the fragment balances were  $1.02 \pm 0.05$  and  $1.01 \pm 0.01$  ( $C_6/C_8$  and  $C_{7Tol}/C_{7Ald}$  respectively). The  $\alpha/\beta$  selectivity for PPE at 345  $^{\circ}$ C is was found to be 3.9 when diluted in biphenyl (Table 1), but only 2.9 as neat solution.<sup>2</sup> This indicates that there is a slight concentration dependence to the product selectivity which is surprising since no concentration dependence was observed at 375  $^{\circ}$ C.<sup>2</sup>

**Table 1. Reaction Rates and Product Selectivity from the Thermolysis of Substituted PPE's at 345  $^{\circ}$ C in Biphenyl**

Compound	% Conversion	Rate (%/h)	a/b
PPE	3.8	1.7	3.9
<i>o</i> '-OCH <sub>3</sub> -PPE	3.6	8.5	4.6
<i>p</i> '-OCH <sub>3</sub> -PPE	4.6	10.7	3.0
$\alpha$ -OH-PPE	1.9	2.0	3.4
<i>p</i> -OH-PPE	2.1	10.4	5.0
<b>a</b> , <i>p</i> -OH-PPE	-*	-*	-*

-\* Fragment balances were not close to unity, see text. % Conversion based on reaction products and starting charge of material. Rate based on % conversion over the corrected reaction time (see experimental).

***o*'-OCH<sub>3</sub>-PPE.** The pyrolysis of the *o*'-OCH<sub>3</sub>-PPE produced products consistent with the proposed free radical pathway described for PPE. The major products include styrene and guaiacol in a 1:1 ratio, and less than 10 mol % each of toluene, ethyl benzene, anisole, phenol, and *o*-anisaldehyde. The mass balance was 95.3% at 3.6% conversion. The reaction rate increased 5-fold for *o*'-OCH<sub>3</sub>-PPE compared to PPE. It has been reported that the *o*-methoxy substituent weakens the C-O bond by ca. 4 kcal mol<sup>-1</sup> so a rate enhancement was expected. In the FVP of *o*'-OCH<sub>3</sub>-PPE (where only unimolecular reactions can occur), the *o*-methoxy substituent enhanced the rate of decomposition by 4-fold compared to PPE.<sup>5</sup>

The  $\alpha/\beta$  selectivity increased 20 % for *o*'-OCH<sub>3</sub>-PPE compared to PPE. This increase in selectivity could be a consequence of a reduction in the hydrogen abstraction rate constant for hydrogen abstraction at the  $\beta$ -carbon or a reduced rate constant for the 1,2-O, C-phenyl shift (so that bimolecular hydrogen transfer between the  $\alpha$  and  $\beta$ -carbons competes) because of steric or electronic effects. In the neophyl rearrangement, electron donating substituents were found to decrease the rate of rearrangement while electron withdrawing substituents increased the rate of rearrangement.<sup>5</sup> Thus, the *o*'-methoxy substituent is expected to reduce the rate of the 1,2-phenyl shift. To investigate the potential role of steric effects in the reaction, the *p*'-methoxy substituted PPE was studied since this substituent should have similar electronic properties but different steric interactions.

***p*'-OCH<sub>3</sub>-PPE.** Products from the pyrolysis of the *p*'-OCH<sub>3</sub>-PPE were analogous to those proposed from the free radical pathway. The major products were styrene and 4-methoxyphenol produced in a 1:1 ratio, analogous to *o*'-OCH<sub>3</sub>-PPE. The mass balance was 97.9 % for a conversion of 4.6%. The reaction rate increased 6.3-fold compared to PPE (and 1.3-fold compared to *o*'-OCH<sub>3</sub>-PPE).

The  $\alpha/\beta$  selectivity for *p*'-OCH<sub>3</sub>-PPE was 35 % smaller than that found for *o*'-OCH<sub>3</sub>-PPE. This indicates that the *o*'-methoxy substituent does impose steric constraints on the reaction. The methoxy-substituent also appears to enhance hydrogen abstraction at the  $\beta$ -carbon.

**$\alpha$ -OH-PPE.** Acetophenone and phenol were the dominant products formed (25.5 and 39.6 mol % respectively) in the thermolysis of  $\alpha$ -OH-PPE. Benzene, toluene, styrene, benzaldehyde, phenol, benzyl alcohol, phenylacetaldehyde, and dehydrated  $\alpha$ -OH-PPE were formed in smaller amounts (0.80-7.0 mol %). The mass balance was 95.7% at a conversion of 1.9 %. It is seen from Table 1, that the selectivity of  $\alpha$ -OH-PPE is only 13% smaller than PPE, and the reaction rate only 1.2x larger than PPE, indicating that the  $\alpha$ -hydroxy substituent has little impact on the reaction selectivity.

To account for the additional products found in the reaction mixture, there are two possible phenyl shifts that can follow hydrogen abstraction at the  $\beta$ -carbon. If the aryl ring connected to the oxygen shifts, then the products of the  $\beta$ -scission are benzaldehyde and the  $\alpha$ -hydroxybenzyl radical (Figure 3a). The  $\alpha$ -hydroxybenzyl radical can either abstract hydrogen from the starting material (which is the most likely source of hydrogen at low conversions) to give benzyl alcohol, or it may lose a hydrogen atom to give benzaldehyde. If the other aryl ring shifts, i.e., 1,2 phenyl shift, the phenoxy radical and the tautomer of phenylacetaldehyde are formed following  $\beta$ -scission (Figure 3b). All of these compounds were detected in the reaction mixture. Again this is difficult to predict without further exploration for the decomposition of the  $\alpha$ -hydroxybenzyl radical.

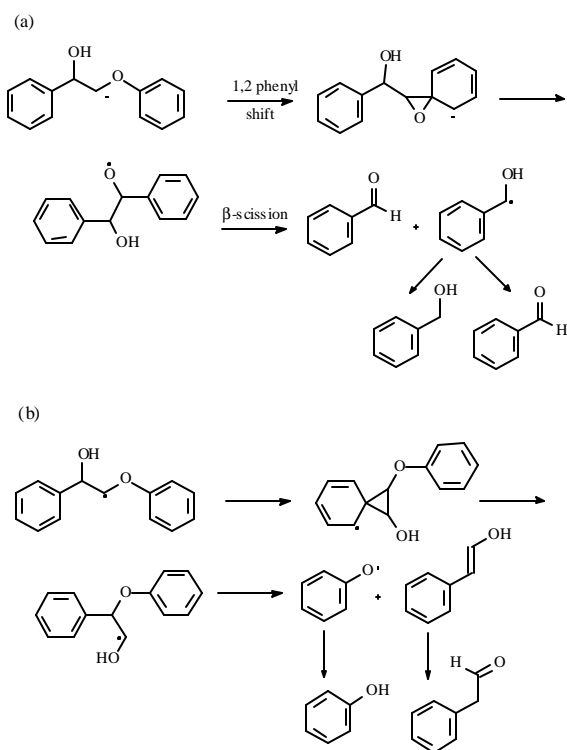


**Figure 3.** Possible pathways following  $\beta$ -hydrogen abstraction.

***p*-OH-PPE.** Products from the pyrolysis of *p*-OH-PPE are analogous to those that follow the free radical pathway. Phenol and *p*-vinylphenol make up the largest fraction of the product mixture, 41.4 mol % and 37.2 mol % respectively, from the hydrogen abstraction at the  $\alpha$ -carbon. Benzaldehyde and *p*-cresol (8.3 mol% and 7.3 mol% respectively), which are formed from the  $\beta$ -hydrogen abstraction, followed by the 1,2-O, C-phenyl shift and  $\beta$ -scission, were formed in ca. a 1:1 ratio. However, the *p*-OH-PPE had a low, and slightly irreproducible mass balance of 88.5% at a conversion of 2.1%. The fragment balances showed reasonable agreement with a  $C_6/C_8$  value of  $1.07 \pm 0.05$ , and  $C_7/C_7$  value of  $1.14 \pm 0.0$ . The rate was enhanced by 5.8x, but the selectivity was only enhanced by 1.3x for *p*-OH-PPE compared to that of PPE. The increase in reaction rate may be attributed to participation of the *p*-hydroxy group in the hydrogen abstraction reactions, however no new products are seen. This is under additional investigation.

**a, *p*-OH-PPE.** The pyrolysis of the  $\alpha$ ,*p*-OH-PPE left many unanswered questions. This compound was completely consumed in 15 minutes at 345 °C. The mass balance was ca. 60.8 %, and the fragment balances were poor, which indicate that many of the primary products undergo secondary reactions. One problem is the reactivity of the hydroxybenzyl alcohol, which is a potential product in the reaction but was not observed. A preliminary investigation of the reactivity of hydroxy and methoxy substituted benzyl alcohols at 345 °C, indicates that these compounds are not stable under the reaction conditions and undergo ionic and free radical reactions.

## Conclusions

In general, the free radical chain mechanism proposed for PPE explains most of the pyrolysis products formed from the substituted PPE's. The rate of reaction increases if the substituent can stabilize the radicals formed from the C-O homolysis (such as a methoxy group), or if the substituent increases the rate constant for hydrogen abstraction. A subtle balance between rates for competitive hydrogen abstraction, 1,2-phenyl shift, and  $\beta$ -scission steps controls the product selectivities. Unfortunately, the rate constants for hydrogen

abstraction by phenoxy or substituted phenoxy radical from hydrocarbons are not known, and as a consequence of polar effects in the hydrogen abstraction reaction, they cannot be reliably estimated by standard thermochemical kinetic techniques. Similarly, rate constants for the O, C-phenyl shift are not known. To predict the decomposition of the oxygenated materials, the rate constants for these processes are needed. Future studies include the study of the fast pyrolysis of the lignin model compounds by atmospheric pressure flow pyrolysis with on-line monitoring of products by molecular beam mass spectrometry to address these issues through direct kinetic measurements.

**Acknowledgement.** This research was sponsored by the Division of Chemical Sciences, Geosciences, and Biosciences, Office of Basic Energy Sciences, U.S. Department of Energy under contract DE-AC05-00OR22725 with Oak Ridge National Laboratory, managed and operated by UT-Battelle, LLC. MKK was supported by an appointment to ORNL Postdoctoral Research Associated program administered jointly by Oak Ridge Institute for Science and Education and ORNL.

## References

- (1) *Lignin: Historical, Biological, and Materials Perspectives*; Glasser, W. G., Northey, R. A., Schultz, T. P., Eds.; ACS Symposium Series 742: American Chemical Society: Washington, DC, 2000. Chapter 15.
- (2) Britt, P. F.; Buchanan, A. C. III; Malcolm, E. A.; *J. Org. Chem.* **1995**, *60*, 6523.
- (3) Klein, M. T.; Virk, P. S.; *Ind. Eng. Chem. Fundam.* **1983**, *22*, 35.
- (4) Cooney, M. J.; Britt, P. F.; Buchanan, A. C. III *Prepr. Pap.-Am. Chem. Soc., Div. Fuel Chem.* **1997**, *42*, 89.
- (5) Britt, P. F.; Buchanan, A. C. III; Cooney, M. J.; Martineau, D. R.; *J. Org. Chem.* **2000**, *65*, 1376.
- (6) Britt, P. F.; Buchanan, A. C. III; Hitsman, V. H.; *Prepr. Pap.-Chem. Soc., Div. Fuel Chem.*, **1991**, *36*, 529
- (7) Stein, S. E. *J. Am. Chem. Soc.* **1989**, *111*, 1423.
- (8) *Reactive Molecules*; Wentrup, C.; John Wiley & Sons, Inc.: Canada, 1984.